

Using spectral reflectance in soybean breeding: evaluating genotypes for soybean sudden death
disease resistance and grain yield

by

Ethan J. Menke

B.S., Newman University, 2014

A THESIS

submitted in partial fulfillment of the requirements for the degree

MASTER OF SCIENCE

Department of Agronomy
College of Agriculture

KANSAS STATE UNIVERSITY
Manhattan, Kansas

2018

Approved by:

Major Professor
William T. Schapaugh

Copyright

© Ethan Menke 2018.

Abstract

Sudden Death Syndrome (SDS) in soybean, (*Glycine max* (L.) Merr.) caused by *Fusarium virguliforme*, is an increasing problem in commercial soybean production due to the yield loss associated with the disease. Screening for genetic resistance requires extensive visual evaluations. Canopy spectral reflectance may be an indirect tool for selection of SDS resistance as well as grain yield in large segregating populations. The objective of this study was to estimate SDS resistance and seed yield in large diverse soybean populations using canopy spectral reflectance. Spectral reflectance, disease index, maturity and yield were measured on two populations consisting of 160 nested association mapping recombinant inbred lines and checks; and 140 commercial cultivars with checks. Populations were grown in three environments in 2015 and 2016 with historic SDS disease pressure. Entry, environment, and entry by environment sources of variation were significant for disease index, yield, maturity and spectral reflectance. Changes in season average reflectance were correlated to disease index, yield and maturity. Estimation models of disease index, yield and maturity were created with season averages as well as individual day readings for both populations. Season average and individual day models accounted for 11% to 77% of the phenotypic variation in disease and 41% to 93% of yield variation when measurements were taken at the height of disease pressure. Models for disease index and yield models were able to predict significant portions of the phenotypic variation between entries at most environments. These results suggest that it may be possible to estimate resistance to SDS and grain yield in soybeans using spectral reflectance in breeding populations.

Table of Contents

List of Figures	vi
List of Tables	xi
Acknowledgements	xiii
Dedication	xiv
Chapter 1 - Review of Literature	1
Introduction	1
Soybean Sudden Death Syndrome	2
SDS Management	5
Yield Loss due to SDS	6
SDS and SCN Synergy	7
Seed Treatments for SDS	7
High Throughput Phenotyping	9
Spectral Reflectance	9
Estimating Chlorophyll Content	10
Reflectance Indexes	11
Reflectance for Grain Yield	11
Reflectance for Disease	12
References	15
Chapter 2 - Evaluating Genotypes for Soybean Sudden Death Resistance and Grain Yield using Spectral Reflectance	23
Introduction	23
Soybean Sudden Death Syndrome	23
Genetic Resistance to SDS	26
Phenotyping with Spectral Reflectance	27
Material and Methods	33
Results and Discussion	37
Agronomic Data	37
NAM	37
SVPT	38

Spectral Reflectance Readings.....	40
NAM.....	40
SVPT.....	41
Dx and Reflectance Correlations	42
NAM Season Average	42
NAM Individual Days.....	44
SVPT Season Average.....	45
Reflectance Curve Change Due to Disease.....	45
Reflectance and Yield Correlations	46
NAM Season Average	46
NAM Individual Days.....	47
SVPT Season Average.....	47
Correlations with Maturity, Dx and Yield	47
Regression Equations for Dx Prediction.....	48
NAM Season Average	48
NAM Individual Days.....	49
SVPT Season Average.....	49
Regression Equations for Yield Prediction.....	50
NAM Season Average	50
NAM Individual Days.....	51
SVPT Season Average.....	51
Maturity Estimation Models	52
DX and Yield Estimation based on Maturity Groups.....	52
Check Models	54
Conclusions.....	57
References.....	59
Tables and Figures	67

List of Figures

Figure 2.1 a. Distribution of season average disease index scores for recombinant inbred lines in a nested association mapping population grown in Manhattan in 2015.	75
Figure 2.1 b. Distribution of season average disease index scores for recombinant inbred lines in a nested association mapping population grown in Manhattan in 2016.	75
Figure 2.1 c. Distribution of season average disease index scores for recombinant inbred lines in a nested association mapping population grown in Rossville in 2016.	76
Figure 2.2 a. P-values for entry main effect for individual waveband reflectance measurements of individual day readings for a nested association mapping population grown at Manhattan in 2015.....	76
Figure 2.2 b. P-values for entry main effect for individual waveband reflectance measurements of individual day readings for a nested association mapping population grown at Manhattan in 2016.	77
Figure 2.2 c. P-values for entry main effect for individual waveband reflectance measurements of individual day readings for a nested association mapping population grown at Rossville in 2016.....	77
Figure 2.3 a. P-values for entry main effect for individual waveband reflectance measurements of individual day readings for the Soybean Variety Performance Test Population grown at Manhattan in 2015.	78
Figure 2.3 b. P-values for entry main effect for individual waveband reflectance measurements of individual day readings for the Soybean Variety Performance Test Population grown at Manhattan in 2016.	78
Figure 2.3 c. P-values for entry main effect for individual waveband reflectance measurements of individual day readings for the Soybean Variety Performance Test Population grown at Rossville in 2016.....	79
Figure 2.4 a. Pearson’s correlation (r) between disease index and season average waveband reflectance for a nested association mapping population grown at Manhattan in 2015. Significant correlation at $\alpha = .05$ is equal to $r \leq -.15$ and $r \geq .15$. Significant correlation at $\alpha = .01$ is equal to $r \leq -.20$ and $r \geq .20$	79
Figure 2.4 b. Pearson’s correlation (r) between disease index and season average waveband reflectance for a nested association mapping population grown at Manhattan in 2016.	

Significant correlation at $\alpha = .05$ is equal to $r \leq -.15$ and $r \geq .15$. Significant correlation at $\alpha = .01$ is equal to $r \leq -.20$ and $r \geq .20$	80
Figure 2.4 c. Pearson's correlation (r) between disease index and season average waveband reflectance for a nested association mapping population grown at Rossville in 2016. Significant correlation at $\alpha = .05$ is equal to $r \leq -.15$ and $r \geq .15$. Significant correlation at $\alpha = .01$ is equal to $r \leq -.20$ and $r \geq .20$	80
Figure 2.5 a. Pearson's correlation (r) between disease index and August 8 waveband reflectance for a nested association mapping population grown at Rossville in 2016. Significant correlation at $\alpha = .05$ is equal to $r \leq -.15$ and $r \geq .15$. Significant correlation at $\alpha = .01$ is equal to $r \leq -.20$ and $r \geq .20$	81
Figure 2.5 b. Pearson's correlation (r) between disease index and September 2 waveband reflectance for a nested association mapping population grown at Rossville in 2016. Significant correlation at $\alpha = .05$ is equal to $r \leq -.15$ and $r \geq .15$. Significant correlation at $\alpha = .01$ is equal to $r \leq -.20$ and $r \geq .20$	81
Figure 2.6 a. Pearson's correlation (r) between disease index and season average waveband reflectance of the soybean variety performance test population grown at Manhattan in Significant correlation at $\alpha = .05$ is equal to $r \leq -.15$ and $r \geq .15$. Significant correlation at $\alpha = .01$ is equal to $r \leq -.20$ and $r \geq .20$	82
Figure 2.6 b. Pearson's correlation (r) between disease index and season average waveband reflectance of the soybean variety performance test population grown at Manhattan in 2016. Significant correlation at $\alpha = .05$ is equal to $r \leq -.15$ and $r \geq .15$. Significant correlation at $\alpha = .01$ is equal to $r \leq -.20$ and $r \geq .20$	82
Figure 2.6 c. Pearson's correlation (r) between disease index and September 9 waveband reflectance of the soybean variety performance test population grown at Rossville in 2016. Significant correlation at $\alpha = .05$ is equal to $r \leq -.15$ and $r \geq .15$. Significant correlation at $\alpha = .01$ is equal to $r \leq -.20$ and $r \geq .20$	83
Figure 2.7 a. Average spectral reflectance curves of SDS susceptible lines and SDS resistant lines at Manhattan 2015.....	83
Figure 2.7 b. Average spectral reflectance curves of SDS susceptible lines and SDS resistant line at Manhattan 2016.....	84
Figure 2.7 c. Average spectral reflectance curves of SDS susceptible lines and SDS resistant lines at Rossville in 2016.....	84

Figure 2.8 a. Pearson’s correlation (r) between yield and season average waveband reflectance for the nested association mapping population grown at Manhattan in 2015. Significant correlation at $\alpha = .05$ is equal to $r \leq -.15$ and $r \geq .15$. Significant correlation at $\alpha = .01$ is equal to $r \leq -.20$ and $r \geq .20$ 85

Figure 2.8 b. Pearson’s correlation (r) between yield and season average waveband reflectance for the nested association mapping population grown at Manhattan in 2016. Significant correlation at $\alpha = .05$ is equal to $r \leq -.15$ and $r \geq .15$. Significant correlation at $\alpha = .01$ is equal to $r \leq -.20$ and $r \geq .20$ 85

Figure 2.8 c. Pearson’s correlation (r) between yield and season average waveband reflectance for the nested association mapping population grown at Rossville in 2016. Significant correlation at $\alpha = .05$ is equal to $r \leq -.15$ and $r \geq .15$. Significant correlation at $\alpha = .01$ is equal to $r \leq -.20$ and $r \geq .20$ 86

Figure 2.9 a. Pearson’s correlation (r) between yield and August 8 waveband reflectance for a nested association mapping population grown at Rossville in 2016. Significant correlation at $\alpha = .05$ is equal to $r \leq -.15$ and $r \geq .15$. Significant correlation at $\alpha = .01$ is equal to $r \leq -.20$ and $r \geq .20$ 86

Figure 2.10 a. Pearson’s correlation (r) between yield and season average waveband reflectance for the soybean variety performance test population grown at Manhattan in 2015. Significant correlation at $\alpha = .05$ is equal to $r \leq -.15$ and $r \geq .15$. Significant correlation at $\alpha = .01$ is equal to $r \leq -.20$ and $r \geq .20$ 87

Figure 2.10 b. Pearson’s correlation (r) between yield and season average waveband reflectance for the soybean variety performance test population grown at Manhattan in 2016. Significant correlation at $\alpha = .05$ is equal to $r \leq -.15$ and $r \geq .15$. Significant correlation at $\alpha = .01$ is equal to $r \leq -.20$ and $r \geq .20$ 87

Figure 2.10 c. Pearson’s correlation (r) between disease index and September 9 waveband reflectance for the soybean variety performance test population grown at Rossville in 2016. Significant correlation at $\alpha = .05$ is equal to $r \leq -.15$ and $r \geq .15$. Significant correlation at $\alpha = .01$ is equal to $r \leq -.20$ and $r \geq .20$ 88

Figure 2.11 a. Pearson’s correlation (r) between maturity and season average waveband reflectance for the nested association mapping population grown at Manhattan in 2015.

Significant correlation at $\alpha = .05$ is equal to $r \leq -.15$ and $r \geq .15$. Significant correlation at $\alpha = .01$ is equal to $r \leq -.20$ and $r \geq .20$	88
Figure 2.11 b. Pearson's correlation (r) between maturity and season average waveband reflectance of the Nested association mapping population grown at Manhattan in 2016. Significant correlation at $\alpha = .05$ is equal to $r \leq -.15$ and $r \geq .15$. Significant correlation at $\alpha = .01$ is equal to $r \leq -.20$ and $r \geq .20$	89
Figure 2.11 c. Pearson's correlation (r) between maturity and season average waveband reflectance for the nested association mapping population grown at Rossville in 2016. Significant correlation at $\alpha = .05$ is equal to $r \leq -.15$ and $r \geq .15$. Significant correlation at $\alpha = .01$ is equal to $r \leq -.20$ and $r \geq .20$	89
Figure 2.12 a. Pearson's correlation (r) between maturity and August 8 waveband reflectance for the nested association mapping population grown at Rossville in 2016. Significant correlation at $\alpha = .05$ is equal to $r \leq -.15$ and $r \geq .15$. Significant correlation at $\alpha = .01$ is equal to $r \leq -.20$ and $r \geq .20$	90
Figure 2.13 a. Pearson's correlation (r) between yield and season average waveband reflectance for the soybean variety performance test population grown at Manhattan in 2015. Significant correlation at $\alpha = .05$ is equal to $r \leq -.15$ and $r \geq .15$. Significant correlation at $\alpha = .01$ is equal to $r \leq -.20$ and $r \geq .20$	90
Figure 2.13 b. Pearson's correlation (r) between yield and season average waveband reflectance for the soybean variety performance test population grown at Manhattan in 2016. Significant correlation at $\alpha = .05$ is equal to $r \leq -.15$ and $r \geq .15$. Significant correlation at $\alpha = .01$ is equal to $r \leq -.20$ and $r \geq .20$	91
Figure 2.13 c. Pearson's correlation (r) between disease index and September 9 waveband reflectance for the soybean variety performance test population grown at Rossville in 2016. Significant correlation at $\alpha = .05$ is equal to $r \leq -.15$ and $r \geq .15$. Significant correlation at $\alpha = .01$ is equal to $r \leq -.20$ and $r \geq .20$	91
Figure 2.14 a. Relationship between observed disease index score and predicted disease index score based on stepwise regression model using season average reflectance values for the NAM population at Manhattan in 2015.	92

Figure 2.15 a. Relationship between observed disease index score and predicted disease index score based on stepwise regression model using season average reflectance values and maturity as a covariate for the NAM population at Rossville2016.....	92
Figure 2.16 a. Relationship between observed disease index score and predicted disease index score based on stepwise regression model for September 2 reflectance values for the NAM population at Rossville 2016.....	93
Figure 2.17 a. Relationship between observed yield and predicted yield based on a stepwise regression model using season average reflectance values for the NAM population at Rossville 2016.....	93
Figure 2.18 a. Relationship between predicted yield and observed yield based on a stepwise regression model for the check reflectance value for the NAM population at Rossville 2016.	94
Figure 2.19 a. Relationship between observed disease index score and predicted disease index score for the check reflectance model for the NAM population at Rossville 2016....	94
Figure 2.20 a. Relationship between observed disease index score and predicted disease index score for the NAM RILs based on the NAN Check model population at Manhattan 2015.	95
Figure 2.21 a. Relationship between predicted yield and observed yield for the NAM RILs based on the NAM Check model population at Rossville 2016.	95
Figure 2.22 a. Relationship between observed disease index and predicted disease index for the NAM population at Rossville in 2016 based on the NAM Grand means model.....	96
Figure 2.23 a. Relationship between observed yield and predicted yield for the NAM population at Rossville in 2016 based on the NAM Grand means model.	96
Figure 2.24 a. Relationship between observed yield and predicted yield for the NAM population at Manhattan in 2016 based on the NAM Grand means check model.....	97
Figure 2.25 a. Relationship between observed disease index and predicted disease index for the NAM population at Rossville in 2016 based on the NAM Grand Means check model.	97

List of Tables

Table 2.1. Analysis of variance F-values for disease index, disease incidence, disease severity, yield, and maturity for a nested association mapping population.....	67
Table 2.2. Least square means and ranges for disease index, disease incidence, disease severity, yield and maturity for a nested association mapping population.....	67
Table 2.3. Soybean variety performance test entries analysis of variance F-values for disease index, disease incidence, disease severity, yield and maturity in three environments.	68
Table 2.4. Soybean Variety Performance Test Entry least square means and ranges for disease index, disease incidence, disease severity, yield and maturity.	68
Table 2.5. Pearson’s correlations (r) between entry means for disease index, yield and maturity at all three environments for both the nested association mapping population and soybean variety performance test population.....	69
Table 2.6. Coefficient of determination (R^2) values for stepwise regression models for disease index, yield and maturity based on season averages in the total population, early maturity group, middle maturity group, and late maturity group, checks, and season average model including maturity for the nested association mapping population. Coefficient of determination (R^2) values for stepwise regression models for the disease index, yield and maturity based on season averages and common entry models for soybean variety performance test population.....	70
Table 2.7. Wavebands selected by stepwise regression models to predict disease index, yield, and maturity based on reflectance values using season averages, individual days, and checks entries only for both 2015 and 2016 in Manhattan.	71
Table 2.8. Wavebands selected by stepwise regression models to predict disease index, yield, and maturity using season average, individual days, and checks for 2016 in Rossville.	72
Table 2.9. Wavebands selected by stepwise regression models to predict disease index, yield, and maturity using nested association mapping population divided into early, middle, and late maturity groups for 3 environments.....	73
Table 2.10. Wavebands selected by stepwise regression models to predict disease index, yield, and maturity soybean variety performance test population season average at 3 environments.....	74

Table 2.11. Wavebands selected by stepwise regression models to predict disease index, yield, and maturity using nested association mapping population grand means. 74

Acknowledgements

I would like to thank Dr. William Schapaugh for the opportunity to pursue my masters at Kansas State University. His support and expertise were fundamental in the success of my research. I would like to thank my committee Dr. Krishna Jagadish and Timothy Todd for their valuable input and time on this project. To the Soybean project crew Jake Peterson, Rene Hessel and Cheyenne Stephens for their help in setting up, planting, maintaining and harvesting experiments and Brent Christenson for his knowledge of spectral equipment and data processing. To the Soybean Project undergraduate workers who helped to make my research possible. Thank you to the faculty and staff of the agronomy department who allow for the smooth operation of the Department.

Finally, thank you to my parent for supporting me through my education, and unending support and encouragement in all that I have done.

Dedication

To my family and friends without their support my education would not have been possible.

Chapter 1 - Review of Literature

Introduction

Soybean (*Glycine max* (L.) Merr.) is the second largest field crop produced in the United States (US), behind corn. In 2016 approximately 34 million hectares of soybean were planted across the United States which was an increase from 2015 (USDA NASS). The United States average production was 3.5 tons per hectare⁻¹ (t ha⁻¹) bushels per acre for a total production of 117 million metric tons of grain (USDA ERS). This production made the US the largest producer of soybean in the world and accounted for 33% of the world production (USDA FAS). The US is the largest exporter of soybean to the world, exporting about 50% of total production for a cash value of approximately \$22.6 billion. The US along with Brazil and Argentina account for almost 90% of the world production and exports of soybean (USDA FAS). Soybean is primarily grown to produce oil and protein from the seed. Soybean is the second largest source of vegetable oil in the world behind palm oil. The byproduct of crushing for oil is soybean meal which is extremely high in protein and is used as a feed stock for animals.

By 2050, the world's production will need to increase at least 100% over current levels to sustainably feed the world population (Godfray et al. 2010; Phalan et al., 2011; Ray et al., 2013). Currently, a 1.3% yield increase per year is being archived by breeders for soybean (Ray et al., 2013). It is estimated that yield will need to increase as a rate of 2.4% per year to feed world population by 2050 (Ray et al., 2013). To increase the rate of gain in production we may need to focus on multiple approaches such as better management and better resistance to abiotic and biotic stresses that cause large scale yield losses (Phalan et al., 2011; Ray et al., 2013). The US, between 2006 and 2009 approximately 10.8 million metric tons of soybean were lost per year to plant disease; this is approximately 13% loss of total production (Koenning and Wrather, 2010).

The largest yield loss due to disease was caused by soybean cyst nematode (SCN), which accounted for roughly 30% of yield loss to diseases in each of these years. SCN, seedling disease, Phytophthora root rot, soybean sudden death syndrome, and Sclerotinia stem rot were the top five diseases that caused major yield loss to soybean production (Koenning and Wrather, 2010). Soybean sudden death syndrome was the fourth leading cause of yield loss, accounting for about 6% of the total yield loss during these yields (Koenning and Wrather, 2010).

Soybean Sudden Death Syndrome

Soybean sudden death syndrome was first observed in 1971 in Arkansas, but was not officially named until 1983. Sudden death syndrome in North America is caused by the soil born fungi *Fusarium virgulifrome* (Aoki et al., 2003), formally known as *Fusarium solani* f. sp. *Glycines* (Roy et al., 1989; Roy et al., 1997) Since 1971, SDS has spread across much of the US soybean producing areas (Roy et al., 1997). SDS has been observed in South American and South African soybean production, but the causative agents are *Fusarium tucucmaniae* and *Fusarium brasiliens*, respectively (Aoki et al., 2003; Tewoldemedhin et al., 2017). *F. virgulifrome* is distinguished from other fusarium that infects soybean roots by the blue spores that are produced in pure cultures (Roy et al., 1989; Roy et al., 1997; Aoki et al., 2003). The pathogen is difficult to extract and culture from diseased plants due to its slow growth (Roy et al., 1989; Roy et al., 1997; Aoki et al., 2003). *F. virgulifrome* is considered asexual and a colonial species, which is another defining feature distinguishing it from the South American pathogens (Covert et al., 2007). *F. virgulifrome* survives as chlamydospores between infections. These chlamydospores allow the fungus to survive outside host, in the soil, plant material and in soybean nematode cysts. Once conditions are favorable for the disease, the spores germinate and infect soybean roots. Once infected, the disease progresses and *F. virgulifrome* produces

macroconidia which can be spread through the soil by flowing water and tillage (Hartman et al., 2015).

F. virguliforme initially infects the roots of young soybean plants and then the fungal population increases as the growing season proceeds. The fungi can initially infect the lateral roots of the soybean plant before moving into the tap root (Ortiz-Ribbing and Eastburn, 2004). Infection causes significant loss of root length, surface area and volume (Ortiz-Ribbing and Eastburn, 2004). Root infections were shown to occur earlier on in the plant's life cycle, with older plants were shown to have decrease root severity, potentially due to increased suberin production in older roots (Gongora-Conal and Leandro, 2011). Root damage has not been shown to correlate with foliar symptoms. This is due to different environment conditions being favorable for the development of symptoms in the roots versus leaves (Wrather et al. 1995; Scherm and Yang 1996; Kandel et al. 2016). Root rot symptoms have been correlated negatively with seed yield (Lou et al., 1999). *F. virguliforme* does not colonize the soybean plant beyond the roots (Roy et al., 1997). Foliar symptoms are caused by the production of toxins in the roots that are transported via the xylem to the leaves (Brar et al., 2011; Chang et al., 2015). One in the leaves, the toxins target cellular machinery to induce cell death which leads to leaf chlorosis and necrosis (Brar et al.; 2011; Chang et al., 2015). In the presence of light, the toxins produced by *F. virguliforme* degraded the rubisco enzymes which initiates a chain reaction leading to the creation of reactive oxygen species and the eventual shutdown of the photosynthetic pathway. These changes can lead to cell death and eventually leaf necrosis (Ji et al., 2006).

Foliar symptoms in soybean affected by SDS tend to occur later in the growing season, typically at the onset of flowering (R1) (Fehr et al., 1971, Roy et al., 1997). Initial symptoms appear as small, light green or yellow chlorotic spot on leaves, with some crinkling of young

leaves. (Roy et al., 1997; Westphal et al., 2008; Hartman et al., 2015). After the onset of symptoms chlorotic spots continue to enlarge and their severity increases. Eventually the chlorotic tissue can become necrotic and spread to all the leaf tissue, except that directly around the major veins. (Roy et al., 1997). Eventually, the necrosis can cause the premature loss of the leaves, with only the petioles remaining attached to the plant. The cortex of the lower root will have a tan or brown appearance in diseased plants. The pith in the stem of infected plants will be unaffected. (Roy et al., 1997; Westphal et al., 2008; Hartman et al., 2015). The diseased plant will lack vigorous roots, as stated above, and may have blue *F. virguliforme* spores on the root at the soil surface. Symptoms tend to start in the upper most leaves and move towards the lower leaves as the disease progresses. SDS causes the abortion of pods and flowers if the disease is severe during the flowering (Roy et al., 1997). Severely infected plants are easy to pull from the soil due to their decreased root structure. If the infection is severe enough, and the plant is susceptible, SDS can cause premature death of the plant (Roy et al., 1997; Westphal et al., 2008; Hartman et al., 2015)

Foliar symptoms of SDS at the onset of disease are similar to several soybean diseases, making it at times hard to distinguish which pathogen is responsible for the disease (Westphal et al., 2008; Hartman et al., 2015). The attached petioles as well as brown cortical discoloration in the roots is the best way to identify *F. virguliforme* as the causative agent of disease (Roy et al., 1997; Westphal et al., 2008; Hartman et al., 2015).

Sudden death syndrome research is typically performed in fields with a historic record of the disease being present. But, field level research is difficult with SDS due to the highly variable distribution of the fungi in the field. Roy et al., (1989) first isolated *F. virguliforme* from the roots of infected plants collected in infested fields. To try and make more consistent evaluations of

plant response, multiple methods of field and greenhouse inoculations have been attempted (Melgar and Roy., 1994; Goa et al., 2006). Melger and Roy (1994) used a greenhouse assay to screen for SDS resistance in soybean cultivars using *F. virguliforme* isolated from infected roots and soybean cyst nematode cysts. The fungi are cultured on sterile grain sorghum or popcorn, and placed in furrow with the soybean seed to artificial inoculate the soil with *F. virguliforme* (Li et al, 2000; de Farias Neto et al., 2006). This method provided an adequate method of inoculating non-infested soil with *F. virguliforme* to evaluate genotypic response to the pathogen, with the effect lasting multiple years (de Faris Neto et al., 2006). Artificial inoculation of non-infested soil is achievable but requires additional effort and expense during planting, especially in large scale trials.

SDS Management

F. virguliforme is also highly variable in its ability to cause SDS due to environmental factors such as temperature and rainfall. This variability across environments poses a similar problem to research as the distribution of SDS in the field. High soil moisture has been shown to increase the severity and progress of SDS (Melger et al., 1994; Scherm and Yang, 1996; Roy et al., 1997; Leandro et al., 2013). Leandro et al. (2013) showed that years with SDS epidemics tended to happen in years with above average rain fall. Melgar, Roy and Abney (1994) showed that irrigation increased the severity of the foliar symptoms associated with SDS, especially if the soils were wet prior to flowering. Similar results were seen in a greenhouse experiment that showed an increase in disease symptoms with irrigation (Roy et al., 1989). Irrigation during the late vegetative and reproductive growth stages were shown to have a significant impact in the severity of SDS (de Farias Neto et al., 2006). Low soil temperatures at planting were shown to have less effect on foliar symptoms for SDS, but did increase the severity of the root symptoms

(Schrem and Yang 1994). Tillage that reduced soil compaction and improved drainage has been shown to help reduce the severity of SDS symptoms (Vick et al., 2003). Shallow tillage, less than 10cm, that only disturbed the upper soil surface was also shown to have an effect on decreasing the severity of SDS as compared to no till systems by increasing soil temperature (Wrather et al., 1995). Later planting dates have been shown to decrease the effects of SDS, but delayed planting was also shown to decrease seed yield (Hershman et al., 1990; Wrather et al., 1995). Crop rotation has been shown to reduce the *F. virguliforme* populations, but the traditional corn and soybean rotation that is common practice was shown to have no effect on reducing the symptoms of SDS (Xing and Westphal, 2009). These studies provide important insight into the management of SDS both for farmers who are trying to avoid the disease and for researchers looking to better evaluate soybean genotypes for their resistance to SDS.

Yield Loss due to SDS

Yield loss in soybean is primarily caused by severe infection during the reproductive stages of grain fill (Rupe et al., 1989). Njiti et al. (1998) saw a significant reduction in the yield components of both resistant and susceptible soybean plants when infected by *F. virguliforme*. This included a reduction of the number of flowers that were on the plant, which indicates that yield loss can occur before visible leaf symptoms appear (Njiti et al., 1998). Increased foliar severity has been shown to decrease seed size as well as total seed weight per plant (Njiti et al., 1998; Lou et al., 1999). These reductions in yield components accounted for approximately 18% yield loss of individual plants (Njiti et al., 1998), which can translate into losses of 18 -29 kg/ha (Lou et al., 2000) on moderately resistant cultivars that have been infected.

SDS and SCN Synergy

Soybean cyst nematode, *Heterodera glycines*, is the most prevalent and destructive pathogen to soybean in the US. A synergistic effect between SDS and SCN has been observed, with SCN population increasing the severity of the SDS foliar symptoms (Roy et al., 1989). *F. virgulifrome* has the ability to survive in SCN cysts for up to six months, which allows it to survive until the next growing season (Mclean and Lawrence, 1993). SDS is shown to reduce the population of cyst nematodes through increased root necrosis, but this decrease in population is not significant enough to prevent the cyst nematode from colonizing soybean roots in the future (Mclean and Lawrence 1993; Mclean and Lawrence 1995). SCN resistance has been shown to help reduce the symptoms of SDS in the field (Hershman et al., 1990; Njiti et al., 1996). This is possibly due to the relation of the resistance QTL, Rfs2, for SDS on Chromosome 18 (linkage group G) that is also located close to the Rhg1 gene that encodes for SCN resistance (Njiti et al., 1996; Meksem et al., 1999; Pruhba et al., 1999; Wen et al., 2014).

Seed Treatments for SDS

Prior to 2015, there were no commercially available seed treatments that could be used to control sudden death syndrome. In 2015, Bayer Crop Science released the ILevo® seed treatment to help control SCN and SDS. The active ingredient in ILevo® is Fluopyram. Fluopyram was shown to decrease the plant stand from 3-8% (Kendal et al., 2016ab). However, the seed treatment also was shown to decrease root rot severity, as well as reduce foliar symptoms due to *F. virgulifrome* (Kendal et al., 2016ab). Yield was also positively impacted using ILevo®, with an increase of 5-30% in yield over untreated seed (Kendal et al., 2016; Adee, 2015). Seed treatment had the largest yield benefits when used with a susceptible variety but

were most effective at preventing disease when used with resistant genotypes (Adee, 2015; Adee, 2016).

Genetic Resistance to SDS

SDS resistance is a quantitative, polygenic trait which makes it difficult to breed total resistance to the disease into new elite cultivars (Hnetkovsky et al., 1996; Njiti et al., 1996). Of the 18-30 quantitative trait loci (QTLs) reported to contribute to SDS resistance, it is thought that 8- 10 of these must be present in the genome to provide adequate resistance (Lightfoot, 2015). This level of pyramiding QTLs is extremely effective in terms of durability, but extremely challenging for breeders to consistently integrate all resistance loci into a single line. Confirmed QTLs to SDS resistance are mapped and confirmed on linkage groups C2 (Chm. 6), D2 (Chm. 17), G (Chm 18), J (Chm 16), and N (Chm 3) (Lightfoot, 2015). These associations were made using bi-parental mapping populations to track inheritance of resistance and susceptible genes. Wen et al., (2014) reporting on the first genome wide association mapping (GWAS) study for SDS resistance found seven previously discovered QTLs along with 13 new independent QTLs. Rfs2 and Rhg1 were identified on chromosome 18 (linkage group G) to consistently provide both resistances to SCN and SDS as previously stated (Meksen, 1999; Prabhu, 1999; Wen et al., 2014). The use of GWAS allowed for the dissection of multiple genetic backgrounds instead of just two as in the case of bi parental mapping populations. This and previous studies could not determine if Rfs2 and Rhg1 are independent QTLs that are linked on chromosome 18, if they are controlled by a single pleiotropic gene, or they represent a copy number variation in the Rhg1 loci (Luckew et al., 2013; Wen et al., 2014). The polygenic nature of SDS resistance makes it tough to determine the exact effects of genes, but new GWAS and mapping techniques will

allow breeders to better understand the genetic mechanisms contributing to resistance and allow breeders to create durable resistance.

High Throughput Phenotyping

In recent years the advancement in the field of genetics and genomics using next generation sequencing techniques have allowed for breeders to better understand the genetics of the plants that they are working with. These tools have given breeders new methods of selecting for desirable traits, as well as increase the number of lines that can be evaluated at a given time. New selection models, such as GWAS, allow breeders to predict how a line will preformed even before it is planted. A major challenge of using these systems is the large amount of phenotypic data that is needed to create accurate predictive models. This challenge has been called the phenotyping bottleneck (Furbank and Tester, 2011; White et al., 2012). This problem arises from the less robust growth in new techniques for assessing plants phenotypic qualities when compared to genotyping tools. These phenotypic evaluations still require visual or physical evaluation by breeders and scientists, and are usually labor intensive as well as subjective. To elevate this bottleneck, breeders have been looking to use high-throughput phenotyping through remote sensing. These techniques include the use of spectral reflectance measurements for evaluating plant heath through non-destructive, in-season measurements (Cabrera-Bosquet et al., 2012).

Spectral Reflectance

Spectral reflectance of leaves has been used by researchers to measure many different plant heath characteristics. The techniques of remote measurements are based on the principals of light reflectance and absorbance in the leaf parts (Kumar and Silva, 1973). Visible light, 400-700nm, is absorbed mainly in by the epidermis and palisade mesophyll due to the presence

chloroplast and plant pigments that use the light to drive photosynthesis (Woolley, 1971; Kumar and Silva, 1973). Near infrared is reflected 700-1300 nm, is not widely absorbed by the plant to drive photosynthesis, for this reason when it hits the spongy mesophyll in the plant leave it is reflected out of the plant. (Woolley, 1971; Kumar and Silva, 1973). Chlorophyll a, chlorophyll b, and plant pigments absorb light to drive photosynthesis (Chappelle et al., 1992; Jensen 2007). The red edge is one on the most critical portions of the plant reflectance curve. This region is where plant pigments stop absorbing light and began to reflect it (Horler et al., 1983). With these measurements of the light that is reflected by the leaves plant health, chlorophyll content, biomass, yield, abiotic stress, and disease can be estimated (Chappelle et al., 1992; Carter 1993, Penueles et al., 1993; Filella and Penueles, 1994; Penueles et al., 1997)

Estimating Chlorophyll Content

Canopy chlorophyll content which is a key indicator of plant health and photosynthetic ability has been estimated through the use of leaf spectral reflectance. Chlorophyll a, chlorophyll b, and carotenoids were best characterized in soybeans by reflectance observed at 675nm, 650nm, and 500nm wavelengths respectively in soybean (Chappelle et al., 1992). Chlorophyll a was estimated by using the simple reflectance ratio ($675\text{nm} / 700\text{nm}$), to characterize total photosynthesis ability. (Chappelle et al., 1992). The reflectance ratio explained 93% of the phenotypic variation observed in chlorophyll a content. Leaf reflectance in the near infra-red and red edge of the reflectance spectrum has explained up to 95% of the variation in chlorophyll content in maize and soybean (Gitson et al., 2005). In wheat, chlorophyll content has been used to detect nitrogen in the plant canopy and to aid in decision making for fertilizer applications (Fitzgerald et al., 2010).

Reflectance Indexes

Most applications using spectral reflectance measurements rely on ratios of reflectance values measured from different wavelengths. This was seen above in the use of the simple ratio of red reflectance divided by reflectance of the red edge or NIR was to estimate chlorophyll content (Chappell et al., 1992). One of the most used reflectance measurements is the normalized difference vegetative index (NDVI) which was developed by (Deering, 1978; Tucker et al., 1979) to estimate green biomass. They estimated biomass by using a relationship between the near infrared reflectance and the reflectance of Red light, $NDVI = (NIR - Red) / (NIR + Red)$.

Reflectance for Grain Yield

Marti et al. (2007) estimated wheat yield and biomass at the milk stage using NDVI. NDVI measurements accounted for 77% of the variation in biomass and 75% of the variation in yield. Barber et al. (2006) was able to use NDVI as a selection tool in a wheat breeding to select 20-80% of the top 20% best performing varieties in a three-year study. Royo et al. (2003) found that reflectance measurements taken at the milk stage of wheat development were the most predictive for yield. Aparicio et al. (2000) used reflectance measurements to characterize yield of durum wheat in both irrigated and dryland plots. Measurements from dryland plots explained more of the phenotypic difference in yield as compared to irrigated treatments. Bandyopadhyay et al. (2014) used water stress indexes created from reflectance measurements to estimate the effects of water stress on wheat yields and were able explain up to 87% of the phenotypic variation in yield.

Weber et al. (2012) used a partial least squares model to estimate corn yield from reflectance spectra but was only able to account for 40% of the phenotypic variation in yield, which would limit the effectiveness of the tool for selection due to the large portion of

unexplained variation. Sakamoto et al (2013) used reflectance data from satellites to estimate corn yields and accounted for approximately 75% of the yield variation at a regional level. Spectral reflectance has been used to estimate yield in other grain crops, such as in canola (Sulik and Long, 2016), as well as in salt and water stressed forage crops (Poss et al., 2006). NDVI reflectance was used to model total yield for the growing season for forage sorghum and accounting for 80% of the yield variation (Tagarakis et al., 20017).

Ma et al., (2001) were the first to use spectral reflectance measurements to quantify grain yield in soybean, using historical lines with known yield differences. An NDVI, created using 813nm for the NIR reflectance and 613nm as the red reflectance, taken at the R5 growth explained from 45% to 80% of the phenotypic variation in yield, depending on environment and year (Ma et al., 2001). They suggested that measurements be taken at R5 were the most informative and reduced the effects of soil reflectance on the measurement. Christenson et al., (2016) found similar results when examining soybean for differences in spectral reflectance as a predictor of grain yield. Their models explained 44% of the variation in yield when derived from individual waveband measurements and 58% of the yield variation when the model was based on reflectance indexes. In this study, maturity groupings were also incorporated into the models.

Reflectance for Disease

Vigier et al. (2004) used canopy spectral reflectance to evaluate soybean symptoms from the fungal disease *Sclerotinia* stem rot. In this study, they observed spectral reflectance differences primarily in the blue and red regions of the visible spectrum, as well as in the NIR and Red edge regions. Reflectance of red wavebands between 675nm and 695nm accounted for 87% of the differences in response to disease in the plants.

Nutter et al. (2002) used canopy spectral reflectance to estimate SCN populations in the soil, yield, oil and protein content of soybean. Using percent reflectance at 810nm, 48% of the initial SCN population in the soil variation was explained. This same waveband explained 90% of yield, 14% of oil and 49% of protein variation. Yield and oil content increased with an increase of percent reflectance at 810nm, whereas initial SCN population measurements and protein decreased with an increase in reflectance at 810nm. Protein is negatively correlated to yield and oil. This indicates that higher reflectance in the NIR is a positive indicator of plant health and lower stress on the plant from disease (Nutter et al., 2002). Nutter et al. (2002) in addition to ground measurements, used aerial and satellite measurements to estimate the traits, all three methods provide similar estimates. Yang et al. (2016) used satellite imagery to predict the occurrence of SDS in Iowa soybean field, with the use of NDVI measurements in June, this allowed for large scale estimation of disease area as well as to determine the risk SDS poses to a field.

Fletcher et al. (2014) looked at the relationship between charcoal root rot and reflectance in soybean. The authors observed a negative correlation between reflectance in the visible, red edge and NIR with an increase in the pathogen colonization in the plant. In this experiment, strongest correlation between disease and reflectance were observed in the NIR (960-1200nm). This characterization of disease by spectral reflectance may aid in the development of spectral indices that can be used to predict a cultivar's response to charcoal root rot early, in season before foliar systems are visible.

Bajwa et al. (2017) used leaf reflectance to characterize the severity of disease caused by SDS and SCN individually and in combination. They observed an increase in reflectance of light in the visible portion of the spectrum and a greater absorption of light in the NIR when under

disease pressure. Plants that were inoculated with SDS had high red reflectance and decreased biomass. This reduced reflectance is due to a reduction in chlorophyll content in the leaves. Spectral reflectance measurements between 500-700nm tended to correlate best with disease symptoms. Models developed from the wavebands that could classify healthy plants from diseased plants 97% of the time, while diseased plants were identified 58% of the time. Lower accuracy in diseased plants came from the inability of the model to classify slightly diseased plants from healthy plants. Reflectance measurements tended to be less informative when taken closer to planting, making early disease estimates difficult. Diseased plants were not able to be separated into SCN and SDS classes. Similar results were seen in Aslan et al. (2014).

Muhammed (2005) used hyperspectral reflectance to characterize fungal disease severity in wheat. He showed that disease severity affects absorption of light in the visible spectrum, especially in the blue and green regions. Disease also caused greater adsorption of NIR light above 750nm. Disease results in a decrease in the above ground green biomass and a reduction of the NIR light reflecting light back to the sensor. The model created from these measurements was able to estimate disease severity to 96% accuracy with corresponding field assessment. Franke and Menz (2007) used multi-spectral remote sensing to estimate powdery mildew infections in wheat plots. They found that spectral readings later in the season increased the accuracy of the predictive model when compared to ground truth data. Early models could classify plant as disease or healthy 57% of the time, whereas models from later measurements increased 89% correct classification between diseased and healthy plants (Franke and Menz, 2007). The model also classified diseased plots more accurately than healthy plots (Franke and Menz, 2007).

References

- Adee, E. 2015. Effects of seed treatment on sudden death syndrome symptoms and soybean yield. Kansas Agricultural Experiment Research Report 1(2):1-6. doi.org/10.4148/2378-5977.1006.
- Adee, E. 2016. Interaction between seed treatment and variety on sudden death syndrome symptoms and soybean yield. Kansas Agricultural Experiment Research Reports 2(5):1-5. doi.org/10.4148/23787-5977.1224.
- Aslan, H. 2015. Using remote sensing in soybean breeding: estimating soybean grain yield and soybean cyst nematode populations. (Masters Thesis) Available from K-Rex-electronic Thesis and Dissertation, and Report.
- Aoki, T., K. O'Donnell, Y. Homma, and A. Lattanzi. 2003. Sudden death syndrome of soybean is caused by two morphologically and phylogenetically distinct species within the *Fusarium solani* species complex – *F. vurguleforme* in North America and *F. tucumaniae* in South America. Mycology 95(4):660-684.
- Aparicio, N., D. Villegas, J. Casasesus, J. Araus, and C. Royo. 2000. Spectral vegetation indices as nondestructive tools for determining durum wheat yield. Agron. J. 92:83-91.
- Bajwa, S., J. Rupe, and J. Mason. 2017. Soybean disease monitoring with leaf reflectance. Remote Sensing 9 (127):1-14. doi:10.3390/rs9020127.
- Bandyopadhyay, K., S. Pranhan, R. Sahoo, R. Singh, V. Gupta. 2014. Characterization of water stress and prediction of yield of wheat using spectral indices under varied water and nitrogen management practices. Agricultural Water Management 146:115-123.
- Brar, H., S. Swaminathan, and M. Bhattacharyya. 2011. The *Fusarium viguliforme* toxin FvTox1 causes foliar sudden death syndrome-like symptoms in soybeans. MPMI 24(10):1179-1188. doi:10.1094 /MPMI -12-10-0285.
- Cabrera-Bosquet, L., J. Crossa, J. Zitzewitz, M. Serret, and J. Araus. High -throughput phenotyping and genomic selection: the frontiers of crop breeding converge. J. of Integrative Plant Bio. 54(5):312-320.
- Carter, G. 1993. Responses of leaf spectral reflectance to plant stress. American J. of Bot. 80 (3):239-243.

- Chappelle, M. Kim, and J. McMurtrey. 1992. Ratio analysis of reflectance spectra (RARS): an algorithm for the remote estimation of the concentrations of chlorophyll a, chlorophyll b, and carotenoids in soybean leaves. *Remote Sensing the Env.* 39:239-247.
- Chang, H., L. Domier, O. Radwan, C. Yendrek, M. Huddson, and G. Hartman. 2015. Identification of multiple phytotoxins produced by *Fusarium virguliforme* including a phytotoxic effector (FvNIS1) associated with sudden death syndrome foliar symptoms. *MPMI* 29(2):96-108.
- Christenson, B., W. Schapaugh, N. An, K. Prince, V. Prasad, and A. Fritz. 2016. Predicting soybean relative maturity and seed yield using canopy reflectance. *Crop Sci.* 56:625-643.
- Covert, S., K. O'Donnell, D. Starkey, A. Holiday, D. Geiser, F. Cheung, C. Town, A. Storm, J. Juba, M. Scandiani, and X. Yang. 2006. Sexual reproduction in the soybean sudden death pathogen *Fusarium tucumaniae*. *Fungal Gen. and Bio.* 44:799-807.
doi:10.1016/j.fgb.2006.12.009.
- Curran, P., J. Dungan, and D. Peterson. 2001. Estimating the foliar biochemical concentration of leaves with reflectance spectrometry. *Remote Sensing the Env.* 76:349-359.
- Curran, P., J. Dungan, and H. Gholz. 1990. Exploring the relationship between reflectance red edge and chlorophyll content in slash pine. *Tree Physiology.* 7:3-48.
- Deering, D., 1978. Rangeland reflectance characteristics measured by aircraft and spacecraft sensors. Ph.D. diss., Texas A&M University, College Station.
- de Farias Neto, A., G. Hartman, W. Pedersen, S. Li., G. Bollero, and B. Diers. 2006. Irrigation and inoculation treatments that increase the severity of soybean sudden death syndrome in the field. *Crop Sci.* 46:2547-2554.
- Fehr, W., C. Caviness, D. Burmond, and J. Pennington. 1971. Stages of development descriptions for soybeans, *Glycine max* (L.) Merr. *Crop Sci.* 11:929-931.
- Fletcher, R., J. Smith, A. Mengistu, J. Ray. 2014. Relationships between Microsclerotia content and hyperspectral reflectance data in soybean tissue infected by *Macrophomina phaseolina*. *American J. of Plant Sci.* 5:3737-3744.
- Filella, I., and J. Penuelas. 1994. The red edge position and shape as indicators of plant chlorophyll content, biomass and hydric status. *Int. J. of Remote Sensing.* 15 (7):1459-1470.

- Fitzgerald, G., D. Rodrigues, and G. O'Leary. 2010. Measuring and predicting canopy nitrogen nutrition in wheat using spectral index- The canopy chlorophyll content index (CCCI). *Field Crop Research* 116:318-324.
- Franke, J., and G. Menz. 2007. Multi-temporal wheat disease detection by multi-spectral remote sensing. *Precision Agric.* 5:161-172.
- Furbank, R., and M. Tester. 2011. Phonemics- technologies to relieve the phenotyping bottleneck. *Trends in Plant Sci.* Vol. 16. No.12: 635-644.
doi:10.1016/j.tplants.2011.09.005.
- Gao, X., T. Jackson, G. Hartman, and T. Niblack. 2006. Interaction between the soybean cyst nematode and *Fusarium solani* f. sp. *Glycines* based on greenhouse factorial experiments. *Phytopathology.* 96:1409-1415.
- Gitelson, A., A. Vina, V. Ciganda, D. Rundquist, and T. Arkebauer. 2005. Remote estimation canopy chlorophyll content in crops. *Geophysical Research Letters* 32:L08403.
doi:10.1029/2005GL022688.
- Godfray, H. J. Beddington, I. Crute, L. Haddad, and D. Lawrence, J. Muir, J. Pretty, S. Robinson, S. Thomas, C. Thoulmin. 2010. Food security: the challenge of feeding 9 billion people. *Sci* 327:812-818.
- Gongora- Canul, C., F. Leandro. 2011. Plant age affects root infection and development of foliar symptoms of soybean sudden death syndrome. *Plant Dis.* 95(3):242-247.
- Hartman, G., H. Chang, and L. Leandro. 2015. Research advances and management of soybean sudden death syndrome. *Crop Pro.* 73:60-65.
- Hartman, G., G. Noel, and L. Gray. 1995. Occurrence of soybean sudden death syndrome in East- Central Illinois and associated yield losses. *Plant Dis.* 79:314-318.
- Hatfield J., A. Gitelson, J. Schepers, and C. Walthall. 2008. Application of remote sensing for agronomic decisions. *Agron. J.* 100:S117-S131. doi:10.2134/agronj2006.0370c.
- Hershman, D., J. Hendrix, R. Stuckey, P. Bachi, and G. Henson. 1990. Influence of planting date and cultivar on soybean sudden death syndrome in Kentucky. *Plant Dis.* 74:761-766.
- Hnetkovsky, H., S. Chang, T. Doubler, P. Gibson, and D. Lightfoot. 1996. Genetic mapping of loci underlying field resistance to soybean sudden death syndrome (SDS). *Crop Sci.* 36:394-400.

- Horler, D., M. Dockray, and J. Barber. 1983. The red edge of plant leaf reflectance. *Int. J. of Remote Sensing*. 4(2):273-288.
- Ji, J., M. Scott, and M. Bhattacharyya. 2006. Light is essential for degradation of ribulose- 1,5 bisphosphate carboxylase- oxygenase large subunit during sudden death syndrome development in soybean. *Plant Bio*. 8:597-505.
- Kandel, Y., K. Wise, C. Bradley, A. Tenuta, and D. Mueller. 2016. Effect of planting date, seed treatment, and cultivar on plant population, sudden death syndrome, and yield of soybean. *Plant Dis*. 100:1735-1743.
- Kandel, Y., K. Wise, C. Bradley, A. Tenuta, and D. Mueller. 2016. Fungicide and cultivar effects on sudden death syndrome and yield of soybean. *Plant Dis*. 100:1339-1350.
- Koenning, S., and J. Wrather. 2010. Suppression of soybean yield potential in the Continental United States by plant disease from 2006-2009. Online. *Plant Health Progress* doi:10.1094/PHP-010-1122-01-RS.
- Kummar, R., and L. Silva. 1973. Light ray tracing through leaf cross section. *Applied Optics*. 12(12):2950-2954.
- Leandro, L., A. Robertson, D. Mueller, and X. Yang. 2013. Climatic and environmental trends observed during epidemic and non-epidemic years of soybean sudden death syndrome in Iowa. Online. *Plant Health Progress* doi:10.1094/PHP-2013-0529-01-RS.
- Li, S., Y. Tam, and G. Hartman. 2000. Molecular differentiation of *Fusarium solani* f. sp. *glycines* other *F. solani* based on mitochondrial small subunit rDNA sequences. *Phytopathology* 90(5):491-497
- Lightfoot, D. 2015. Two decades of molecular marker-assisted breeding for resistance to soybean sudden death syndrome. *Crop Sci*. 56:1460-1484.
- Lou, Y., O. Meyer, D. Lightfoot, and M. Schmidt. 1999. Root colonization of soybean cultivars in the field by *Fusarium solani* f. sp. *glycines*. *Plant Dis*. 83(12):1155-1159.
- Lou, Y., K. Hildebrand, S. Chong, O. Myers, and J. Russin. 2000. Soybean yield loss to sudden death syndrome in relationship to symptom expression and root colonization by *Fusarium solani* f. sp. *glycines*. *Plant Dis*. 84:914-920.
- Luckew, A., L. Leandro, M. Bhattacharyya, D. Nordman, D. Lightfoot, and S. Cianzio. 2013. Usefulness of 10 genomic regions in soybean associated with sudden death resistance. *Theory of Applied Genetics* 126:2391-2403.

- Ma, B., L. Dwyer, C. Costa, E. Cober, and M. Morrison. 2001. Early prediction of soybean yield from canopy reflectance measurements. *Agron. J.* 93:1227-1234.
- Marti, J., J. Bort, G. Slafer, and J. Araus. 2007. Can wheat yield be estimated by early measurements of normalized difference vegetation index? *Annals of Applied Biology* 150:253-257.
- McLean, K., and G. Lawrence. 1993. Interrelationship of *Heterodera glycines* and *Fusarium solani* in sudden death syndrome of soybean. *J. of Nematology* 25(3): 434-439.
- McLean, K., and G. Lawrence. 1995. Development of *Heterodera glycines* as affected by *Fusarium solani*, the causal agent of sudden death syndrome of soybean. *J. of Nematology* 27(1)70-77.
- Melgar, J., and K. Roy. 1994. Soybean sudden death syndrome: cultivar reactions to inoculation in a controlled environment and host range and virulence of causal agent. *Plant Dis.* 78: 265-268.
- Melger, J., K. Roy, and T. Abney. 1994. Sudden death syndrome of soybean: etiology, symptomatology, and effects of irrigation and *Heterodera glycines* on incidence and severity under field conditions. *Canadian J. of Bot.* 72:1647-1653.
- Meksem, K., T. Doubler, K. Chanchaoenchai, V. Njiti, S. Chang, A. Roa Arelli, P. Cregan, L. Gray, P. Gibson, and D. Lightfoot. 1999. Clustering among loci underlying soybean resistance to *Fusarium solani*, SDS and SCN in near-isogenic lines. *Theor. Appl. Genet.* 99:1131-1142.
- Montes J., A. Melchinger, and J. Reif. 2007. Novel throughput phenotyping platforms in plant genetic studies. *Trends in Plant Sci.* Vol12. No.10:433-436.
- Muhammed, H. 2005. Hyperspectral crop reflectance data for characterizing and estimating fungal disease severity in wheat. *Biosystems Engineering* 91(1):9-20.
doi:10.1016/j.biosystemseng.2005.02.007
- Njiti, V., A Sheanaut, R. Sutter, M. Schmidt, and P. Gibson. 1996. Soybean response to sudden death syndrome: inheritance influenced by cyst nematode resistance in Pyramid x Douglas progenies. *Crop Sci.* 36:1165-1170.
- Njiti, V., T. Doubler, R. Sutter, L. Gray, P. Gibson, and D. Lightfoot. 1998. Resistance to soybean death syndrome and root colonization by *Fusarium solani* f. sp. *Glycine* in near-isogenic lines. *Crop Sci.* 38:472-477.

- Nutter, F., G. Tylka, J. Guan, A. Moreira, C. Maret, T. Rosburg, J. Basart, and C. Chong. 2002. Use of remote sensing to detect soybean cyst nematode-induced plant stress. *J. of Nematology* 34(3):222-231.
- Ortiz- Ribbing, L., and D. Eastburn. 2004. Soybean root systems and sudden death syndrome severity: taproot and lateral root infection. *Plant Dis.* 88:1011-1016.
- Penuelas, J., I. Filella, C. Biel, L. Serrano, and R. Save. 1993. The reflectance at the 950-970 nm regions as an indicator of plant water status. *Int. J. of Remote Sensing* 14(10):1887-1905.
- Penuelas, J., R. Isla, I. Filella, and J. Araus. 1996. Visible and near infrared reflectance assessment of salinity effects barley. *Crop Sci.* 37:198-202.
- Penuelas, J., and I. Filella. 1998. Visible and near-infrared reflectance techniques for diagnosing plant physiological status. *Sci.* 3(4):151-155.
- Phalan, B., M. Onial, A. Balmford, and R. Green. 2011. Reconciling food production and biodiversity conservation: land sharing and land sparing compared. *Sci.* 333:1289-1291.
- Prasad, A., L. Chai, R. Singh, and M. Kafatos. 2006. Crop yield estimation model for Iowa using remote sensing and surface parameters. *Int. J. of Applied Earth Obs. and Geoinformation* 8: 26-33. doi:10.1016/j.jag.2005.06.002.
- Prabhu, R., V. Njiti, B. Bell-Johnson, J. Johnson, M. Schmidt, J. Klien, and D. Lightfoot. 1999. Selecting soybean cultivars for dual resistance to soybean cyst nematode and sudden death syndrome using two DNA markers. *Crop Sci.* 39:982-987.
- Printer Jr., P., J. Hatfield, J. Shepers, E. Barnes, and M. Moran. 2003. Remote sensing for crop management. *Photogrammetric Engineering and Remote Sensing* 69(6):647-664.
- Ray, D., N. Muller, P. West, and J. Foley. 2013. Yield trends are insufficient to double global crop production by 2050. *PLoS ONE* 8(6):e66428.
- Roy, K., J. Rupe, D. Hershman, and T. Abney. 1997. Sudden death syndrome of soybean. *Plant Dis.* 81(10):1000-1111.
- Roy, K., G. Lawrence, and K. Mclean. 1989. Isolation and identification of *Fusarium solani*, the cause of sudden death syndrome of soybean. *Plant Diagnostic Quarterly* 10: 17-27.
- Royo, C., F. Alvaro, V. Martos, A. Ramdani, J. Isidro, D. Villegas, and L. Garcia del Moral. 2007. Genetic changes in durum wheat yield components and associated traits in Italian and Spanish varieties during the 20th Century. *Euphytica* 155:259-270. doi 10.1007/s10681-006-9327-9.

- Rupe, C. 1989. Frequency and pathogenicity of *Fusarium solani* recovered from soybeans with sudden death syndrome. *Plant Dis.* 73:581-584.
- Sakamoto, T., A. Gitelson, and T. Arkebauer. 2013. MODIS-based corn grain yield estimation model incorporating crop phenology information. *Remote Sensing of Env.* 131: 215-231.
- Scherm, H., and X. Yang. 1996. Development of sudden death syndrome of soybean in relation to soil temperature and soil water matric potential. *Phytopathology* 86(6): 642-649.
- Sulik, J., and D. Long. 2016. Spectral considerations for modeling yield in canola. *Remote Sensing the Env.* 184: 161-174. [.doi.org/10.1016/j.rse.2016.06.016](https://doi.org/10.1016/j.rse.2016.06.016).
- Tagarakis, A. Q. Keterings, S. Lyons, and G. Godwin. 2017. Proximal sensing to estimate yield of brown midrib forage sorghum. *Agron. J.* 109:107-114.
[doi:10.2134/agronj2016.07.0414](https://doi.org/10.2134/agronj2016.07.0414).
- Tewoldemedhin, Y., S. Lamprecht, M. Vaughan, and G. O'Donnell. 2017. Soybean SDS in South Africa caused by *Fusarium brailiense* and a novel undescribed *Fusarium sp.* *Plant Dis.* 101:150-157.
- Tucker, C., J. Elgin, and J. McMurtrey. 1978. Monitoring corn and soybean crop development by remote sensing techniques. NASA Technical Memorandum 79607.
- USDA Economic Research Service. 2017. Oil Crops Data. <http://www.ers.usda.gov/data-products/oil-crops-yearbook.aspx>.
- USDA FAS. 2017. Oilseeds: World Markets and Trade.
<https://apps.fas.usda.gov/psdonline/app/index.html#/app/downloads>.
- USDA FAS. 2017. World Agricultural Production.
- USDA NASS. 2016. Acreage Report. ISSN 1949-1522.
- Vick, C., S. Chong, J. Bond, and J. Russin. 2003. Response of soybean sudden death syndrome to subsoil tillage. *Plant Dis.* 87:629-632.
- Vigier, B., E. Pattey, and I. Strachan. 2004. Narrowband vegetation indexes and detection of disease damage in soybeans. *GeoSci and Remote Sensing Letter.* 1(4):255-259.
- Weber, V., J. Araus, J. Cairns, C. Sanchez, A. Melchinger, and E. Orsini. 2012. Prediction of grain yield using reflectance spectra of canopy and leaves in maize plants grown under different water regimes. *Field Crop Research* 128:82-90.
- Westphal, A., T. Abney, L. Xing, G. Shaner. 2008. Sudden death syndrome of soybean. *The Plant Health Instructor* [doi:10.1094/PHI-I-2008-0102-01](https://doi.org/10.1094/PHI-I-2008-0102-01).

- White, J. P. Andrade-Sanchez, M. Gore, K. Bronson, T. Coffelt, M. Conley, K. Feldmann, A. French, J. Heun, D. Hunsaker, G. Wall, and G. Wang. 2012. Field based phonemics for plant genetic research. *Field Crop Research* 133:101-112.
- Woolley, J. 1971. Reflectance and transmittance of light by leaves. *Plant Phy.* 47: 656-662.
- Wen, Z., R. Tan, J. Yuan, C. Bales, W. Du, S. Zhang, M. Chilvers, C. Schmidt, Q. Song, P. Cregan, and D. Wang. 2014. Genome-wide association mapping of quantitative resistance to sudden death syndrome in soybean. *BMC Genomics* 15:809.
- Wrather, J., S. Kending, S. Anand, T. Niblack, and G. Smith. 1995. Effects of tillage, cultivar, and planting date on percentage of soybean leaves with symptoms of sudden death syndrome. *Plant Dis.* 79: 560-562.
- Xing, L., A. Westphal. 2006. Interaction of *Fusarium solani* f. sp. *Glycines* and *Heterodera glycines* in sudden death syndrome of soybean. *Phytopathology* 93: 763-770.
- Yang, S., X. Li, C. Chen, P. Kyveryga, X. Yang. 2016. Assessing field-specific risk of soybean sudden death syndrome using satellite imagery in Iowa. *Phytopathology* 106(8): 842-853. <http://dx.doi.org/10.1094/PHYTO-11-15-0303-R>

Chapter 2 - Evaluating Genotypes for Soybean Sudden Death Resistance and Grain Yield using Spectral Reflectance

Introduction

Soybean (*Glycine Max* (L.) Merr.) is one of the most important crops in the world. It is the second most cultivated crop in the United States (US) occupying about 30% of the planted acres (USDA ERS). The US produced 107 million metric tons or 33% of the world production in 2015 (USDA FRS). With predicted growth in the human population, production will need to increase at least 100% by the year 2050 to adequately feed the world (Ray et al., 2013). To accomplish this task there will need to be a major increase in the land area used for agriculture production, or an increase in the efficiency of current agronomic lands (Godfray et al., 2010; Phalan et al., 2011; Tscharntke et al., 2013; Ray et al., 2013). To contribute improvements in efficiency, breeders will have to roughly double the genetic gain that is currently achieved. For soybean, this would mean an increase from 1.3% increase in yield per year to 2.4% (Ray et al., 2013). A yield increase can also be accomplished by decreasing the losses caused by disease. Between 2006 and 2009, yield loss due to diseases ranged from 296 million bushels in 2007 to 484 million bushels in 2009 (Koenning and Wrather, 2010). These losses equate to roughly 10 to 15% of total production. The fourth most destructive soybean disease in the US during this time was soybean sudden death syndrome (SDS), which was responsible for the loss of 20-34 million bushels of yield between 2006 and 2009 (Koenning and Wrather, 2010).

Soybean Sudden Death Syndrome

Soybean sudden death (SDS) is the term for the foliar disease that is caused by the soybean fungal pathogen *Fusarium virguliforme* (Roy et al., 1997; Aioki et al., 2003). SDS was first observed in Arkansas in 1971 and spread north into most soybean producing states (Roy et

al., 1997; Westphal et al, 2008; Hartman et al., 2015). The disease tends to cause the most losses in the central US soybean production area (Koenning and Wrather, 2010). SDS has been observed in both South America and South African soybean production areas, but the causative agent is *Fusarium tucumaniae* and *Fusarium brasiliense*, respectively (Aoki et al., 2003; Tewoldemedhin et al., 2017). *F. virguleforme* is an asexual reproducing colonial soil borne fungi with low genetic diversity. Its asexual reproduction separates the North American pathogen from its South American relative (Covert et al., 2006). The fungus produces distinct blue colonies when pure cultures are obtained and purified in the lab (Roy et al., 1989; Roy et al., 1997; Aoki et al., 2003). The fungus survives in the soil in chlamydospores until favorable conditions are present for it to invade soybean roots and cause sudden death syndrome disease symptoms (Westphal et al. 2008; Hartman et al., 2015)

F. virguleforme begins by invading the roots of the young soybean plants shortly after emergence. Upon initial infection, there are no visible aboveground symptoms. Root symptoms include a decrease in root surface area, length, and volume (Ortiz-Ribbing and Eastburn, 2004). Younger roots are more susceptible to infection than older roots. This is thought to be due to increased suberin production in older roots (Conal and Leandro, 2011). Root colonization has been negatively correlated to seed yield in soybean plants (Lou et al., 2000). Infected roots can be identified from other root diseases due to the brown or rust discoloration of the root cortex as well as the potential blue colony formation on the root at or just below the soil surface (Brar et al., 2011; Chang et al., 2015). *F. virguleforme* does not move out the soybean roots and cause foliar symptoms (Roy et al., 1997). The aboveground foliar symptoms observed with SDS are the result of multiple toxins produced by the fungi in the roots that are transported to the leaves via the xylem (Brar et al., 2011; Chang et al., 2015). These toxins trigger programmed cell death,

which normally is used to protect plants from pathogens (Brar et al., 2011). Toxins from SDS are dependent on light to cause necrosis in plant leaves. It is speculated that this is caused by the toxin producing reactive oxygen species that lead to the disruption of photosynthesis (Ji et al., 2006).

Once toxins are transported to the leaves, foliar symptoms begin to appear. Initial symptoms appear as small pale green or yellow spots of chlorosis. These spots increase in size and eventually turn necrotic as symptoms progress. The chlorosis can continue to increase in size until all the leaf tissue is necrotic, with the exception of the tissue close to major veins. At this point, if the disease continues to progress the leaves will prematurely drop from the plant leaving only the petiole attached to the stem. Initial foliar symptoms are similar to other biotic and abiotic stresses, such as Charcoal Root Rot and drought stress, which makes initial identification of SDS difficult. Diseased plants observed to have interveinal necrosis, leaf loss with attached petioles, and brown or rust colored cortex tissue in the roots are all positive indicators of SDS (Rupe et al., 1989; Roy et al., 1997; Hartman et al., 2015). Foliar symptoms are not always indicative of grain yield losses due to the relationship between disease symptoms and plant development (Njiti et al., 1998; Ortiz-Ribbing and Eastburn, 2004).

Disease management options are limited and only partially control disease losses. Planting date can affect the onset and severity of the disease, with earlier planting dates tending to lead to higher disease severity (Hershman et al., 1990; Wrather et al., 1995). Delayed planting does help reduce the risk of SDS, but delaying planting also reduces yield regardless of SDS (Kandel et al., 2016). Lower soil temperatures at planting also have been shown to increase the severity of the disease, as well as decrease plant heath in general (Schrem and Yang, 1996). Different field tillage practices have been shown to reduce the severity of SDS. Shallow, or strip-

till practices, which tend to warm the soil temperatures, have been shown to decrease SDS severity (Wrather et al., 1995). Also, improving soil drainage has been shown to decrease disease severity (Vick et al., 2003). Soil compaction when reduced with tillage was not shown to decrease SDS, but did have a positive impact on seed yield (de Farias Neto et al., 2006). Soil moisture, from rainfall or irrigation, might be the single largest environmental driver of disease severity of SDS. Rainfall during planting as well as high soil moisture, from rainfall or irrigation, during the late reproductive (R4) phase of soybean growth greatly contributes to disease severity (de Faris Neto et al., 2006).

In 2015, Bayer Crop Science released ILevo® seed treatment to help control soybean cyst nematode and SDS. Fluopyram, the active ingredient in ILevo®, decreases the plant stand from 3-8%, but was shown to decrease root rot severity, as well as reduce foliar symptoms (Kendal et al., 2016). Yield was also positively impacted with an increase of 5-30% in yield over untreated seed (Adee, 2015; Kendal et al., 2016). Yield benefits are greater when used with susceptible varieties, but when used with SDS resistant varieties disease symptoms are almost entirely eliminated (Adee, 2015; Adee, 2016).

Genetic Resistance to SDS

SDS resistance is controlled by many genes (Hnetkovsky et al., 1996; Njiti et al., 1996). Lightfoot (2015) found eight quantitative trait loci (QTLs) on five chromosomes reported in literature. These QTLs were discovered in biparental mapping population studies. The first Genome Wide Association Mapping study (GWAS) for SDS resistance was performed by Wen et al. (2014) identified seven of the previously discovered QTLs along with 13 additional QTLs. Durable resistance is thought to require 8 - 10 QTLs in the genome to provide adequate resistance (Lightfoot, 2015.) The need for the large number of QTLs to provide resistance

increases the difficulty of integrating resistance into a cultivar, but if achieved, resistance should remain durable due to clonal nature of the pathogen and the large pyramid of QTLs used to provide resistance. The Rfs2 gene, located on linkage group G, chromosome 18, is the only cloned resistant quantitative trait locus (QTL) (Chang et al., 1996; Meksem et al., 1999; Prabhu et al., 1999; Wen et al., 2014). This QTL is possibly the same as, or closely linked to the Rhg1 gene which provides resistance to SCN (Meksem et al., 1999; Prabhu et al., 1999; Wen et al., 2014). It is unknown if resistance to SCN and SDS provided from this region of chromosome 18 is controlled by two different genes, controlled by a single pleiotropic gene, or due to the copy number of a gene providing resistance to both pathogens. (Luckew et al., 2013; Wen et al., 2014).

Phenotyping with Spectral Reflectance

In last 20 years there has been substantial increases made in the understanding of plant genetics and the ability to use new techniques to increase the genetic gain achieved through plant breeding (Furber and Tester, 2011; White et al., 2012). These new techniques and methods have led to the use of genomic selection, where the genetic makeup of the plant is used to predict the performance of new genotypes. While genomic selection has increased the genetic gain achieved by breeders, development of these genomic models require large amounts of phenotypic data (Furber and Tester, 2011; White et al., 2012; Cabrera-Bosquet et al., 2012; Araus and Cairns, 2014). Collection of phenotypic data is still primarily obtained through visual or physical evaluations (Furber and Tester, 2011; White et al., 2012). In the case of disease ratings, visual evaluations of symptoms are often used. These ratings tend to rely on observations by skilled personnel and can be inconsistent between raters and across environments. These phenotypic evaluations can be time consuming and expensive to collect, which can lead to a

bottleneck in the ability to phenotype new genetic material. To alleviate this bottleneck, breeders and researchers have begun to use remote sensing as a noninvasive way to screen germplasm (Cabrerria-Basquet et al., 2012).

Spectral reflectance is a remote sensing method that uses the reflectance of light from the plant to predict the health and performance of the plant (Printer et al., 2003). Remote sensing relies on the principal that different portions of the light spectrum are absorbed and reflected by different components of the leaf (Kummar and Silva, 1973). Chlorophyll primarily absorbs light in the visible portion of the spectrum to drive photosynthesis, with greater absorption in the blue- (400-500nm) and red (600-700nm) portions of the spectrum, versus the green region (500-600nm). Around the red edge (700- 750nm) region there is a sharp increase in the reflectance since it does not provide energy to drive photosynthesis (Horler et al., 1983). Light in the near infra-red (NIR) (above 750nm) region does not drive cellular function, but has been shown to be related to plant water content (Penuelas et al., 1993). Cellular structure in the plant leaf also affects the path of light as it travels through the palisade mesophyll cells where most photosynthesis occurs. When the light reaches the spongy mesophyll, the remaining photosynthetic active light is absorbed and the NIR is scattered and reflected due to the air the leaves (Kummar and Silva, 1973). Changes in plant health effect the way that light travels through these cells and thus can be used as an indicator of disease or stress (Adams et al., 1999).

Reflectance in the visible parts of the spectrum tends to correlate to the chlorophyll concentration in the leaves (Gitelson and Merzlyak, 1996). Gitelson et al. (2005) used spectral reflectance to estimate 92% and 98% of the variation in chlorophyll content in the leaves of soybean and corn plants respectively. The authors showed that a model using reflectance in the NIR divided by reflectance of the red edge minus 1, $(R_{NIR}/R_{red-edge})-1$, provided the most accurate

estimation of chlorophyll in both corn and soybean. The effects of canopy architecture were shown to influence the estimation of chlorophyll due to greater absorption in the soybean leaves in the visible spectrum (400-700 nm), causing higher estimation of chlorophyll content than in corn (Gitelson et al., 2005). Daughtry et al. (2000) demonstrated that nitrogen was associated with leaf chlorophyll contents, and chlorophyll content could be estimated using spectral reflectance. The authors observed an interaction between reflectance and leaf area, and this interaction accounted for a large amount of the variation that was observed between chlorophyll content and spectral reflectance. Chappelle et al., (1992) characterized individual wavelengths to estimate the reflectance of plant pigments in soybean leaves. The authors identified reflectance at 675nm, 650nm, and 500nm as absorption bands for chlorophyll a, b and carotenoids, respectively (Chappell et al., 1992). A relationship between chlorophyll a content in soybean leaves with the rate of photosynthesis was observed, with the ability to accurately estimate 93% of the variation in chlorophyll a content with a simple reflectance ratio (SR) of 675nm / 700nm (Chappell et al., 1992.) Gitelson and Merzlyak (1996) used green wavelength reflectance to replace the red wavelength reflectance to estimate chlorophyll content creating the Green normalized vegetative index ($GNDVI = (R_{NIR} - R_{green}) / (R_{NIR} + R_{green})$) which they demonstrated was more sensitive to a wider range of chlorophyll content than the normal NDVI = $(R_{NIR} - R_{red}) / (R_{NIR} + R_{red})$. The Normalized Differences Vegetative Index (NDVI), which is calculated by the formula $(NIR - Red) / (NIR + Red)$ as described by Deering et al. (1977) and Tucker (1978) to estimate above ground biomass. NDVI is one of the most commonly used indices to predict plant health and yield in many agricultural crops (Ma et al., 2001; Prasad et al., 2006; Marti et al., 2007).

Chlorophyll content has been shown to be a secondary measurement for yield (Buttery and Buzzel, 1973; Shimada et al., 1995), thus allowing spectral reflectance to be used to estimate yield. It has been used in corn, wheat, soybean, milo, and canola (Ma et al., 2002; Royo et al., 2003; Marti et al., 2007; Weber et al. 2012; Christenson et al., 2016; Sulik and Long, 2016; Tagarakis et al., 2017). Weber et al. (2012) used canopy reflectance and partial least square regression to estimate roughly 40% of the variation in grain yield in corn. This estimation technique would be useful as an early screening tool, but with so much phenotypic variation was left unexplained further evaluation of lines would need to be taken. Multiple studies have used spectral reflectance in the evaluation of wheat yield under both irrigated and dryland conditions. Aparicio et al. (2000) used a simple ratio $SR = (R_{NIR}/R_{red})$, NDVI, and photochemical reflectance index (PRI) to estimate grain yield. SR accounted for 52% and NDVI 59% of the yield variation under dryland conditions. Royo et al. (2003) used multiple reflectance wavebands and indices, such as the 550nm, 680nm, water index (WI), as well as the NDVI and SR to predict grain yield in wheat. Reflectance at 680 nm explained 24% to 47% of yield phenotypic variation, while water index accounted for 17% to 32% of the variation in yield. The SR was more useful in predicting yield accounting for 19% to 35% of the yield variation. Both NDVI and SR failed to predict grain yield accurately in environments with decreased biomass (Royo et al., 2003). In this experiment environment played a major factor in any of the indices predictive ability (Royo et al., 2003). Barber et al., (2006) used NDVI to select up to 80% of the 20% highest yielding varieties in recombinant inbred lines (RILs) under irrigation. This study, as in the case of Weber et al. (2012) showed that yield estimation maybe useful for estimation of yield early in testing. Reflective measurements taken at early grain fill and milk stage in wheat

where most informative at estimating yield than those taken closer to maturity (Aparicio et al., 2000; Royo et al 2003; Barber et al., 2006; Marti et al., 2007)

Ma et al. (2000) first used spectral reflectance to characterize grain yield in soybean. The authors identified the R5 growth stages as the most informative time to take measurements in soybean. NDVI measurements taken at R5 accounted for up to 80% of the variation in yield between the 42 varieties (Ma et al., 2000). In this experiment environment effected predictive ability, with lower yielding fields creating better fitting models (Ma et al., 2000). Christenson et al. (2016) used reflectance to account for 44% of the yield variability of observed cultivars waveband reflectance, and using a model containing multiple vegetative indices accounted for 58% of the variation in yield among cultivars. In this experiment, maturity of the genotypes was estimated, and entries divided in to early, middle, and late maturing groups. When divided into maturity groups, the predictive ability of the models increased to account for 55%, and 48% of the variability in for the early and middle maturity groups respectively. Predictive ability declined, explaining only 18% of the variability in yield for the late maturing group (Christenson et al., 2016). The decrease in predictive ability of the late maturity group may be due to not continuing scans all the way through the growing season of late entries (Christenson et al., 2016)

Spectral reflectance has been used to identify diseases symptoms in crops. Muhammed (2005) used reflectance to estimate fungal disease severity of wheat accounting for 95% of the variation between disease estimates and observed ratings. Franke and Menz (2007) used reflectance to quantify powdery mildew in wheat. Measurements could identify 95% of infected plants and 78% of healthy plants that were measured. Spectral reflectance readings were more informative as disease symptoms increased. Vigier et al. (2004) used spectral reflectance to estimate Sclerotinia stem rot in soybean. Using narrow band reflectance between 675-695 nm

explained 87 % of the phenotypic differences in disease. Nutter et al. (2002) used spectral reflectance to estimate the initial infection of soybean with SCN, yield, protein, and oil. Using reflectance at 810nm they could account or 48% of initial SCN population in the soil, which was shown to negatively influence the yield. Bajwa et al. (2017) used spectral reflectance to characterize SDS and SCN severity in combination in soybean. The authors used models with individual wavelengths and spectral indices to estimate disease severity. Reflectance models identify 94% of healthy plants, but were less successful at predicting diseased plants or distinguishing between SDS and SCN. This study as, with previous studies, found that later readings taken after the onset of disease symptoms were more informative at predicting disease. Fletch et al. (2014) examined charcoal root rot in soybean relationship with spectral reflectance. The authors found overall decrease in reflectance with increased disease pressure across all wavebands, with reflectance in the NIR most correlated to pathogen content in the plant (Fletch et al. 2014)

With the difficulties associated with developing new cultivars possessing high yield and resistance to SDS resistance, large populations and extensive phenotypic evaluation is required to identify new genotypes. Spectral reflectance has been shown to help quantify resistance in the field to disease, but these experiments tended to have a limited number of genotypes involved. The objective of this study was to determine if spectral reflectance measurements could be used to evaluate SDS resistance and yield in a breeding program.

Material and Methods

This study was conducted at three environments across two years, during the 2015 and 2016 growing seasons. All three environments were chosen due to having historical SDS outbreaks. In 2015, plots were located at the Kansas State University Research Farm at Manhattan, KS (39° 08' 31" N, 96° 37' 46" W, 315m of elevation) on a Eudora silt loam soil (Coarse-silty, mixed, superactive, mesic Fluventic Hapludolls). In 2016, plots were located near Rossville, KS (39° 07' 08" N, 95° 55' 29" W, 281m of elevation) on a Eudora silt loam soil (Coarse-silty, mixed, superactive, mesic Fluventic Hapludolls) and at Manhattan, KS (39°08' 34" N, 96°37' 43" W, 315m of elevation) on Belvue silt loam soil (Coarse-silty, mixed, superactive, nonacid, mesic Typic Udifluvents).

Genotypes evaluated included 140 F5 derived RILs from a cross between LD00-3009 and IA 3023 from the SOY NAM population (Diers, 2012). This NAM population was selected due to the resistance of LD00-3309 and the susceptibility of IA3023 to SDS. With the addition of checks for yield and SDS resistance, the population evaluated totaled 160 genotypes. SDS resistant checks selected from maturity groups three, four, and five were LD06-7862, Ripley and LS09-1920, respectively. SDS susceptible checks from maturity groups three, four, and five and were Morgan, Spencer and V82-2191, respectively. V82- 2191 was only included in 2015 experiments, due to its late maturity it was removed from the 2016 test to aid in harvest. A second population totaling 140 entries, consisting of commercial cultivars and the previously stated SDS checks were evaluated as part of the Kansas State University Variety Performance test (SVPT). SVPT entries differed between years; with 24 cultivars evaluated in both 2015 and 2016. The experimental units were 2-row plots (3.4 m long with rows spaced 76 cm apart). The experimental design was a randomized complete block with four replications of the NAM

population and three replications for the SVPT population. In 2015, plots were planted on May 13 at Manhattan. In 2016, plots were planted on May 12 at Rossville and on May 18 at Manhattan. Weed pressure at all environments was controlled with herbicide and hand weeding to prevent weed pressure from being a limited factor. Irrigation was applied throughout the growing season at all environments to maintain adequate soil moisture and to help increase the severity of SDS.

Maturity, height, lodging and seed yield were collected on all plots both years. Maturity was recorded as the date after August 31st when 95% of the pods on the plants had reached mature color. Height was recorded from the base of the plant to the top of the main stem in cm. Lodging was scored on a scale from one to five with one indicating all plants were erect and five indicating all plants were prostrate. Plots were harvested with a two-row plot combine cutting both rows of the plot. Grain yield was a function of the total seed weight of the plot and adjusted to uniform moisture. SDS ratings were taken at the R6 growth stage of the plants (Fehr, 1973). Disease severity (Ds) and incidence (Di) ratings were taken on all the plots. Incidence ratings were scored from 0-100 % on 5% increments based the infected area of the plot. Disease severity was scored on a 0-9 scale, with 0 = no visual symptoms, 1 = 10 % chlorosis or 5 % necrosis, 2 = 20 % chlorosis or 10 % necrosis, 3 = 40 % chlorosis or 20 % necrosis, 4 = 60 % chlorosis or 40 % necrosis, 5 = greater than 60 % chlorosis or 40 % necrosis, 6 = up to 1/3 premature defoliation, 7 = less than 2/3 premature defoliation, 8 = greater than 2/3 premature defoliation, and 9 = premature plant death. A disease index (Dx) was calculated using the formula: $Di * Ds / 9 = Dx$.

Canopy spectral reflectance measurements were collected with two Ocean Optics USB 2000 spectroradiometers (Ocean Optics, Dunedin Florida) controlled by the CDAP-2 (CALMIT University of Lincoln Nebraska, Lincoln, NE) for data acquisition, integration and processing.

The use of two passive spectroradiometers allowed for the calculations of average reflectance for comparisons between days. This is accomplished by using one sensor to collect down-welling light coming from the sky, and the second up-welling sensor to collect light being reflected from the leaf surface. Spectral reflectance was collected from the soybean canopy from 350-1027nm in electromagnetic spectrum, with a field of view of 25° and collection interval of 0.37nm. Data in the ultra violet (350 to 400 nm) portion was removed due to atmospheric interference. A spectrolan panel (Labssphere, Sutton, N.H.) was used as a white reference to calibrate the spectroradiometer at the start of each collection session. Sensors were mounted on an adjustable monopod and were held so that the sensors were vertical to the plots. Sensors were held approximately a half a meter above the plot to produce a 25-cm field of view. The first and last meter of the plot were excluded from the measurement to reduce end-row effect. Ten scans were taken and automatically averaged by the CDAP-2 software to produce a single measurement for each plot. Spectral data was collected on near cloud free days within two and half hours of solar noon, 10:00 to 15:00 hours. Reflectance readings were taken weekly from R2-R6 in all environments. Six, five and four collection dates were taken in 2015 at Manhattan, in 2016 at Manhattan and 2016 at Rossville, respectively.

Reflectance data were averaged to create 10 nm waveband regions, between 400 to 1027 nm, to reduce the size of the data set, limit the collinearity of near spectral bands and reduce the variation associated with individual waveband measurements (Curran et al., 2001; DeJong et al., 2003; Lin et al., 2012; Christenson et al., 2014). Individual wavelength measurements that were averaged tended to be highly correlated, so this step is thought to cause minimal loss of information (Christenson et al., 2014).

SAS 9.4 (SAS Institute, 2016) was used to analyze all spectral and phenotypic data. PROC MIXED was used for analysis of variance for yield, disease incidence, disease severity, disease index and maturity, using block as the random effect. Least square means were calculated by PROC MIXED. PROC GLM procedure was used for ANOVA of the spectral wavebands to check for significant differences between entries for reflectance at individual wavebands. PROC CORR was used to characterize the relationship between yield, maturity, disease index and individual wavebands. PROC REG using the stepwise procedure was used to create estimation models for disease index, yield, maturity using the waveband reflectance measurements.

Results and Discussion

Agronomic Data

NAM

Nested Association Mapping (NAM) population entries differed significantly ($p < .0001$) for average yield over all three environments (Table 2.1). A significant ($p < .0001$) entry by environment interaction was observed for yield (Table 2.1). Entry mean yields ranged from 1.65 t ha⁻¹ to 4.4 t ha⁻¹ at Manhattan in 2015, .89 t ha⁻¹ to 4.3 t ha⁻¹ at Manhattan in 2016, and 1.0 t ha⁻¹ to 3.7 t ha⁻¹ at Rossville in 2016 (Table 2.2). Mean yields were significantly different between Rossville in 2016 (2.5 t ha⁻¹) and both years in Manhattan (3.0 t ha⁻¹ and 2.8 t ha⁻¹ in 2015 and 2016, respectively) (Table 2.2).

NAM population entries differed in maturity and a significant entry by environment interaction was observed for maturity (Table 2.1). Maturities at Manhattan and Rossville in 2016 averaged a few days earlier than maturities at Manhattan in 2015 (Table 2.2). Entry means for maturity at Manhattan in 2015 ranged from 14 to 33 days, at Manhattan in 2016 ranged 14 to 36 days and at Rossville 2016 ranged from 15 to 25 days after August 31 (Table 2.2). In 2016 at Manhattan, all lines were mature by Sep. 28 except for LS09-1920 which matured on Oct. 6. In 2016 at Rossville, LS09-1920 was not harvested due to not being mature at that time the rest of the plots were harvested.

Although the range in disease incidence (Di) among entries at each environment was slightly larger at Manhattan in 2015, averaged across all entries, Di was higher at the 2016 environments (32.6% and 37.4%) than at Manhattan in 2015 (24.3%) (Tables 2.1 and 2.2). Di was significantly different ($p < .0001$) between entries at all environments (Table 2.1). Entry means for

disease incidence ranged from 0-90% at Manhattan in 2015, 2-80% at Manhattan in 2016 and 2-85% in Rossville at 2016 (Table 2.2).

Disease severity (Ds) differed among all three environments with the highest severity observed at Rossville in 2016 (3.4) and the lowest severity observed at Manhattan in 2015 (1.9) (Table 2.2). The interaction between entry and environment was also observed to be significant ($p < .0001$) for Ds (Table 2.1). Entry means for disease severity scores ranged from 0-6 in Manhattan in 2015, from 1-8 at Manhattan in 2016, and from 0-7 at Rossville in 2016 (Table 2.2).

Mean Dx score of 8.5 in 2015 at Manhattan was significantly lower than the Dx scores at both environments in 2016 (Tables 2.1 and 2.2). A significant ($P < .0001$) entry by environment interaction was observed for Dx (Table 2.1). Entry means for disease index ranged from 0 to 57 at Manhattan in 2015, 0 to 67 at Manhattan in 2016, and 1 to 69 at Rossville in 2016 (Table 2.2 and Fig. 2.1). NAM RILs tended to be normally distributed for Dx at Manhattan and Rossville in 2016 (Fig. 2.1bc), but the 2015 Manhattan distribution was not normally distributed, probably due to the lower disease pressure at that environment (Fig. 2.1a).

Disease index will be used in this study as the primary disease assessment tool since it accounts for both the severity as well as the amount of disease present in the plot. This gives Dx a more accurate prediction of disease pressure than either Di or Ds measurements.

SVPT

SVPT entries had significant ($p < .0001$) entry differences for mean seed yield (Table 2.3). Environment and the environment by entry sources of variation were significant for seed yield as well (Table 2.3). Average seed yield for SVPT entries at Manhattan 2015 was 3.5 t ha^{-1} and ranged for $.79 \text{ t ha}^{-1}$ to 4.8 t ha^{-1} (Table 2.4). In 2016 at Manhattan, SVPT entries had a mean yield of 3.4 t ha^{-1} , with a range of yield from $.33 \text{ t ha}^{-1}$ to 4.6 t ha^{-1} . Mean yield for all entries at

Rossville in 2016 was 3.1 t ha⁻¹ and entry means ranged from 1.2 t ha⁻¹ to 5.5 t ha⁻¹. Mean yields of entries were significantly different all three environments (Table 2.3). Entries in the SVPT population tended to have higher yields than the NAM RILs, because the SVPT population was comprised of mostly cultivars used in commercial seed production.

Maturity was significantly different ($p < .0001$) between entry for SVPT entries (Table 2.3). Maturity was significantly different ($p < .0001$) between environment, and significant ($p < .0001$) entry by environment interaction was observed for maturity (Table 2.3). Maturity for entries was significantly different at all environments (Table 2.3). Maturity of all entries ranged from 19 to 46 days after August 31st at Manhattan 2015 (Table 2.4). SVPT entries at 2016 Manhattan and Rossville had maturity that ranged from 18-56 day and 17-53 days after August 31 at respectively (Table 2.4). The maturity range was greater in the SVPT population than in the NAM population due to the inclusion of many maturity group five entries, whereas the NAM population was comprised of mainly maturity group 3 and early maturity group 4 genotypes.

Disease index scores significantly differed ($p < .0001$) between entry and environment for the SVPT entries (Table 2.3). Entry by environment interaction was significant ($p < .0001$) for disease index scores (Table 2.3). Entries in the SVPT had significantly different Dx scores between all three environments (Table 2.4). SVPT entries at Manhattan 2015 mean disease index score ranged from 0-76. In 2016 at Manhattan and Rossville all SVPT entries had ranges in disease index scores from 0-92 and 0-83 respectively (Table 2.4).

SVPT c entries had significant differences between disease incidence and severity for both entry and environment (Table 2.3). Significant interactions were observed between entry by environment for both Di and Ds (Table 2.3). SVPT disease incidences were significantly different between at between years but not environments in 2016 (Table 2.4). Mean disease

severities were different between all environments for SVPT entries (Table 2.4). Mean disease incidence ranged from 2 to 85% for all SVPT entries at Manhattan 2015, and between 0-100% for all SVPT entries in 2016 at both Manhattan and Rossville (Table 2.4). Mean disease severity scores for SPVT entries ranged from 1-8 in 2015 at Manhattan (Table 2.4). In 2016 at both Manhattan and Rossville all SVPT line mean Ds scores ranged from 0-8 (Table 2.4).

The entry by environment source of variation for yield, maturity, Di, Ds and Dx was significant for the NAM and SVPT populations (Tables 2.1 and 2.3). The entry by environment interaction tended to account for a smaller portion of the phenotypic variance than the entry main effect. Regardless, in this study, both the grand entry means for the agronomic traits across all environments, and the individual environment entry means will be used to examine the relationships between the spectral reflectance measurements and Dx and seed yield.

Spectral Reflectance Readings

NAM

For each genotype, a single seasonal average reflectance value was calculated for each waveband region using the reflectance values from the significant days in which differences were detected among genotypes for any waveband region ($p \leq 0.1$). Reflectance data from 905-1025nm was removed due to poor data quality across all scans. For the NAM population at Manhattan in 2015, three dates (August 11, August 30 and September 14) were used to calculate the season average (Fig. 2.2a). In 2016 at Manhattan, four dates (August 3, August 10, September 1, and September 6) were used to calculate the season average (Fig. 2.2b). In 2016 at Rossville three days (August 4, August 8, and September 2) were used to calculate the season average reflectance (Fig. 2.2c).

At Manhattan 2015, the August 11 and 31 reflectance readings were significantly different among entries in both the blue (400-500nm) and green (500-600nm) regions (Fig. 2.2a). August 11 reflectance readings were significant different among entries in the red (600-700 nm) and red edge (705-730nm) regions. August 31 reflectance readings in the NIR (>730 nm) differed significantly among entries. September 14 waveband reflectance only differed significantly among entries in portions of the red (600-700nm) and NIR (>730nm) regions. At Manhattan 2016, entries differed in reflectance on August 3 and 10 in the green (500-600nm) and red (600-700 nm) regions (Fig. 2.2b). On August 10, entry differences were observed in the NIR (>730nm) region. On September 1 and 6 significant entry differences in the visible (400-700nm) as well the NIR (>703nm) were detected. September 6 had significant entry differences for reflectance in the red edge (700-730nm) region. In 2016 at Rossville, August 3 and 8, and September 2 had significant different in reflectance among entries in most portions the visible spectrum (400-700nm) (Fig.2.2c). On August 8 and September 1 reflectance readings were significantly different among entries in most portions of the red edge (700-730nm) and NIR (>.700nm). Readings collected in the middle of August during the R4-R5 growth stages, tended to not to detect differences among entries even though visible disease symptoms were present. This may have occurred because of environmental factors, but literature indicated that measurements at this time should be informative.

SVPT

SVPT individual day spectral readings were examined for significant differences between entries for waveband reflectance. Significance levels in reflectance among entries was set a $P < .1$. At Manhattan 2015, four dates (August 7, 11 and 20, and September 14) had entries with significant differences in waveband reflectance (Fig 2.3a). Five dates at 2016 Manhattan (August

3, 10, and 16, and September 1 and 12) had waveband reflectance values that significantly differed between entries (Fig. 2.3b). Entry differences in waveband reflectance were observed on only two dates at Rossville 2016 (August 4 and September 9) (Fig. 2.3c). At both Manhattan 2015 and 2016, reflectance tended to be significantly different between entries in both the visible spectrum (400-700nm) and NIR (>730nm) regions (Fig. 2.3ab). September 9 at Rossville 2016 reflectance differed between entries in portion of the blue (500-600nm), red (600-700nm) and most NIR (>735nm) (Fig. 2.3c). Spectral readings from August 4 at Rossville were only significantly different between entries at a small number of wavebands and thus were discarded.

Dx and Reflectance Correlations

NAM Season Average

Pearson's correlations were calculated between Dx and season average reflectance readings for each waveband region to identify waveband regions associated with Dx. Correlations ranged from -.26 to .35 at Manhattan 2015, -.18 to .26 at Manhattan 2016, and -.39 to .19 at Rossville 2016 between Dx and wavelength (Fig. 2.4abc). Dx scores tended to increase as waveband reflectance increased in the visible spectrum (400-700nm) in both years at Manhattan, and as Dx scores increased, waveband reflectance tended to decrease in the NIR (>700nm) at all environments (Fig. 2.4abc). The inversion of the spectral reflectance correlations with dx from positive to negative tended to be centered around 705nm, which corresponds to the red edge region where plants start to reflect non-photosynthetically active light (Horler et al., 1983; Penuelas et al., 1993).

Correlations in the blue spectral region (400-500nm) varied between years at Manhattan. At Manhattan 2015 only two wavebands 485nm and 495 correlated with dx, where as in 2016 the entire region was significant (Fig. 2.4ab). No significant correlations were observed at

Rossville between blue waveband reflectance and Dx (Fig. 2.4c). Correlations in the green (500-600nm) spectral region tended to be significant towards the transition from blue to green and green to red at Manhattan both years (Fig. 2.4ab). Green waveband reflectance and Dx were not correlated at Rossville (Fig. 2.4c). At all three environments, the red waveband reflectance (600-700 nm) was positively correlated to Dx (FIG. 2.4abc). All environments, NIR (>700 nm) reflectance measurements were negatively correlated to Dx (Fig. 2.4abc). Reflectance at 675nm has been reported to be informative at quantifying chlorophyll a absorption, and estimating photosynthesis with minimal effects from other plant pigments (Chappelle et al., 1992). Reflectance at 775 nm had the highest correlation to Dx in both years at Manhattan, while at Rossville 755nm reflectance was most correlated to Dx (Fig. 2.4abc). At both Manhattan environments, the correlations went from positive to negative at 715nm, while at Rossville the transition occurred at 705 nm (Fig. 2.4abc). This transition at the red edge is an important factor in predicting plant health and shifts towards the shorter wavelengths as plants undergo stress. This shift is accompanied by an increase in absorption of light in the NIR due to low water and nitrogen (Filella and Penuelas, 1994). The shift of the red edge observed at Rossville to lower wavelengths could have been due to increased disease pressure experienced at that environment. Decreased photosynthetic activity was observed in plants infected with SDS (Bajwa et al., 2015). This supports the positive correlations that were observed between reflectance and Dx in the visible region (400-700nm). Readings in the NIR (905nm-1023) were on average not significant and as previously discussed were removed from analysis for poor data quality.

2016 Rossville tended to have unusual green (500-600nm) reflectance patterns relative to disease pressure, compared with the other environments. This difference in reflectance observed

at Rossville maybe due to the greater disease pressure damaging the leaf pigments causing increased absorption of the green wavebands.

NAM Individual Days

Individual day reflectance correlations with Dx tended to follow the trends seen in the season averaged readings, except for the August 8, 2016 Rossville reading. At Manhattan in 2015 August 31 was the most informative of day based on correlations as compared to other scans. 605nm was the most informative band at $R=.41$ in the visible range and 775nm ($r=-.18$). For Manhattan 2016 September 1 was the correlated day with Dx at 675nm was the most significant ($r=.3$) in the visible spectrum and 765nm ($r=-.17$) in the NIR. At Rossville 2016, August 8 was the most significant day for visible reflectance with highest correlation in the visible wavelength at 575nm ($r=.25$) and 705nm was most significant ($r=.3$) in the NIR (Fig. 2.6). September 2nd was extremely informative in the NIR ($r=.38$) at 755nm and in the visible region at 675nm ($r=.2$). The reflectance became negatively correlated to Dx at 715nm the same as in the season averages for both 2015 and 2016 in Manhattan. On September 2 at Rossville the trend was the same in season average, but August 8 negative correlation didn't happen until 735nm (Fig. 2.5a). These individual days that were selected the spectral reading taken nearest to the visual disease evaluation, this insured that disease pressure was the greatest for evaluation. August 8 was included in the individual day due to September 2 data only having significant correlation to disease in the portions of the red (600-700nm) and NIR (>730nm) region (Fig2.5b).

Correlation between disease index and waveband reflectance tended to be similar between season average reflectance and individual day reflectance for the NAM population. Reflectance measurements that were taken during the height of disease pressure tended to have

the highest correlation to disease index, except for Sept 8 at Rossville 2016. This increased disease pressure has greater foliar symptoms which leads greater differences between entries reflectance, similar results were seen in estimation of powdery mildew in wheat and charcoal rot root and SDS in soybeans (Franke and Menz, 2007; Fletch et al.,2014; Bajwa et al., 2017). Increased reflectance in the visible waveband region is in line with Bajwa et al. (2017) which also showed that reflectance in the visible region increased with SDS disease pressure. Reflectance in the NIR region was shown to decrease with an increase in disease pressures (Bajwa et al., 2017; Fletch et al.; 2014). 675nm tended to be the most correlated, this is like Vigier et al. (2014) where reflectance between 675-695nm was used to estimate sclerotia stem rot in soybeans. As previously shifts in the red edge were observed in reflectance of the NAM population towards lower wavelengths due to increased disease pressure.

SVPT Season Average

SVPT season average waveband reflectance and Dx correlations for Manhattan 2016 were the only measurements that followed the general trends observed in the NAM population, with positive correlation in the visible wavelengths (400-700nm) and then becoming negatively correlated in the NIR region (>700nm) (Fig.2.6abc). In 2015 at Manhattan, no significant correlations between Dx and waveband reflectance were observed for the season average measurements (Fig 2.6a). At Rossville 2016 negative correlations between Dx and waveband reflectance in the blue (400-500 nm) and green (500-600 nm) regions as well as the NIR(>700nm) (Fig. 2.6c).

Reflectance Curve Change Due to Disease

Spectral reflectance tended to differ between genotypes that were highly resistant and susceptible to SDS. Resistant genotypes tended to have lower reflectance values in the visible

spectrum as compared to highly susceptible lines. SDS resistant checks (LD06-7862, Ripley, and LS09-1920) and susceptible checks (Morgan, Spencer) were averaged to create spectral reflectance measurements to observe differences among resistant and susceptible genotypes due to disease symptoms (Fig. 2.7abc). In the NIR, resistant genotypes had greater reflectance compared with susceptible genotypes. Genotypes responded similarly across environments in their reflectance patterns. Higher reflectance in the visible spectrum suggests that the plant pigments were damaged in the leaves because of foliar disease symptoms. These results are consistent with other findings on light absorption in relation to plant health and productivity, such as the study reported by Penuelas et al. (1993) where damage from salinity and ozone increased reflectance in the visible spectrum and decreased reflectance in the infrared.

Reflectance and Yield Correlations

NAM Season Average

Correlations between yield and season average reflectance readings for each waveband were used to characterize which wavebands were related to yield. Correlations between reflectance and yield ranged from -.40 to .32 at Manhattan 2015, from -.64 to .48 at Manhattan 2016, and from -.46 and .67 at Rossville 2016 (Fig. 2.8abc). Reflectance in the visible range (400-695nm) tended to be negatively correlated to yield, whereas reflectance in the NIR (705-1023nm) tended to be positively correlated with yield. As with correlations with Dx, reflectance at the 675nm waveband was the most correlated with yield at Manhattan and Rossville in 2016, and was significant at Manhattan 2015. Reflectance at the 675nm waveband has been used to estimate yield (Chappell et al., 1992). Yield was negatively correlated to Dx at all environments (Table 2.6). The change in correlations from negative to positive between yield and reflectance occurs at longer wavelengths (725nm and 715nm for yield, as compared to 715nm and 705nm

for Dx in both years in Manhattan and Rossville, respectively). Yield is positively associated with shifts in red edge absorption of longer wavelength light. (Fillea and Penuelas, 1994; Penuelas et al., 1997).

NAM Individual Days

Correlations between seed yield and reflectance tended to follow the trends that were seen in the season average correlations, except for the August 8 reading at Rossville (Fig. 2.9). On this date only, readings in the visible region were significantly correlated to disease. This may be due to the scan being taken early in the season before the onset of severe disease symptoms and at the height of active growth.

SVPT Season Average

The SVPT correlations between yield and reflectance wavebands only appeared to resemble that of the NAM population at Manhattan in 2016 (Fig. 2.10b). At both Manhattan 2015 and Rossville 2016 reflectance in some portions of the visible spectrum were positively correlated with yield (Fig.2.10ac). All environments were positively correlated to increased reflectance and increased yield in the NIR (>700 nm). Christenson et al. (2014) reported negative correlations between yield and reflectance in the visible spectrum, as well as increased reflectance in the NIR leading to higher yield. Individual dates had similar correlations to yield as season average.

Correlations with Maturity, Dx and Yield

Entry means for disease index and maturity were significant correlated at Manhattan2015($r = .36$, $p < .0001$), but were not correlated in either other environment in 2016 (Table 2.6). Yields were significantly correlated to maturity at all three environments for the NAM population, but only at Rossville for the SVPT population. This is confirmed in

Christenson et al. (2014 and 2015) where yield was significantly correlated to yield. SVPT yields for Rossville were significantly correlated to maturity (Table 2.6). Yield was negatively correlates at all environments with disease index in both the NAM and SVPT populations (Table 2.5) For the NAM population maturity was significantly correlated to individual waveband reflectance at all environments (Fig. 2.11abc). Reflectance in the visible wavebands were negatively correlated to maturity in Manhattan in Rossville in 2016 for the NAM population (Fig. 2.11bc). Manhattan in 2015 had no correlation between maturity and reflectance in the blue (400- 500 nm) or green (500-600 nm) regions, but portions were significant in the red (600- 700nm) region (Fig. 2.11a) for the NAM population. At all environments, the NAM population had significant positive correlations between maturity and reflectance in the NIR (>700nm) region (Fig. 2.11 abc). Maturity trends for NAM individual day measurements were like that of the NAM season average, except for the August 8 were only readings from 405-435nm were correlated to maturity (Fig. 2.12). SVPT had similar significant correlations between maturity and waveband reflectance as the NAM population season average and NAM significant days (Fig. 2.13abc).

Regression Equations for Dx Prediction

NAM Season Average

Season average reflectance was used to create regression equations that best explained the phenotypic variation in Dx among the entire NAM population. Stepwise selection allowed variable to enter the equation at significance of $p < .1$ and variables allowed to stay in the equation at significance level of $p < .05$. Manhattan 2015 produced an equation using two wavebands (535nm and 585nm) which explained 52% of the variation in Dx (Tables 2.6 and 2.7) (Fig. 2.14). In 2016 at Manhattan, three reflectance variables (505nm, 675nm, and 755nm) were used to

create the regression equation which explained only 16% of the phenotypic variance in Dx (Tables 2.7 and 2.8). Rossville in 2016 produced a regression equation with four wavebands which explained 28% of the Dx phenotypic variation (Table 2.6 and 2.8).

A single predictive grand means model was created from the average of the three season averages to predict disease index (Table 2.6 and 2.11). This model 28% of the phenotypic variation in the grand means variation in Dx. When used to predict the performance of entries at all three environments using season averaged data 20% of the phenotypic variation in Dx was explained at Manhattan 2015 and Rossville (Figure 2.22), and in Manhattan 2016 the grand means model only explained 6% of the variation in Dx of the NAM population.

NAM Individual Days

To determine if season averages or individual day measurements were more informative at predicting SDS, individual day spectral measurements taken closest to R6 were evaluated in a similar manner as season averages to produce Dx estimations. Individual day regression equations from Aug 31, 2015 and Sept. 1, 2016 at Manhattan, and September 2, 2016 at Rossville, explained 55%, 11% and 24% of the phenotypic variation of Dx respectively (Tables 2.6, 2.7, 2.8). While the models based on the individual days were not identical to the season average models, they were similar and explained about the same amount of the phenotypic variation in Dx. These findings suggest that scans taken at the height of disease pressure might be sufficient for disease prediction, but might pose a challenge due to the potential maturity effects, and weather conditions.

SVPT Season Average

Season averaged data from Manhattan in 2015 was not able to explain any of the phenotypic variation in Dx (Table 2.6). SVPT scans for Manhattan 2015 were typically collected

later in the day which may lead environment factors affecting their predictive ability. Season averaged reflectance from Manhattan and Rossville in 2016 explained 42% and 31% of the phenotypic variation in Dx, respectively, using five wavebands at Manhattan and three wavebands at Rossville (Tables 2.6 and 2.10).

Disease index estimation was possible using spectral reflectance, but Dx models tended to underestimate disease index across all environments for season averages and individual days (Fig. 2.14, 2.15, 2.16, 2.19). The prediction models tended to estimate less of the phenotypic variation in disease compared to studies such as Bajwa et al. (2017). This may be due to the increased number of lines in each of the population as compared to the limited number used in that study.

Regression Equations for Yield Prediction

NAM Season Average

Regression equations created using NAM season reflectance averages using stepwise selection, estimated 41% and 66% of the yield variation among entries in Manhattan in 2015 and 2016 respectively. Six waveband regions were used for Manhattan 2015 and five wavebands for Manhattan in 2016 (Tables 2.6 and 2.7). The equation for Rossville in 2016 accounted for 78% of the yield variation, using six waveband regions (Tables 2.6 and 2.8) (Fig. 2.17). While maturity was significantly correlated to yield when added as a covariate it did not increase the model's predictive accuracy when estimating yield.

The grand means NAM model for yield explained 71% of the phenotypic variation in the grand means yield (Table 2.6). When applied to individual environment season average reflectance values, 25%, 60% and 62% of the phenotypic variation in yield was explained at Manhattan 2015, Manhattan 2016 and Rossville 2016 (Fig. 2.23), respectively.

NAM Individual Days

Individual day readings for the NAM population were used to create yield estimation models. August 31, 2015 and September 2, 2016 readings at Manhattan, predicted 40% and 54% of the phenotypic variation in yield between entries, using 5 and 3 wavebands respectively (Tables 2.7 and 2.8). The September 2 readings at Rossville created models that accounted 77% of phenotypic yield variation using 6 wavebands (Tables 2.6 and 2.8).

SVPT Season Average

Spectral reflectance models using four to eight wavebands in the SVPT population explained 79% and 43% of the phenotypic variation in yield at Manhattan and Rossville, respectively (Tables 2.6 and 2.10). Season averaged reflectance data from Manhattan in 2015 was not able to explain any of the phenotypic variation in Dx and less than 5% of yield phenotypic variation (Tables 2.6 and 2.10).

Yield models tended to slightly overestimate yield but predictions explained more of the phenotypic variation in yield than for disease index (Fig. 2.17 and 2.18). These models tended to explain similar amounts of phenotypic variation in yield as waveband estimates in studies such as Christenson et al. (2016) and Ma et al. (2002). Ma et al. (2002) stated that yield estimation by spectral reflectance was best suited for use early in the breeding cycle due to not explaining enough phenotypic variation in yield. The variation in estimates seen here would support the recommendation that these estimations should be used as an early selection tool, to evaluate large, segregating populations. Individual days tended to estimate yield similarly to season averages. These results are similar to Ma et al., (2002) and Christenson et al. (2016), which indicates that measurements could be taken during R5 to R6 to predicted yield, thus limiting the number of scans needed to be taken per year.

Maturity Estimation Models

The sometimes-strong correlations of maturity with seed yield and Dx makes it necessary to examine the impact of these relationships on the effectiveness of reflectance data to predict Dx and yield. To initiate this evaluation, season averaged reflectance was used to develop models to predict maturity. The NAM population models accounted for 46%, 56%, and 64% of the phenotypic variation in maturity at Manhattan in 2015 and 2016, as well as Rossville, respectively (Tables 2.6, 2.7, 2.8). Individual day models accounted for 46% on August 31, 2015 and 57% on September 1, 2016 at Manhattan of the phenotypic differences in maturity (Tables 2.6 and 2.7). September 2, 2016 at Rossville accounted for 62% of the phenotypic difference in maturity (Tables 2.6 and 2.8). SVPT reflectance data from Manhattan in 2015 failed to create a predictive model (Table 2.6). Season reflectance averages at Manhattan and Rossville in 2016 accounted for 78% and 74% of the phenotypic variation in maturity, respectively (Tables 2.6 and 2.10). When maturity was added as an additional covariate to wavebands, it increased the predictive accuracy of the model for Rossville in 2016, increasing the explained variation in phenotypic Dx from 28% to 42% (Fig. 2.15) (Tables 2.6 and 2.8). Maturity maybe affecting the accuracy of the season average model in Rossville when predicting Dx.

DX and Yield Estimation based on Maturity Groups

To examine the influence of maturity on the DX and yield models, the NAM population at each environment was divided into early, middle and late maturity groups. Each of these maturity groups were then used to create new stepwise predictive models for Dx and yield. Early maturity group estimation models for Dx explained 37%, 8% and 44% of the phenotypic variation at Manhattan 2015 and 2016, as well as Rossville, respectively (Table 2.7 and 2.10). These same models explained 31%, 39% and 72% of phenotypic variance in yield at respective

environments (Tables 2.6 and 2.9). Early models explained 16% and 24% of the phenotypic variation in maturity at Manhattan in 2015 and 2016 respectively (Tables 2.6 and 2.9). Model for the middle maturity group explained 55%, 35%, 42% of Dx variation for 2015 and 2016 Manhattan and Rossville in 2016 (Tables 2.6 and 2.9). These models accounted for 41%, 60%, and 75% of the yield phenotypic differences between both environments at Manhattan and Rossville (Tables 2.6 and 2.9). 25% and 24% of the variation in maturity was explained at Manhattan and Rossville in 2016 by the middle maturity group (Tables 2.6 and 2.9). Late maturity group predicted 54% and 77% of the phenotypic variation in Dx at 2015 Manhattan and 2016 Rossville (Tables 2.6 and 2.9). These same models predicted 49% and 92% of the yield phenotypic variation respectively (Tables 2.6 and 2.9). No late maturity group models could predict the maturity (Tables 2.6 and 2.9).

Models did not have the same number of entries between environments due to each environment being treated separately. The small number of entries in the 2016 Manhattan late maturity group could account for the low predictive quality. The same low number of entries in Rossville in the late maturity group may have led to over estimation of Dx and yield due to the late maturity group containing a majority of the check lines as compared to the early and middle groups. Due to maturity group models estimating similar amounts of phenotypic variance of Dx and yield as compared to season average models, these models support the conclusion that while reflectance is related to maturity, season average models are estimating Dx and yield without major influence of maturity in the prediction. Christenson et al. (2016) showed a greater increase in predictive ability between models separated by maturity than was seen here.

Check Models

For use as a breeding tool, model prediction must be streamlined to predict phenotypic response. For this reason, a simplified model building process was chosen in which the parents, yield checks, and SDS checks were used to create stepwise predictive models to aid in selection of resistance to SDS and yield. The model created by using the reflectance reading from the parents and checks was then used to predict Dx and yield for the RILs in the NAM population.

Manhattan 2015 check reflectance data created a model with two variables 795nm and 875nm wavebands which explained 68% of the variation in Dx (Tables 2.6 and 2.7) The same data created a yield model using 535nm and 585nm wavebands to predict 56% of the yield variation (Tables 2.6 and 2.7). 2016 Manhattan data predicted 54% of the phenotypic variation in Dx using the 475nm waveband, and 80% of the yield variation with three wavebands (Tables 2.6 and 2.7) Rossville 2016 accounted for 73% of the Dx phenotypic variation using 735nm wavebands, and 93% of the phenotypic variation in yield using 775nm and 875nm (Tables 2.6 and 2.8) (Fig. 2.18 and 2.19). The models respectively identified 46%, 58% and 72% of the phenotypic variation in maturity (Tables 2.6, 2.7, 2.8).

The simplified check regression equations were then used to identify SDS resistance and yield in the NAM RILs from each environment. The check model identified 16 to 61% of the phenotypic variation in yield of the NAM RILs. The check models for Dx only accounted for 5% 10% of the phenotypic variation seen in NAM RILs. In Manhattan in 2015 19 of the 28 of the top performing NAM RILs for yield (20%) were identified when the top 50% of NAM RILs with the highest predicted yields were selected, 17 of the top 28 SDS resistant NAM RILs were identified when selecting the top 50% of predicted NAM RILS of SDS resistance. Nineteen of the top 28 NAM RILs for yield and 20 of the 28 most resistant SDS NAM RILs were selected

for with the top 50% of best predicted NAM RILs for yield and disease resistance in Manhattan 2016. 2016 in Rossville the 25 of the top 28 NAM RILS for yield and 21 of the 28 most SDS resistant NAM RILS were selected when the top 50% of predicted values for yield and Dx selected. For yield all the 20% of entries were always identified if the selection criteria were increased to the 75% best predicted yielding of NAM RILs.

Individual environment check equations were used to predict dx and yield at two other environments. The Manhattan 2015 check equation accounted for 61% and 5% of the phenotypic variation in yield and Disease index when applied to the Manhattan 2016 reflectance data. Manhattan 2015 predicted 56% and 3% of the variation in yield and Dx at Rossville 2016. The Manhattan 2016 data explained 22% and 53% of the variation in yield at Manhattan 2015 and Rossville in 2016. This model explained less than 5% of the phenotypic variation of Dx at both Manhattan 2015 and Rossville 2016. Check models created from Rossville 2016 accounted for 38% and 20% of the phenotypic variation in yield at Manhattan in 2015 and 2016 respectively. 10 % of the phenotypic variation in Dx was explained at Manhattan 2015 and 1% at Manhattan 2016 when predicted using the Roseville 2016 check model.

A single universal check model was created from the season average checks from all three environments (Table 2.6 and 2.11). This model was created by stepwise selection to make a universal selection models. 16%, 64% and 54% of the phenotypic variation in yield of the NAM RILs at Manhattan 2015 and 2016 and Rossville when predicted from the grand means check model (Figure 2.24). The universal check model predicted 25%, 8%, 9% of the phenotypic variation in disease index in NAM reals at Manhattan 2015, Manhattan 2016, and Rossville respectively (Figure 2.25).

Yield models tended to account for greater portions of the phenotypic variation in yield across all environments when compared with Disease index prediction models. Disease index models should only be used at the environment where data was collected due to low prediction accuracy at multiple environments. NAM Check models predicted similar to the models in Christenson et al. (2016) where selection of the top 50% of predicted entries identified a majority of actual top yielding entries. Christenson et al. (2016) also found that increasing the model to select the top 75% of predicted yield selected all the top performing lines. This would indicate that spectral reflectance may be useful as an early selection tool for breeders to evaluate large population, similar to what Ma et al. (2003) suggested.

Conclusions

Large genetic differences occurred in the populations used in this study; these two populations are representative of the genetic diversity that would be found in a breeding program. The NAM population was similar to early testing of segregating populations, whereas the SVPT would be similar to final yield testing of new lines. At all three environments, disease pressure was significant and useful in evaluating resistance to SDS in these populations.

Spectral reflectance measurement changed with the increases of diseases pressure. These changes were similar to those reported in the previous literature that showed the increased disease pressure decreases plant photosynthesis. Disease increased reflectance in the visible region of the spectrum while decreasing reflectance the NIR. A shift in the red edge was observed between Rossville and Manhattan which corresponds with an increase in disease pressure at Rossville. Yield reflectance trends were also observed that were similar to reported literature.

Spectral reflectance was able to characterize up to 73%, 78%, and 64% of phenotypic variation in disease index, yield and maturity. These estimations could be used by breeders to increase the efficiency of breeding cycle. Interactions between maturity and disease index and yield, affected the predictive ability of the models. Separating entries into maturity groups reduced the effect of maturity while still predicting disease index and yield phenotypic variation. Individual day measurements taken near SDS evaluation were shown to have similar predictive abilities as season average models. This would potentially allow breeders to take reflectance measurements at the height of disease pressure to then predict disease performance.

To further simplify the predictive ability of the models, the reflectance of the checks and grand means can be used to create predictive models of disease index and yield. When the

models were applied to the individual environment's NAM RILs, the predictive ability of disease index models was less informative than that of yield models for both grand means and check models. The variability in of the models would limit the model's usefulness too early in the breeding process for initial evaluation of yield and SDS resistance. For reliable estimation of disease resistance to SDS, models should be created from data from a single environment. This variability and need to work with in a single environment limits the ability to of the model for use in large-scale disease resistance breeding. Current methods of evaluations will still need to be performed as a final step in developing new lines.

Further research will need to be done to increase the predictive ability and decrease the variability of individual scans, which is a major limiting factor. Another major limitation to predictive measurements by spectral reflectance is the ability to take measurements on large scale breeding populations, new technologies and automation may elevate these limitations. With optimization of methods spectral reflectance measurement may be a new tool for soybean breeders for SDS resistance.

References

- Adams, M., D. Philpot, and W. Norvell. 1999. Yellowness Index: an application of spectral second derivatives to estimate chlorosis of leaves in stressed vegetation. *Int. J. of Remote Sensing* 20(18):3663-3675.
- Adee, E. 2015. Effects of seed treatment on sudden death syndrome symptoms and soybean yield. *Kansas Agricultural Experiment Research Report* 1(2):1-6. <https://doi.org/10.4148/2378-5977.1006>.
- Adee, E. 2016. Interaction between seed treatment and variety on sudden death syndrome symptoms and soybean yield. *Kansas Agricultural Experiment Research Reports* 2(5):1-5. <https://doi.org/10.4148/23787-5977.1224>.
- Aoki, T., K. O'Donnell, Y. Homma, and A. Lattanzi. 2003. Sudden death syndrome of soybean is caused by two morphologically and phylogenetically distinct species within the *Fusarium Solani* species complex – *F. vurguleforme* in North America and *F. tucumaniae* in South America. *Mycology* 95(4):660-684.
- Aparicio, N., D. Villegas, J. Casasesus, J. Araus, and C. Royo. 2000. Spectral vegetation indices as nondestructive tools for determining durum wheat yield. *Agron. J.* 92:83-91.
- Araus, J., and J. Cairns. 2014. Field high-throughput phenotyping the new crop breeding frontier. *Trends in Plant Sci.* 19(1):52-61.
- Bajwa, S., J. Rupe, and J. Mason. 2017. Soybean disease monitoring with leaf reflectance. *Remote Sensing* 9(127):1-14. doi:10.3390/rs9020127
- Brar, H., S. Swaminathan, and M. Bhattacharyya. 2011. The *Fusarium viguliforme* toxin FvTox1 causes foliar sudden death syndrome-like symptoms in soybeans. *MPMI* 24(10):1179-1188. doi:10.1094 /MPMI -12-10-0285
- Buttery, B., and Buzzell, R. 1977. The relationship between chlorophyll content and rate of photosynthesis in soybeans. *Canadian J. of Plant Sci.* 57:1-5.
- Cabrera-Bosquet, L., J. Crossa, J. Zitzewitz, M. Serret, and J. Araus. High -throughput phenotyping and genomic selection: the frontiers of crop breeding converge. *J. of Integrative Plant Bio.* 54(5):312-320.
- Carter, G. 1993. Responses of leaf spectral reflectance to plant stress. *American J. of Bot.* 80(3): 239-243.
- Chappelle, M. Kim, J. McMurtrey. 1992. Ratio analysis of reflectance spectra (RARS): an algorithm for the remote estimation of the concentrations of chlorophyll a, chlorophyll b, and carotenoids in soybean leaves. *Remote Sensing the Env.* 39:239-247.

- Chang, S., T. Doubler, V. Kilo, R. Sutter, J. Klein, M. Schmidt, P. Gibson, and D. Lightfoot. 1996. Two additional loci underlying durable field resistance to soybean sudden death syndrome (SDS). *Crop Sci.* 36:1684-1688.
- Chang, H., L. Domier, O. Radwan, C. Yendrek, M. Huddson, and G. Hartman. 2015. Identification of multiple phytotoxins produced by *Fusarium virguliforme* including a phytotoxic effector (FvNIS1) associated with sudden death syndrome foliar symptoms. *MPMI* 29(2):96-108.
- Christenson, B., W. Schapaugh, N. An, K. Prince, V. Prasad, and A. Fritz. 2015. Characterizing changes in soybean spectra; response curves with breeding advancements. *Crop Sci.* 54: 1585-1597.
- Christenson, B., W. Schapaugh, N. An, K. Prince, V. Prasad, and A. Fritz. 2016. Predicting soybean relative maturity and seed yield using canopy reflectance. *Crop Sci.* 56:625-643.
- Covert, S., K. O'Donnell, D. Starkey, A. Holiday, D. Geiser, F. Cheung, C. Town, A. Storm, J. Juba, M. Scandiani, and X. Yang. 2006. Sexual reproduction in the soybean sudden death pathogen *Fusarium tucumaniae*. *Fungal Gen. and Bio.* 44: 799-807. doi:10.1016/j.fgb.2006.12.009
- Curran, P., J. Dungan, and D. Peterson. 2001. Estimating the foliar biochemical concentration of leaves with reflectance spectrometry. *Remote Sensing the Env.* 76:349-359.
- Curran, P., J. Dungan, and H. Gholz. 1990. Exploring the relationship between reflectance red edge and chlorophyll content in slash pine. *Tree Physiology* 7:3-48.
- Daughtry, C., c. Walthall, M. Kim, E. Brown de Colstoun, and J. McMurtrey. 2000. Estimating corn leaf chlorophyll concentration from leaf and canopy reflectance. *Remote Sensing the Env.* 74:229-239.
- Deering, D., 1978. Rangeland reflectance characteristics measured by aircraft and spacecraft sensors. Ph.D. diss., Texas A&M University, College Station.
- de Farias Neto, A., G. Hartman, W. Pedersen, S. Li., G. Bollero, and B. Diers. 2006. Irrigation and inoculation treatments that increase the severity of soybean sudden death syndrome in the field. *Crop Sci.* 46:2547-2554.
- De Jong, S., E. Pebesma, and B. Lacaze. 2003. Above-ground biomass assessment of Mediterranean forest using airborne imaging spectrometry: The DAIS Payne experiment. *Int. J. of Remote Sensing.* 24:505-1520.
- Fehr, W., C. Caviness, D. Burmond, and J. Pennington. 1971. Stages of development descriptions for soybeans, *Glycine max* (L.) Merr. *Crop Sci.* 11:929-931.

- Fletcher, R., J. Smith, A. Mengistu, J. Ray. 2014. Relationships between microsclerotia content and hyperspectral reflectance data in soybean tissue infected by *Macrophomina phaseolina*. *American J. of Plant Sci.* 5:3737-3744
- Filella, I., and J. Penuelas. 1994. The red edge position and shape as indicators of plant chlorophyll content, biomass and hydric status. *Int. J. of Remote Sensing.* 15(7):1459-1470.
- Furbank, R., and M. Tester. 2011. Phenomics-technologies to relieve the phenotyping bottleneck. *Trends in Plant Sci.* Vol. 16. No.12:635-644. doi:10.1016/j.tplants.2011.09.005
- Gao, X., T. Jackson, G. Hartman, and T. Niblack. 2006. Interaction between the soybean cyst nematode and *Fusarium solani* f. sp. *Glycines* based on greenhouse factorial experiments. *Phytopathology.* 96:1409-1415.
- Gitelson, A., A. Vina, V. Ciganda, D. Rundquist, and T. Arkebauer. 2005. Remote estimation canopy chlorophyll content in crops. *Geophysical Res. Letters* 32:L08403. doi:10.1029/2005GL022688
- Gitelson, A., and M. Merzlyak. 1996. Signature analysis of leaf reflectance spectra: algorithm development for remote sensing of chlorophyll. *J. of Plant Phy.* 148:494-500.
- Gitelson, A., M. Merzlyak, and Y. Grits. 1996. Novel algorithms for remote sensing of chlorophyll content in higher plant leaves. *Geoscience and Remote Sensing Symposium, IGARSS. 'Remote Sensing for a Sustainable Future.* 4:2355-2357. DOI: 10.1109/IGARSS.1996.516985
- Gitelson, A., Y. Kaufman, R. Stark, and D. Rundquist. 2002. Novel algorithms for remote estimation of vegetation fraction. *Remote Sensing the Env.* 80:76-87.
- Godfray, H. J. Beddington, I. Crute, L. Haddad, and D. Lawrence, J. Muir, J. Pretty, S. Robinson, S. Thomas, and C. Thoulmin. 2010. Food security: the challenge of feeding 9 billion people. *Sci* 327:812-818.
- Gongora- Canul, and C., F. Leandro. 2011. Plant age affects root infection and development of foliar symptoms of soybean sudden death syndrome. *Plant Dis.* 95(3):242-247.
- Hartman, G., H. Chang, and L. Leandro. 2015. Research advances and management of soybean sudden death syndrome. *Crop Pro.* 73:60-65.
- Hartman, G., G. Noel, and L. Gray. 1995. Occurrence of soybean sudden death syndrome in East- Central Illinois and associated yield losses. *Plant Dis.* 79:314-318.
- Hatfield J., A. Gitelson, J. Schepers, and C. Walthall. 2008. Application of remote sensing for agronomic decisions. *Agron. J.* 100:S117-S131. doi:10.2134/agronj2006.0370c.

- Hershman, D., J. Hendrix, R. Stuckey, P. Bachi, and G. Henson. 1990. Influence of planting date and cultivar on soybean sudden death syndrome in Kentucky. *Plant Dis.* 74:761-766.
- Horler, D., M. Dockray, and J. Barber. 1983. The Red edge of plant leaf reflectance. *Int. J. of Remote Sensing.* 4(2): 273-288.
- Ji, J., M. Scott, and M. Bhattacharyya. 2006. Light is essential for degradation of ribulose- 1, 5 biphosphite carboxylase-oxygenase large subunit during sudden death syndrome development in soybean. *Plant Bio.* 8:597-505.
- Kandel, Y., K. Wise, C. Bradley, A. Tenuta, and D. Mueller. 2016. Effect of planting date, seed treatment, and cultivar on plant population, sudden death syndrome, and yield of soybean. *Plant Dis.* 100:1735-1743.
- Kandel, Y., K. Wise, C. Bradley, A. Tenuta, and D. Mueller. 2016. Fungicide and cultivar effects on sudden death syndrome and yield of soybean. *Plant Dis.* 100:1339-1350.
- Krezhova, D. 2011. Spectral remote sensing of the responses of soybean plants to environmental stresses, soybean - genetics and novel techniques for yield enhancement. Prof. Dora Krezhova (Ed.), ISBN: 978-953-307-721-5, InTech.
- Koenning, S., and J. Wrather. 2010. Suppression of soybean yield potential in the Continental United States by plant disease form 2006-2009. Online. *Plant Health Progress* doi:10.1094/PHP-010-1122-01-RS.
- Kummar, R., and L. Silva. 1973. Light ray tracing through leaf cross section. *Applied Optics.* 12(12):2950-2954.
- Lee, D., G. Shannon, and M. Choung. 2011. Application of nondestructive measurement to improve soybean quality by near infrared reflectance spectroscopy, soybean – applications and technology, Prof. Tzi-Bun Ng (Ed.), ISBN: 978-953-307-207-4, InTech.
- Leandro, L., A. Robertson, D. Mueller, and X. Yang. 2013. Climatic and environmental trends observed during epidemic and non-epidemic years of soybean sudden death syndrome in Iowa. Online. *Plant Health Progress* doi:10.1094/PHP-2013-0529-01-RS.
- Lichtenthaler, H., O. Wenzel, C. Buschmann, and A. Gitelson. 1998. Plant stress detection by reflectance and fluorescence. *Annals of the New York Academy of Sci* 851: 271-285. DOI: 10.1111/j.1749-6632.1998.tb09002.x.
- Lightfoot, D. 2015. Two decades of molecular marker-assisted breeding for resistance to soybean sudden death syndrome. *Crop Sci.* 56:1460-1484.

- Lin, W., C. Yang, and B. Kuo. 2012. Classifying cultivars of rice (*Oryza sativa* L.) based on corrected canopy reflectance spectra data using the orthogonal projections of latent structures (O-PLS) method. *Chem. Intell. Lab. Syst.* 115:25-36.
- Lou, Y., O. Meyer, D. Lightfoot, and M. Schmidt. 1999. Root colonization of soybean cultivars in the field by *Fusarium solani* f. sp. *glycines*. *Plant Dis.* 83(12):1155-1159.
- Lou, Y., K. Hildebrand, S. Chong, O. Myers, and J. Russin. 2000. Soybean yield loss to sudden death syndrome in relationship to symptom expression and root colonization by *Fusarium Solini* f. sp. *glycines*. *Plant Dis.* 84:914-920.
- Luckew, A., L. Leandro, M. Bhattaharyya, D. Nordman, D. Lightfoot, and S. Cianzio. 2013. Usefulness of 10 genomic regions in soybean associated with sudden death resistance. *Theory of Applied Genetics* 126:2391-2403.
- Ma, B., L. Dwyer, C. Costa, E. Cober, and M. Morrison. 2001. Early prediction of soybean yield from canopy reflectance measurements. *Agron. J.* 93:1227-1234.
- Mahlein, A., T. Rumpf, P. Welke, H. Dehne, L. Plumer, U. Steiner, and E. Oerke. 2013. Development of spectral indices for detection and identifying plant diseases. *Remote Sensing of Environment.* 128: 21-30. doi.org/10.1016/j.rse.2012.09.019.
- Marti, J., J. Bort, G. Slafer, and J. Araus. 2007. Can wheat yield be estimated by early measurements of normalized difference vegetation index? *Annals of Applied Biology.* 150:253-257.
- Melgar, J., and K. Roy. 1994. Soybean sudden death syndrome: cultivar reactions to inoculation in a controlled environment and host range and virulence of causal agent. *Plant Dis.* 78: 265-268.
- Melger, J., K. Roy, and T. Abney. 1994. Sudden death syndrome of soybean: etiology, symptomatology, and effects of irrigation and *Heterodera glycines* on incidence and severity under field conditions. *Canadian J. of Bot.* 72:1647- 1653.
- Montes J., A. Melchinger, and J. Reif. 2007. Novel throughput phenotyping platforms in plant genetic studies. *Trends in Plant Sci.* Vol12. No.10:433-436.
- Muhammed, H. 2005. Hyperspectral crop reflectance data for characterizing and estimating fungal disease severity in wheat. *Biosystems Engineering* 91(1):9-20. doi:10.1016/j.biosystemseng.2005.02.007.
- Njiti, V., T. Doubler, R. Sutter, L. Gray, P. Gibson, and D. Lightfoot. 1998. Resistance to soybean death syndrome and root colonization by *Fusarium solani* f. sp. *Glycine* in near-isogenic lines. *Crop Sci.* 38:472-477.

- Nutter, F., G. Tylka, J. Guan, A. Moreira, C. Marett, T. Rosburg, J. Basart, and C. Chong. 2002. Use of remote sensing to detect soybean cyst nematode-induced plant stress. *J. of Nematology* 34(3):222-231.
- Ortiz- Ribbing, L., and D. Eastburn. 2004. Soybean root systems and sudden death syndrome severity: taproot and lateral root infection. *Plant Dis.* 88:1011-1016.
- Penuelas, J., I. Filella, C. Biel, L. Serrano, and R. Save. 1993. The reflectance at the 950-970 nm regions as an indicator of plant water status. *Int. J. of Remote Sensing* 14(10):1887-1905.
- Penuelas, J., R. Isla, I. Filella, and J. Araus. 1996. Visible and near infrared reflectance assessment of salinity effects barley. *Crop Sci.* 37:198-202.
- Penuelas, J., and I. Filella. 1998. Visible and near-infrared reflectance techniques for diagnosing plant physiological status. *Sci.* 3(4):151-155.
- Phalan, B., M. Onial, A. Balmford, and R. Green. 2011. Reconciling food production and biodiversity conservation: land sharing and land sparing compared. *Sci.* 333:1289-1291.
- Prasad, A., L. Chai, R. Singh, and M. Kafatos. 2006. Crop yield estimation model for Iowa using remote sensing and surface parameters. *Int. J. of Applied Earth Obs. and Geoinformation* 8: 26-33. doi:10.1016/j.jag.2005.06.002.
- Prasad, B., B. Carver, M. Stone, M. Baber, W. Raun, A. Klatt. 2007. Genetic analysis of indirect selection for winter wheat grain yield using spectral reflectance indices. *Crop Sci.* 47: 1416-1425. doi: 10.2135/cropsci2006.08.0546
- Prabhu, R., V. Njiti, B. Bell-Johnson, J. Johnson, M. Schmidt, J. Klien, and D. Lightfoot. 1999. Selecting soybean cultivars for dual resistance to soybean cyst nematode and sudden death syndrome using two DNA markers. *Crop Sci.* 39:982-987.
- Printer Jr., P., J. Hatfield, J. Shepers, E. Barnes, and M. Moran. 2003. Remote sensing for crop management. *Photogrammetric Engineering and Remote Sensing* 69(6):647-664.
- Ray, D., N. Muller, P. West, and J. Foley. 2013. Yield trends are insufficient to double global crop production by 2050. *PLoS ONE* 8(6):e66428.
- Roy, K, J. Rupe, D. Hershman, and T. Abney. 1997. Sudden death syndrome of soybean. *Plant Dis.* 81(10):1000-1111.
- Roy, K., G. Lawrence, and K. Mclean. 1989. Isolation and identification of *Fusarium solani*, the cause of sudden death syndrome of soybean. *Plant Diagnostic Quarterly* 10:17-27.
- Royo, C., F. Alvaro, V. Martos, A. Ramdani, J. Isidro, D. Villegas, and L. Garcia del Moral. 2007. Genetic changes in durum wheat yield components and associated traits in Italian

- and Spanish varieties during the 20th Century. *Euphytica* 155:259-270. DOI 10.1007/s10681-006-9327-9
- Rupe, C. 1989. Frequency and pathogenicity of *Fusarium solani* recovered from soybeans with sudden death syndrome. *Plant Dis.* 73:581-584.
- Sankaran, S., S. Mishra, R. Ehsani, and C. Davis. 2010. A review of advanced techniques for detecting plant diseases. *Computers and Electronics in Agriculture* 72:1-13. doi:10.1016/j.compag.2010.02.007.
- Scherm, H., and X. Yang. 1996. Development of sudden death syndrome of soybean in relation to soil temperature and soil water matric potential. *Phytopathology* 86(6):642-649.
- Shimada, S., M. Kokubun, and S. Matsui. 1995. Effects of water table on physiological traits and yield of soybean. *Japanese J. of Crop Sci.* 64(2):294-303.
- Sulik, J., D. Long. 2016. Spectral considerations for modeling yield in canola. *Remote Sensing the Env.* 184: 161-174. doi.org/10.1016/j.rse.2016.06.016.
- Swaminathan, S., N. Abeysekara, M. Liu, S. Cianzio, and M. Bhattacharyya. 2015. Quantitative trait loci underlying host response of soybean to *Fusarium virguliforme* toxins that cause foliar sudden death syndrome. *Theory of Applied Genetics.* doi 10.1007/s00122-015-2643-5.
- Tagarakis, A., Q. Keterings, S. Lyons, and G. Godwin. 2017. Proximal sensing to estimate yield of brown midrib forage sorghum. *Agron. J.* 109:107-114. doi:10.2134/agronj2016.07.0414.
- Tewoldemedhin, Y., S. Lamprecht, M. Vaughan, and G. O'Donnell. 2017. Soybean SDS in South Africa caused by *Fusarium brailiense* and a novel undescribed *Fusarium sp.* *Plant Dis.* 101:150-157.
- Tucker, C., J. Elgin, and J. McMurtrey. 1978. Monitoring corn and soybean crop development by remote sensing techniques. NASA Technical Memorandum 79607.
- USDA Economic Research Service. 2017. Oil Crops Data. <http://www.ers.usda.gov/data-products/oil-crops-yearbook.aspx>.
- USDA FAS. 2017. Oilseeds: World Markets and Trade. <https://apps.fas.usda.gov/psdonline/app/index.html#/app/downloads>.
- USDA FAS. 2017. World Agricultural Production.
- USDA NASS. 2016. Acreage Report. ISSN 1949-1522.

- Vick, C., S. Chong, J. Bond, and J. Russin. 2003. Response of soybean sudden death syndrome to subsoil tillage. *Plant Dis.* 87:629-632.
- Vigier, B., E. Pattey, and I. Strachan. 2004. Narrowband vegetation indexes and detection of disease damage in soybeans. *GeoSci and Remote Sensing Letter.* 1(4):255-259.
- Weber, V., J. Araus, J. Cairns, C. Sanchez, A. Melchinger, and E. Orsini. 2012. Prediction of grain yield using reflectance spectra of canopy and leaves in maize plants grown under different water regimes. *Field Crop Research* 128:82-90.
- White, J. P. Andrade-Sanchez, M. Gore, K. Bronson, T. Coffelt, M. Conley, K. Feldmann, A. French, J. Heun, D. Hunsaker, G. Wall, and G. Wang. 2012. Field based phenomics for plant genetic research. *Field Crop Research* 133:101-112.
- Woolley, J. 1971. Reflectance and transmittance of light by leaves. *Plant Phy.* 47: 656-662.
- Wen, Z., R. Tan, J. Yuan, C. Bales, W. Du, S. Zhang, M. Chilvers, C. Schmidt, Q. Song, P. Cregan, and D. Wang. 2014. Genome-wide association mapping of quantitative resistance to sudden death syndrome in soybean. *BMC Genomics* 15:809.
- Wrather, J., S. Kending, S. Anand, T. Niblack, and G. Smith. 1995. Effects of tillage, cultivar, and planting date on percentage of soybean leaves with symptoms of sudden death syndrome. *Plant Dis.* 79:560-562.
- Xing, L., and A. Westphal. 2006. Interaction of *Fusarium solani* f. sp. *Glycines* and *Heterodera glycines* in sudden death syndrome of soybean. *Phytopathology* 93:763-770.
- Yang, S., X. Li, C. Chen, P. Kyveryga, X. Yang. 2016. Assessing field-specific risk of soybean sudden death syndrome using satellite imagery in Iowa. *Phytopathology* 106(8): 842-853. <http://dx.doi.org/10.1094/PHYTO-11-15-0303-R>.

Tables and Figures

Table 2.1. Analysis of variance F-values for disease index, disease incidence, disease severity, yield, and maturity for a nested association mapping population.

Source	df	Disease Index	Disease Incidence	Disease Severity	Yield	Maturity
Entry	159	83.9***‡	51.24***	49.19***	123.07**	111.1***
Environment	2	9.7**†	9.02**	21.17**	12.64**	18.55**
Entry x Environment	318	8.31***	10.16***	6.08***	14.57***	58.09***

†*** indicates significance at <.001

Table 2.2. Least square means and ranges for disease index, disease incidence, disease severity, yield and maturity for a nested association mapping population.

Environment		Disease Index	Disease Incidence	Disease Severity	Yield	Maturity
		(Score)	(%)	(Score)	(t/ha ⁻¹)	(Days after Aug. 31)
2015 Manhattan	Mean	8.5a†	24.3a	1.9a	3.03a	23a
	Range	0 - 57	0-90	0-6	1.65 - 4.4	14-33
2016 Manhattan	Mean	12.1b	32.6b	2.8b	2.8a	20b
	Range	0-67	2-80	1-8	1.0-3.7	14-36
2016 Rossville	Mean	15.4b	37.4b	3.4c	2.5b	20b
	Range	1-69	2-85	0-7	3.0-2.8	15-25

†Number followed by different by the same letter were significantly different at P< .05.

Table 2.3. Soybean variety performance test entries analysis of variance F-values for disease index, disease incidence, disease severity, yield and maturity in three environments.

Source	df	Disease Index	Disease Incidence	Disease Severity	Yield	Maturity
Entry	215	16.5***†	10.7***	7.3***	11.1***	32.4***
Environment	2	47.1***	6.8***	95.1***	46.3***	103.9***
Entry by Environment	199	3.0***	2.0***	1.9***	3.3***	16.9***

†*** indicates significance at <.001

Table 2.4. Soybean Variety Performance Test Entry least square means and ranges for disease index, disease incidence, disease severity, yield and maturity.

Environment		Disease Index (Score)	Disease Incidence (%)	Disease Severity (Score)	Yield (t/ha-1)	Maturity (Days after Aug. 31)
2015 Manhattan	Mean	9.2a†	29.5a	2.1a	3.5a	30a
	Range	0-76	2-85	1-8	.79-4.8	19-46
2016 Manhattan	Mean	14.4b	32.0b	2.9b	3.4a	34b
	Range	0-92	0-100	0-8	.33-4.6	18-56
2016 Rossville	Mean	16.5c	33.9b	3.4c	3.1b	33c
	Range	0-83	0-100	0-8	1.2-5.5	17-53

†Number followed by different by the same letter were significantly different at P< .0

Table 2.5. Pearson’s correlations (r) between entry means for disease index, yield and maturity at all three environments for both the nested association mapping population and soybean variety performance test population.

Environment	n		Yield	Maturity
2015 NAM† Manhattan	159	Maturity	.26***	
		Disease Index	-.65***	-.36***
2016 NAM Manhattan	160	Maturity	.57***	
		Disease Index	-.61***	-.10
2016 NAM Rossville	160	Maturity	.40***	
		Disease Index	-.62***	0.06
2015 SVPT‡ Manhattan	145	Maturity	0.05	
		Disease Index	-.72***	0.11
2016 SVPT Manhattan	140	Maturity	0.01	
		Disease Index	-0.80***	0.01
2016 SVPT Rossville	140	Maturity	.32***	
		Disease Index	-.63***	0.01

† Nested association mapping population (NAM)

‡ Soybean variety performance test (SVPT)

*** indicates significance at $p < .0001$

Table 2.6. Coefficient of determination (R^2) values for stepwise regression models for disease index, yield and maturity based on season averages in the total population, early maturity group, middle maturity group, and late maturity group, checks, and season average model including maturity for the nested association mapping population. Coefficient of determination (R^2) values for stepwise regression models for the disease index, yield and maturity based on season averages and common entry models for soybean variety performance test population.

Environment	Waveband Models	n	Disease Index	Model	
				Yield	Maturity
			R^2		
2015 NAM‡ Manhattan	Season Average (SA)	160	.52***	.41***	.46***
	Early	43	.37***	.31**	.16**
	Middle	64	.55***	.41***	NS
	Late	52	.54***	.49***	NS
	August 31st	160	.55***	.40***	.46***
	Check	19	.68**	.56**	.22*
	SA with Maturity	160	.52***	.41***	
2016 NAM Manhattan	Season Average (SA)	160	.16***	.66***	.56***
	Early	62	.08*	.39***	.24**
	Middle	78	.35***	.60**	.25***
	Late	20	NS	NS	NS
	September 1st	160	.11***	.54**	.57***
	Check	20	.55***	.80***	.58**
	SA with Maturity	160	.18***	.58***	
2016 NAM Rossville	Season Average (SA)	160	.28***	.78***	.64***
	Early	54	.44***	.72***	NS
	Middle	87	.42**	.75***	.24***
	Late	19	.77***	.92***	NS
	September 2nd	160	.24***	.77***	.62***
	Check	19	.73***	.93***	.72***
	SA with Maturity	160	.42***	.81***	
NAM Grand Means	All Lines	160	.29***	.71***	.63***
	Checks	20	.69***	.83**	.72***
2015 SVPT ⁺ Manhattan	Season Average	145	NS	.05**	.03*
2016 SVPT Manhattan	Season Average	145	.42**	.79***	.78***
2016 SVPT Rossville	Season Average	145	.31***	.43***	.74***

* indicates significant at the .05 probability level

** indicates significant at the .001 probability level

*** indicates significant at the .0001 probability level

† NS indicates not significant at the .05 probability level

‡ NAM nested association mapping populations

⁺ SVPT indicates soybean variety performance test

Table 2.7. Wavebands selected by stepwise regression models to predict disease index, yield, and maturity based on reflectance values using season averages, individual days, and checks entries only for both 2015 and 2016 in Manhattan.

2015 NAM [†] Manhattan	Season Average (SA)	31-Aug	Check	SA with Maturity
Disease Index Model Wavebands	535nm, 585nm	415nm, 535nm, 595nm	795nm, 875nm	545nm, 565nm
Yield Model Waveband	405nm, 455nm, 525nm, 585nm	405nm, 495nm, 525nm, 585nm, 595 nm	505nm, 745nm	405nm, 45nm, 525nm, 585 nm
Maturity Model Waveband	645nm, 675nm, 685nm, 695 nm, 785nm, 805nm	415nm, 445nm, 565nm, 605nm	805nm	
2016 NAM Manhattan	Season Average (SA)	1-Sep	Check	SA with Maturity
Disease Index Model Waveband	505nm, 675nm, 755nm	675nm,685nm	475nm	mat, 505nm, 675nm, 755nm
Yield Model Waveband	505nm, 685nm, 755nm, 775 nm, 805nm	665nm, 735nm, 755nm	505nm, 765nm	505nm, 685nm, 755nm, 775nm, 805nm
Maturity Model Waveband	635nm, 675nm, 695 nm, 765nm	495nm, 555nm, 595nm, 635nm, 645nm, 805 nm, 875 nm	505nm, 625nm	

[†] NAM indicates nested association mapping population

Table 2.8. Wavebands selected by stepwise regression models to predict disease index, yield, and maturity using season average, individual days, and checks for 2016 in Rossville.

2016 NAM [†] Rossville	Season Average (SA)	2-Sep	Check	SA with Maturity
Disease Index Model Wavebands	765nm, 805nm, 865nm, 885nm	755nm, 895nm	735nm	mat, 715nm, 765nm, 865nm
Yield Model Wavebands	575nm, 675nm, 685nm, 705nm, 745nm, 755nm	585nm, 675nm, 685nm, 705nm, 815nm, 845nm	775nm, 875nm	mat, 525nm, 575nm, 675nm, 685nm, 715nm, 825nm, 885nm
Maturity Model Wavebands	655nm, 665nm, 675nm, 705nm, 805nm	615nm, 645nm, 835nm	515nm, 585nm	

[†] NAM indicates nested association mapping population

Table 2.9. Wavebands selected by stepwise regression models to predict disease index, yield, and maturity using nested association mapping population divided into early, middle, and late maturity groups for 3 environments.

2015 NAM† Manhattan	Early	Middle	Late
Disease Index Model Wavebands	605nm, 745nm	405nm, 485nm, 525nm, 595 nm, 695nm	535nm, 595nm
Yield Model Wavebands	605nm, 745nm	405nm, 605nm, 765nm, 795nm	545nm, 585nm
Maturity Model Wavebands	665nm	NS‡	NS
2016 NAM Manhattan	Early	Middle	Late
Disease Index Model Wavebands	675nm, 685nm	485nm, 745nm	NS
Yield Model Wavebands	745nm	495nm, 885nm	NS
Maturity Model Wavebands	665nm, 675m	505nm, 695nm	NS
2016 NAM Rossville	Early	Middle	Late
Disease Index Model Wavebands	485nm,565nm	675nm, 805nm, 875nm	805m, 885nm
Yield Model Wavebands	605nm,675nm, 685nm, 695nm	735nm, 775nm, 805nm, 895nm	675nm, 755nm
Maturity Model Wavebands	NS	665nm, 695nm, 805nm	NS

† NAM indicates nested association mapping population

‡ NS indicates that no significant wavebands entered the model at $p < .05$

Table 2.10. Wavebands selected by stepwise regression models to predict disease index, yield, and maturity soybean variety performance test population season average at 3 environments.

2015 SVPT† Manhattan		Season Average (SA)
Disease Index Model Wavebands		NS‡
Yield Model Wavebands		785nm
Maturity Model Wavebands		675nm
2016 SVPT Manhattan		Season Average (SA)
Disease Index Model Wavebands		765nm, 795nm, 825nm, 855nm, 895nm
Yield Model Wavebands		595nm, 625nm, 665nm, 675nm, 685nm, 705nm, 825nm, 845nm
Maturity Model Wavebands		485nm, 495nm, 525nm, 595nm, 635nm, 695nm, 705nm, 825nm
2016 SVPT Rossville		Season Average (SA)
Disease Index Model Wavebands		405nm, 765nm, 805nm
Yield Model Wavebands		555nm, 745nm, 755nm, 895nm
Maturity Model Wavebands		555nm, 805nm, 815nm, 835nm, 855nm

† SVPT indicates soybean variety performance test population

‡ NS indicates that no significant wavebands entered the model at $p < .05$

Table 2.11. Wavebands selected by stepwise regression models to predict disease index, yield, and maturity using nested association mapping population grand means.

NAM† Grand Means	Disease Index	Yield	Maturity
All Entries Model Waveband	775nm, 885nm	505nm, 775nm, 795nm, 895nm	625nm, 675nm, 695nm, 825nm
Check Model Waveband	675nm, 685nm	505nm, 665nm, 805nm	445nm, 715nm, 895nm

† NAM indicates nested association mapping population

‡ NS indicates that no significant wavebands entered the model at $p < .05$

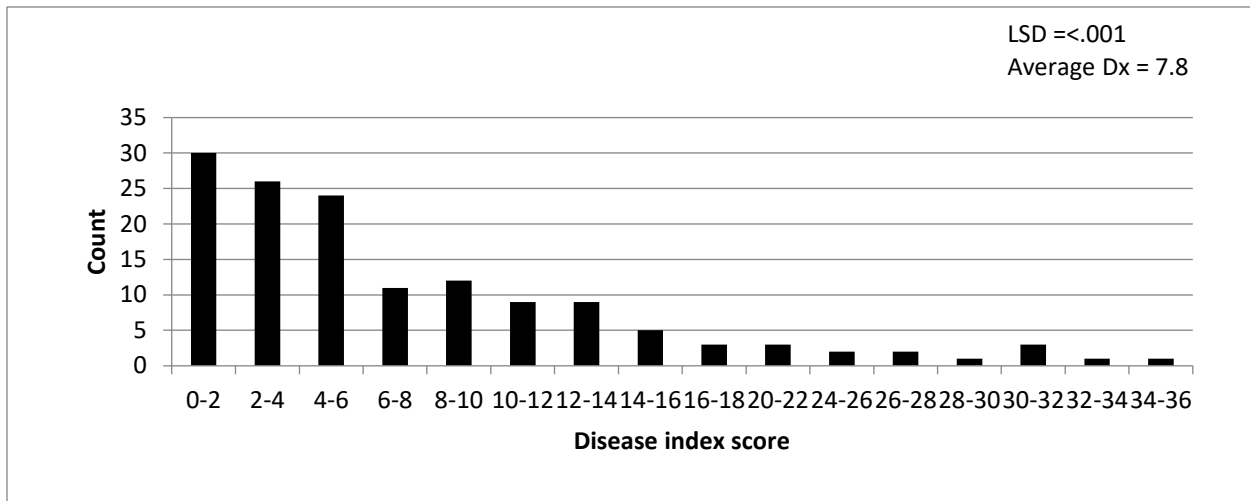


Figure 2.1 a. Distribution of season average disease index scores for recombinant inbred lines in a nested association mapping population grown in Manhattan in 2015.

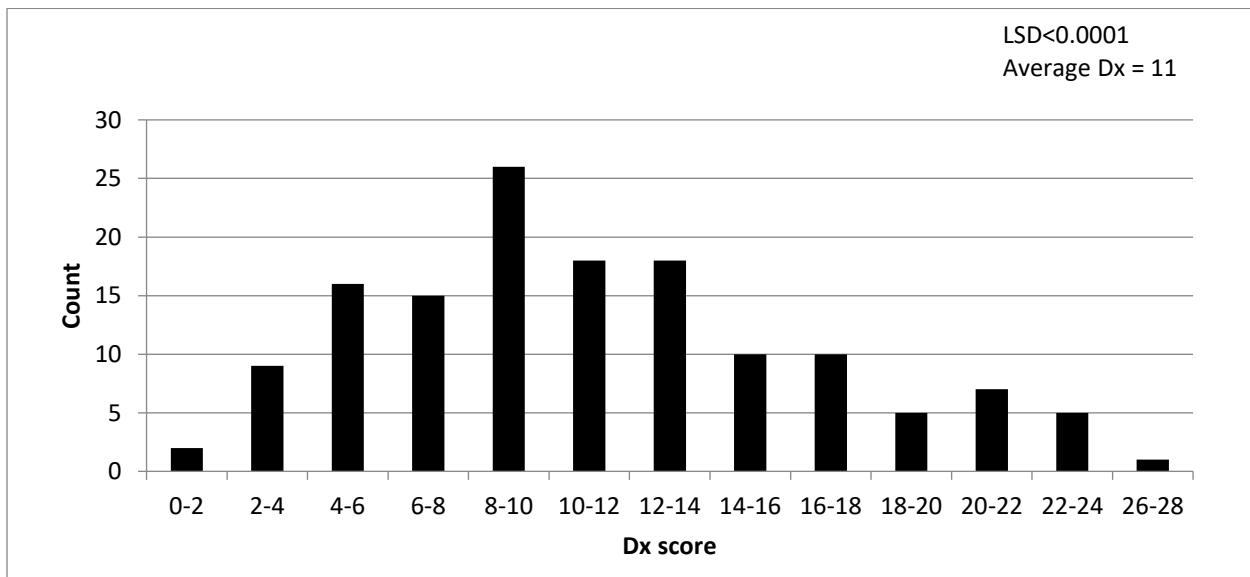


Figure 2.1 b. Distribution of season average disease index scores for recombinant inbred lines in a nested association mapping population grown in Manhattan in 2016.

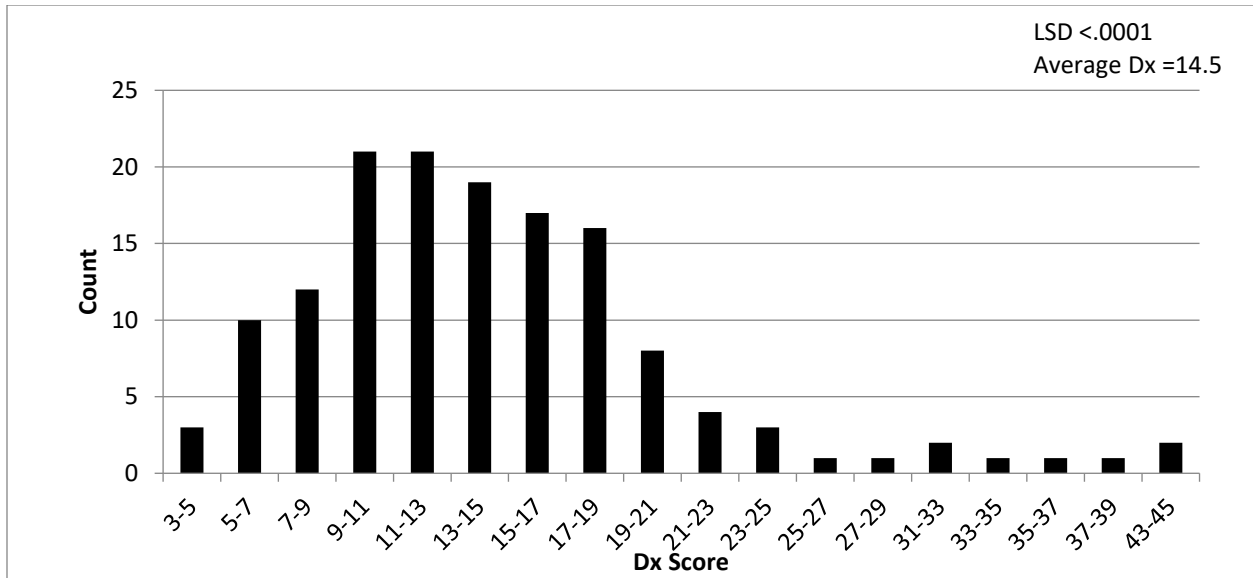


Figure 2.1 c. Distribution of season average disease index scores for recombinant inbred lines in a nested association mapping population grown in Rossville in 2016.

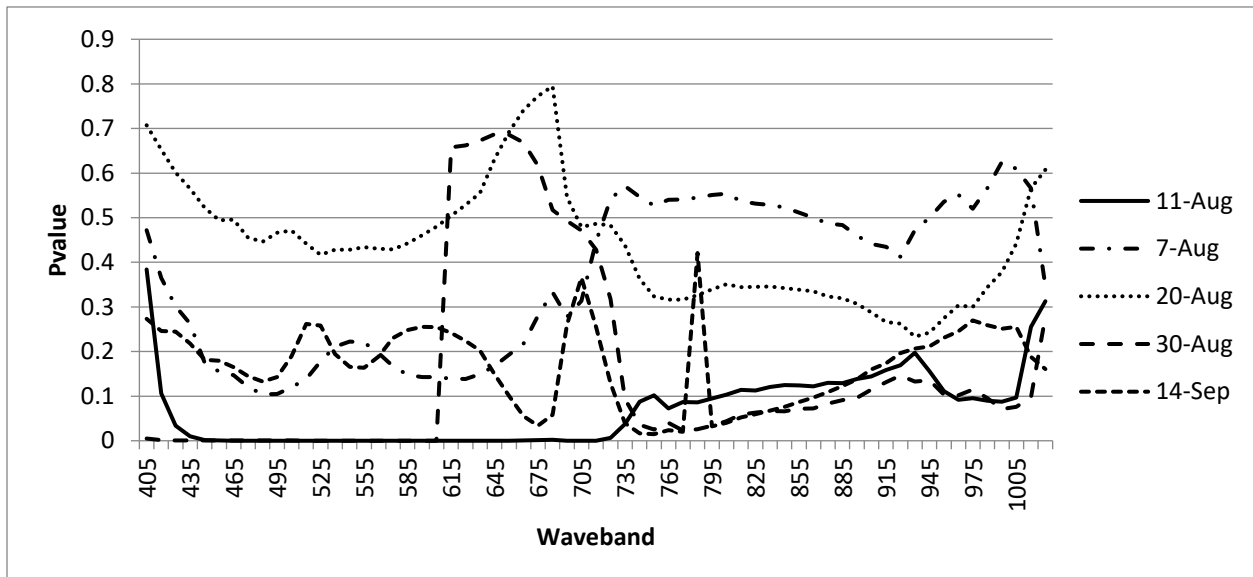


Figure 2.2 a. P-values for entry main effect for individual waveband reflectance measurements of individual day readings for a nested association mapping population grown at Manhattan in 2015.

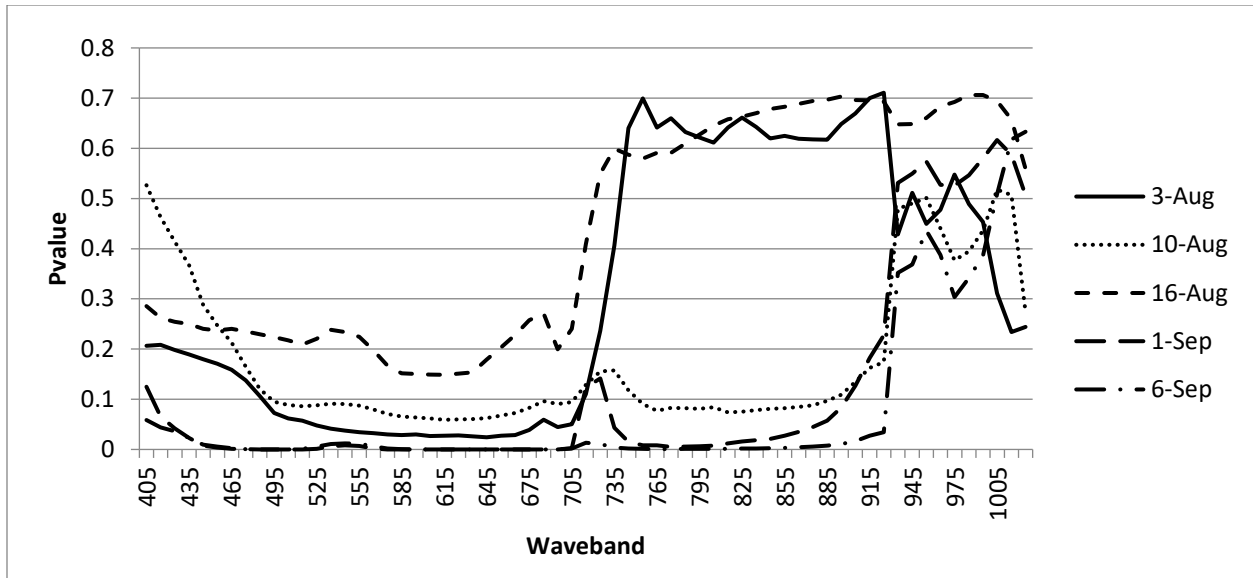


Figure 2.2 b. P-values for entry main effect for individual waveband reflectance measurements of individual day readings for a nested association mapping population grown at Manhattan in 2016.

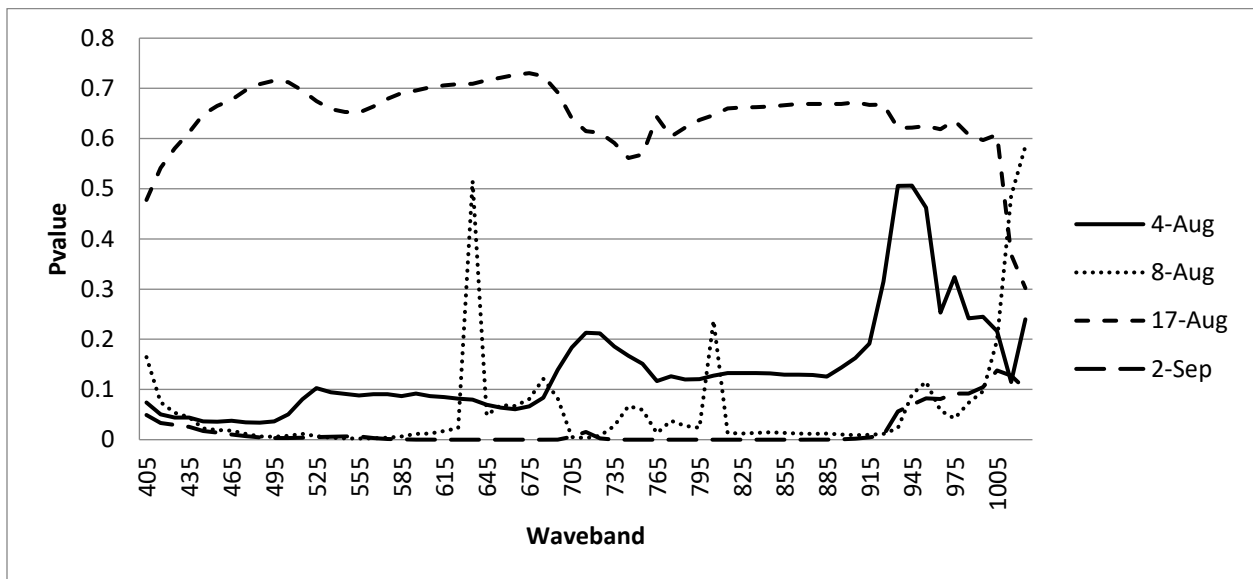


Figure 2.2 c. P-values for entry main effect for individual waveband reflectance measurements of individual day readings for a nested association mapping population grown at Rossville in 2016.

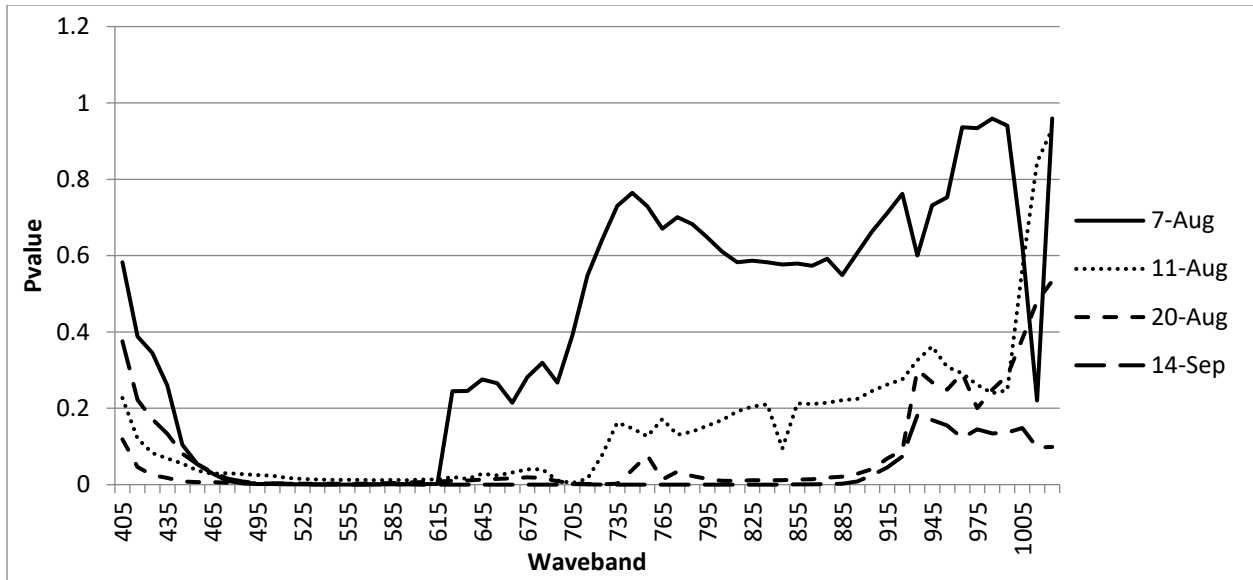


Figure 2.3 a. P-values for entry main effect for individual waveband reflectance measurements of individual day readings for the Soybean Variety Performance Test Population grown at Manhattan in 2015.

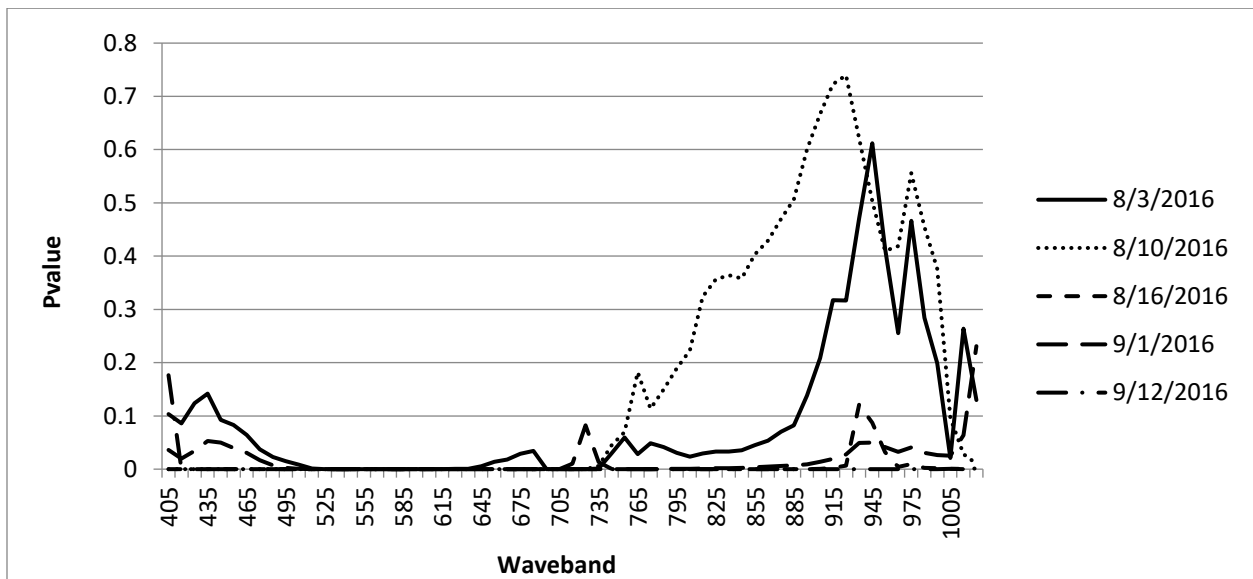


Figure 2.3 b. P-values for entry main effect for individual waveband reflectance measurements of individual day readings for the Soybean Variety Performance Test Population grown at Manhattan in 2016.

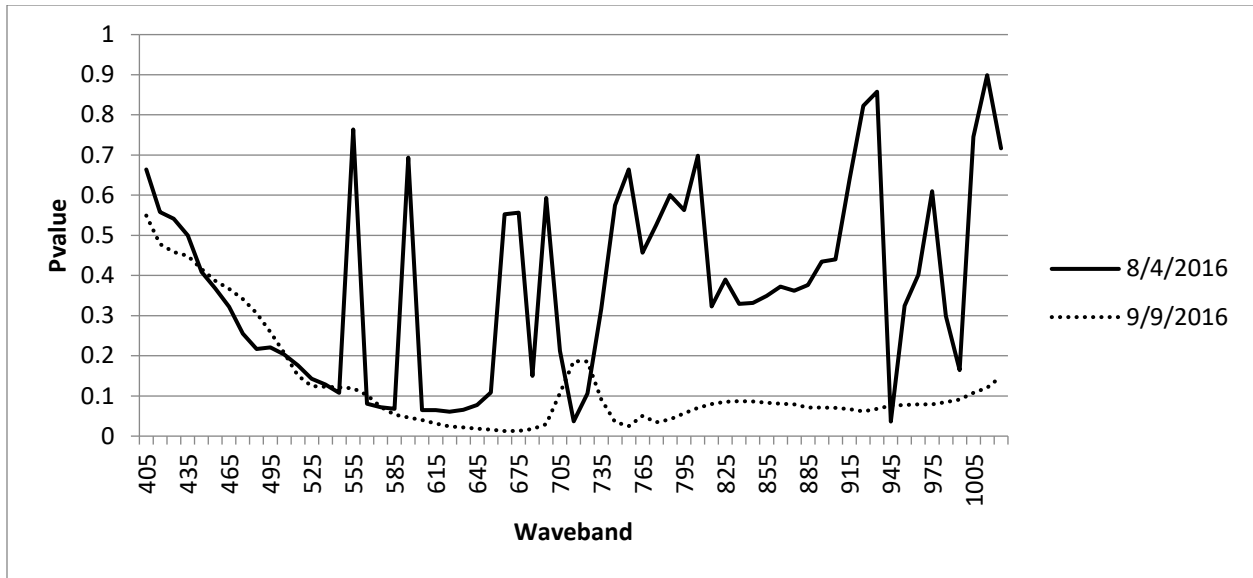


Figure 2.3 c. P-values for entry main effect for individual waveband reflectance measurements of individual day readings for the Soybean Variety Performance Test Population grown at Rossville in 2016.

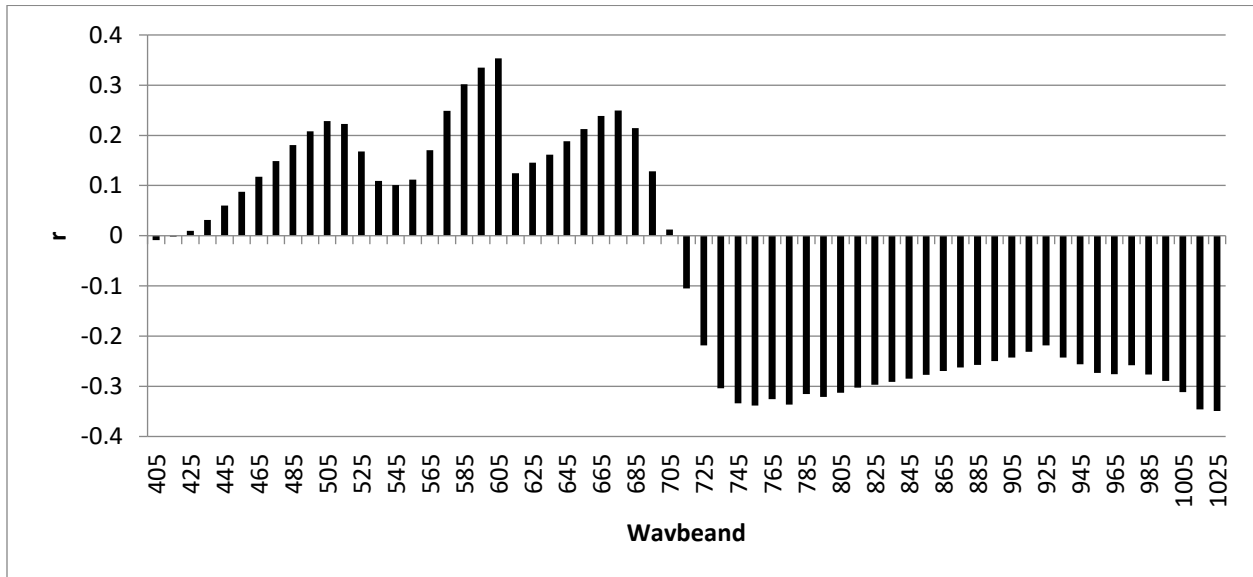


Figure 2.4 a. Pearson's correlation (r) between disease index and season average waveband reflectance for a nested association mapping population grown at Manhattan in 2015. Significant correlation at $\alpha = .05$ is equal to $r \leq -.15$ and $r \geq .15$. Significant correlation at $\alpha = .01$ is equal to $r \leq -.20$ and $r \geq .20$.

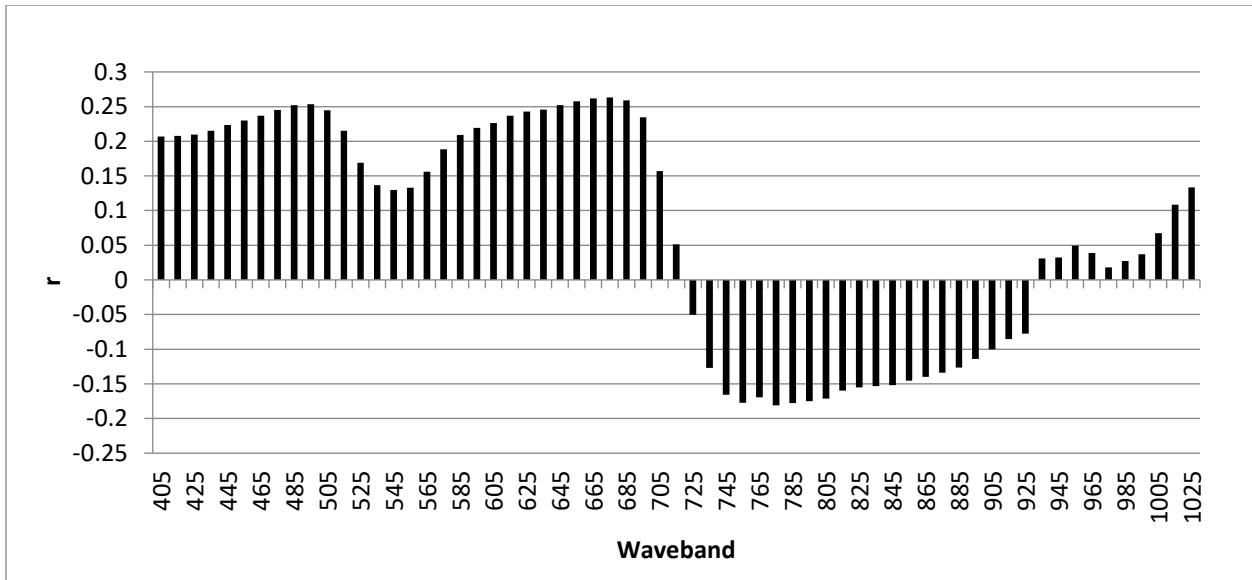


Figure 2.4 b. Pearson's correlation (r) between disease index and season average waveband reflectance for a nested association mapping population grown at Manhattan in 2016. Significant correlation at $\alpha = .05$ is equal to $r \leq -.15$ and $r \geq .15$. Significant correlation at $\alpha = .01$ is equal to $r \leq -.20$ and $r \geq .20$.

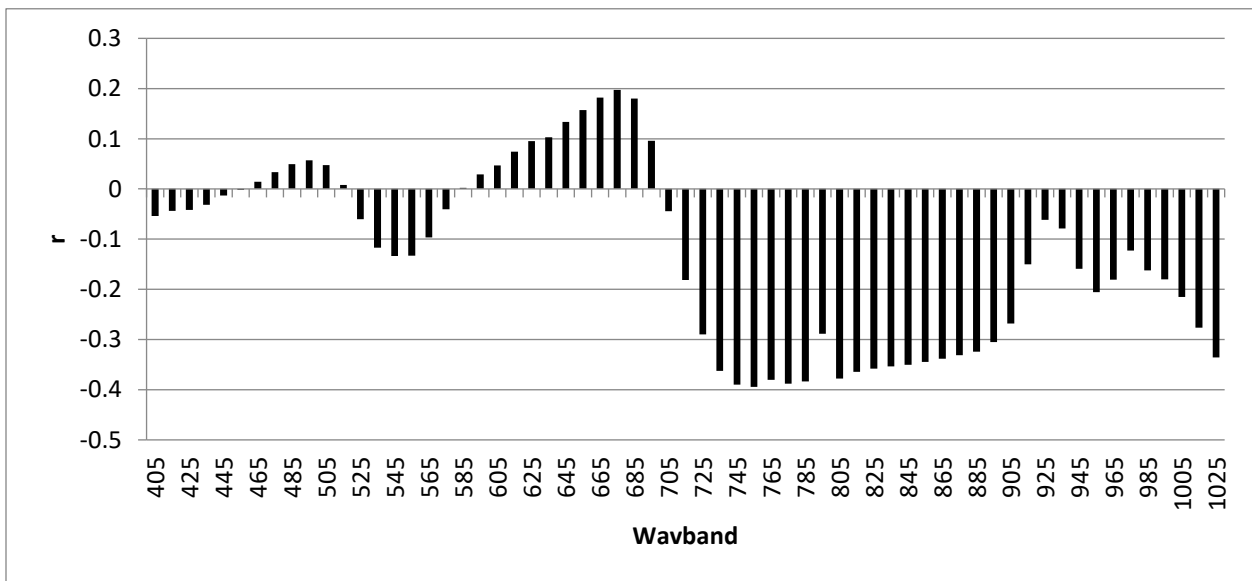


Figure 2.4 c. Pearson's correlation (r) between disease index and season average waveband reflectance for a nested association mapping population grown at Rossville in 2016. Significant correlation at $\alpha = .05$ is equal to $r \leq -.15$ and $r \geq .15$. Significant correlation at $\alpha = .01$ is equal to $r \leq -.20$ and $r \geq .20$.

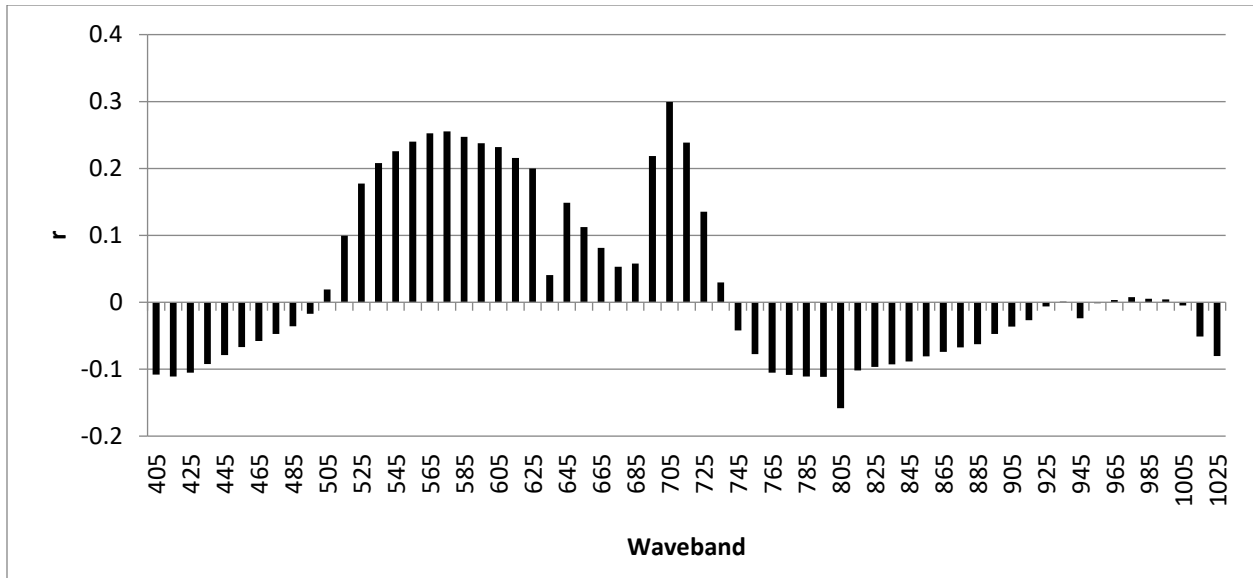


Figure 2.5 a. Pearson's correlation (r) between disease index and August 8 waveband reflectance for a nested association mapping population grown at Rossville in 2016. Significant correlation at $\alpha = .05$ is equal to $r \leq -.15$ and $r \geq .15$. Significant correlation at $\alpha = .01$ is equal to $r \leq -.20$ and $r \geq .20$.

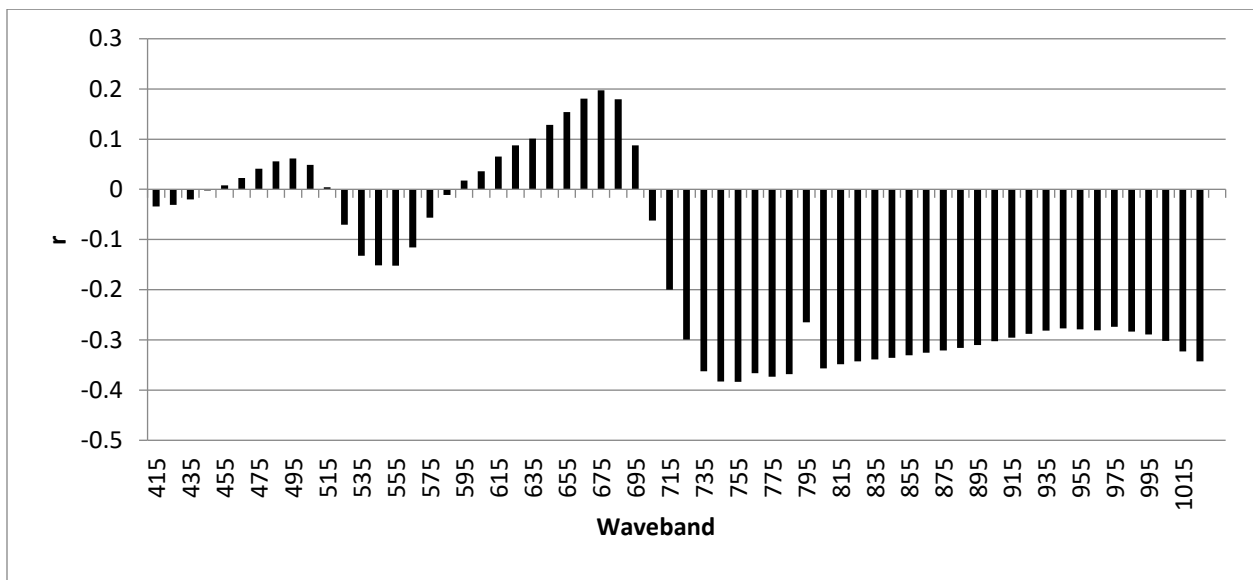


Figure 2.5 b. Pearson's correlation (r) between disease index and September 2 waveband reflectance for a nested association mapping population grown at Rossville in 2016. Significant correlation at $\alpha = .05$ is equal to $r \leq -.15$ and $r \geq .15$. Significant correlation at $\alpha = .01$ is equal to $r \leq -.20$ and $r \geq .20$.

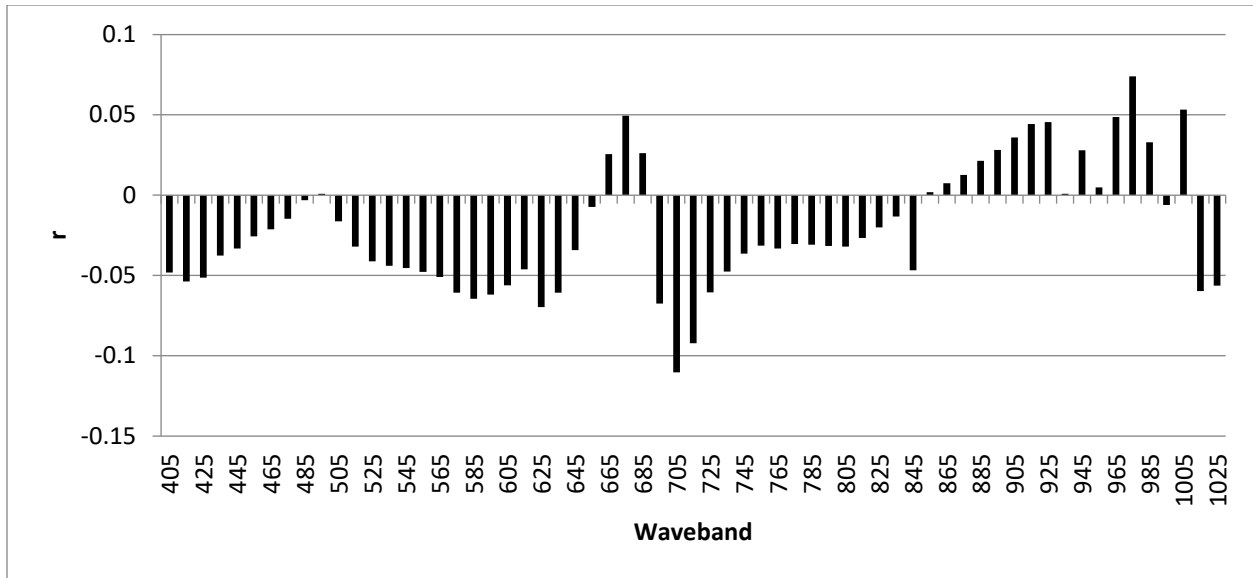


Figure 2.6 a. Pearson's correlation (r) between disease index and season average waveband reflectance of the soybean variety performance test population grown at Manhattan in

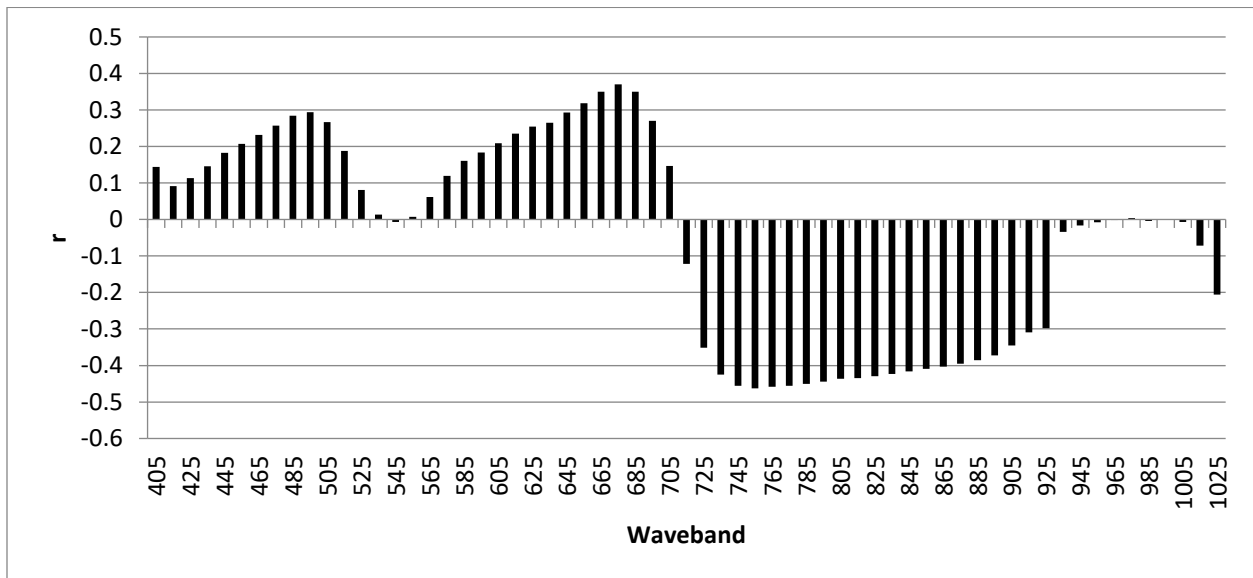


Figure 2.6 b. Pearson's correlation (r) between disease index and season average waveband reflectance of the soybean variety performance test population grown at Manhattan in 2016. Significant correlation at $\alpha = .05$ is equal to $r \leq -.15$ and $r \geq .15$. Significant correlation at $\alpha = .01$ is equal to $r \leq -.20$ and $r \geq .20$

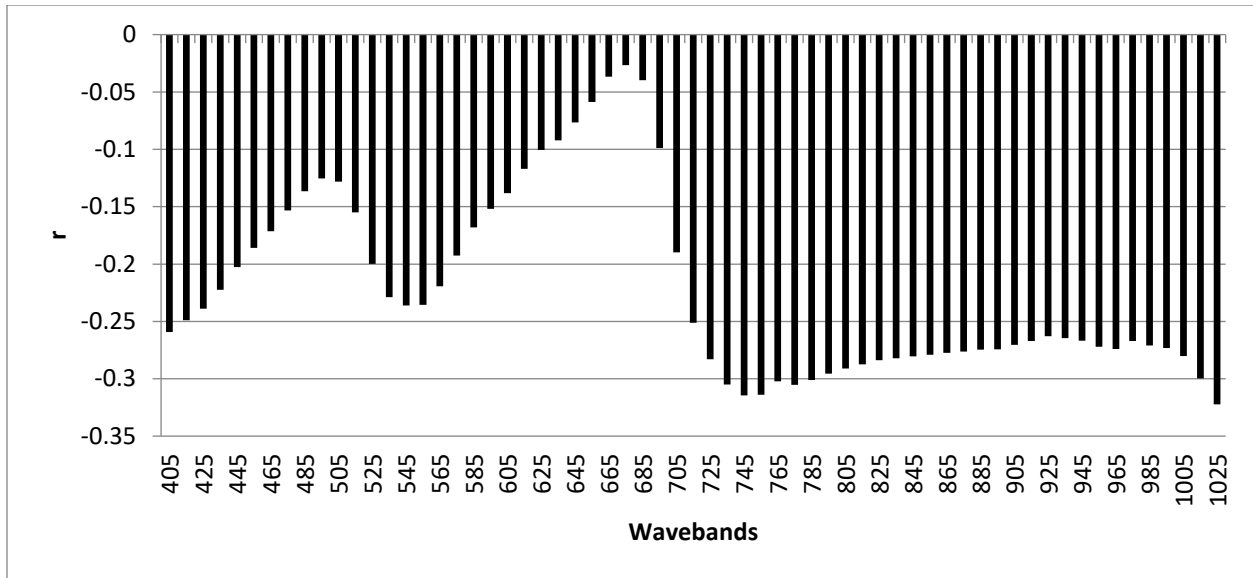


Figure 2.6 c Pearson's correlation (r) between disease index and September 9 waveband reflectance of the soybean variety performance test population grown at Rossville in 2016. Significant correlation at $\alpha = .05$ is equal to $r \leq -.15$ and $r \geq .15$. Significant correlation at $\alpha = .01$ is equal to $r \leq -.20$ and $r \geq .20$.

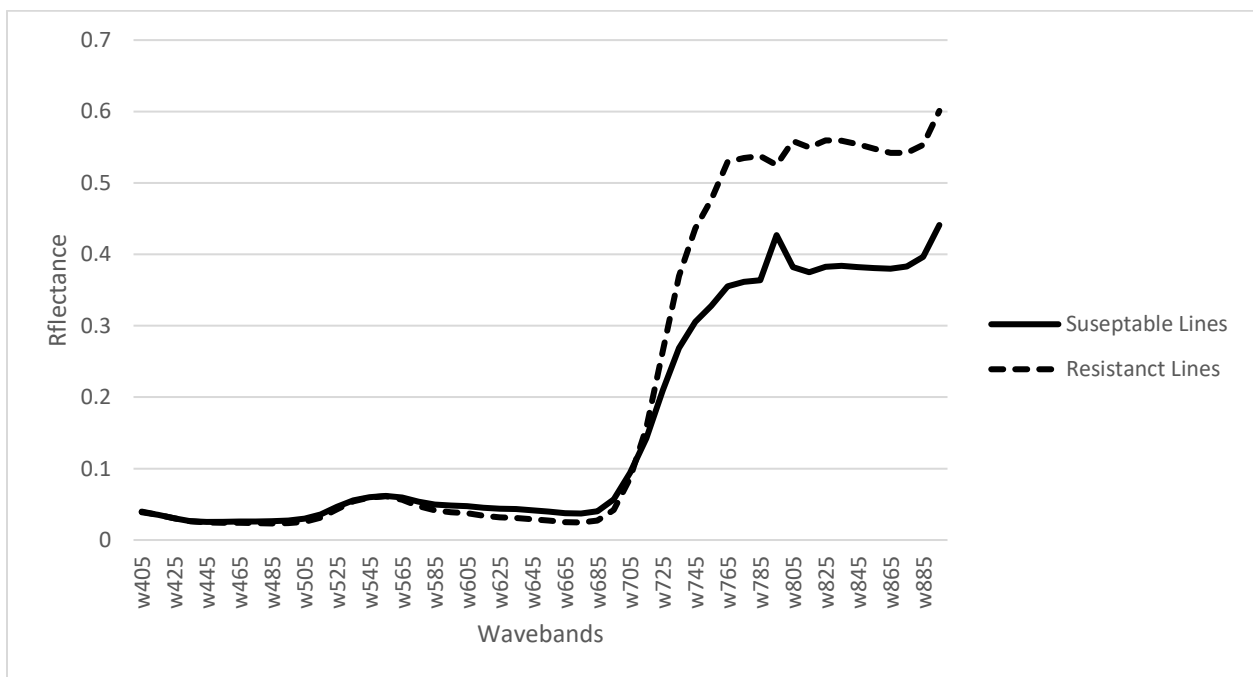


Figure 2.7 a. Average spectral reflectance curves of SDS susceptible lines and SDS resistant lines at Manhattan 2015.



Figure 2.7 b. Average spectral reflectance curves of SDS susceptible lines and SDS resistant line at Manhattan 2016.

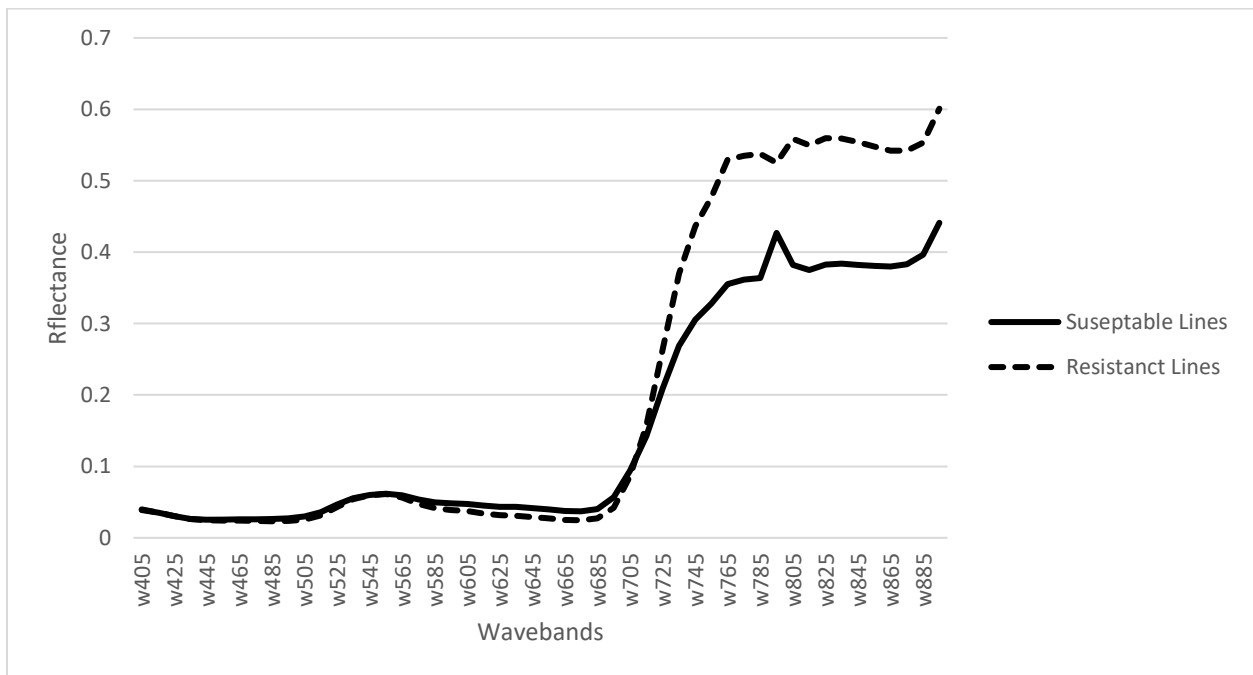


Figure 2.7 c. Average spectral reflectance curves of SDS susceptible lines and SDS resistant lines at Rossville in 2016.

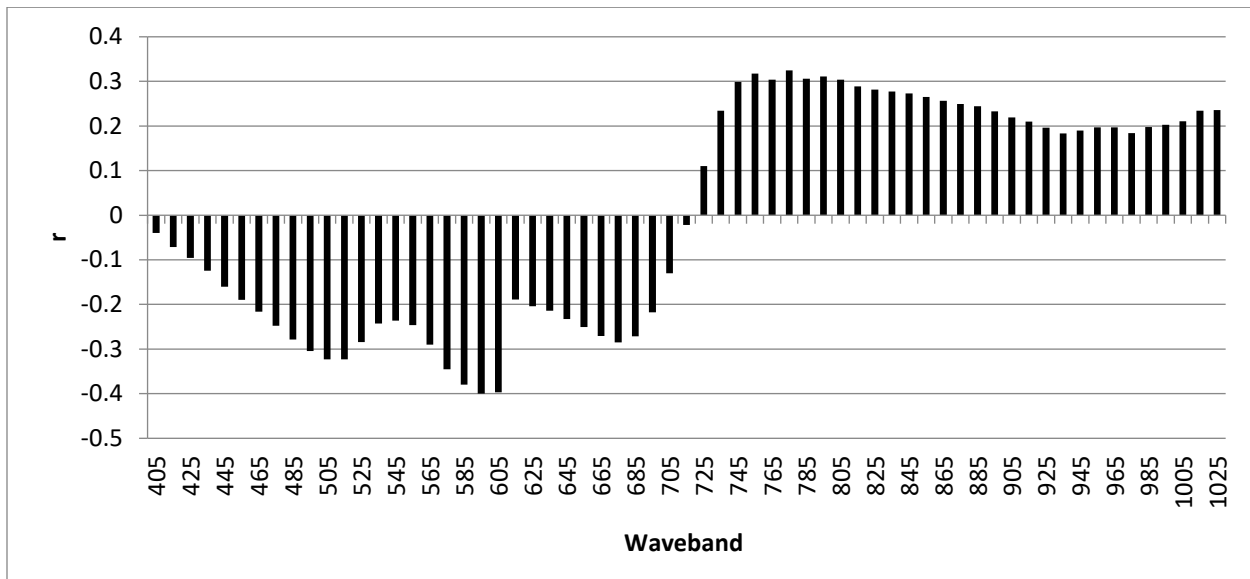


Figure 2.8 a. Pearson's correlation (r) between yield and season average waveband reflectance for the nested association mapping population grown at Manhattan in 2015. Significant correlation at $\alpha = .05$ is equal to $r \leq -.15$ and $r \geq .15$. Significant correlation at $\alpha = .01$ is equal to $r \leq -.20$ and $r \geq .20$.

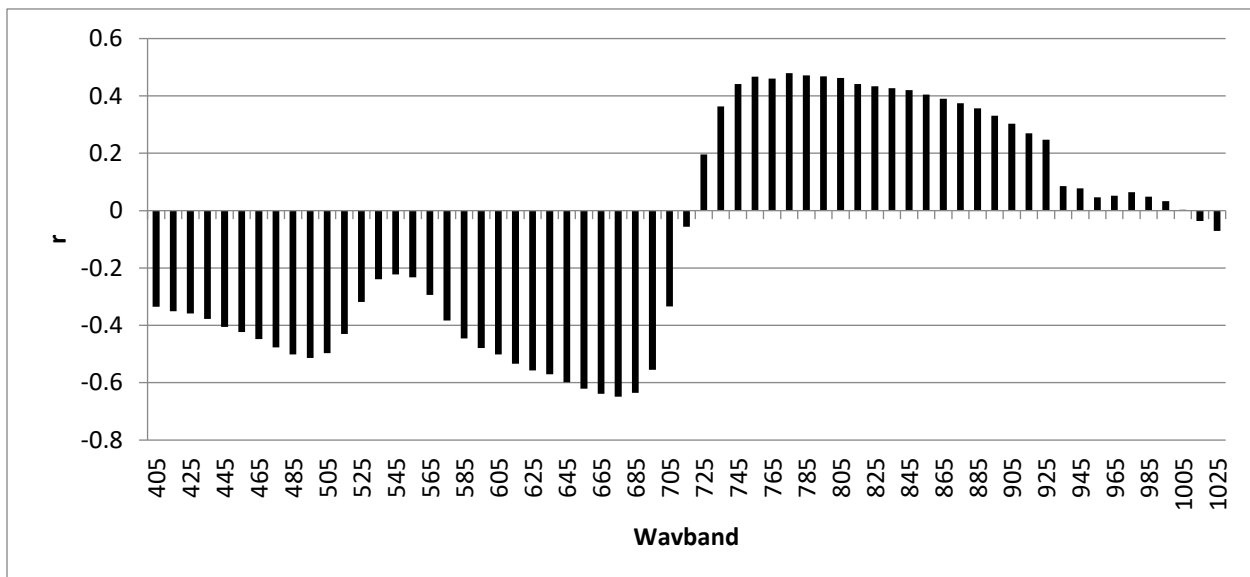


Figure 2.8 b. Pearson's correlation (r) between yield and season average waveband reflectance for the nested association mapping population grown at Manhattan in 2016. Significant correlation at $\alpha = .05$ is equal to $r \leq -.15$ and $r \geq .15$. Significant correlation at $\alpha = .01$ is equal to $r \leq -.20$ and $r \geq .20$.

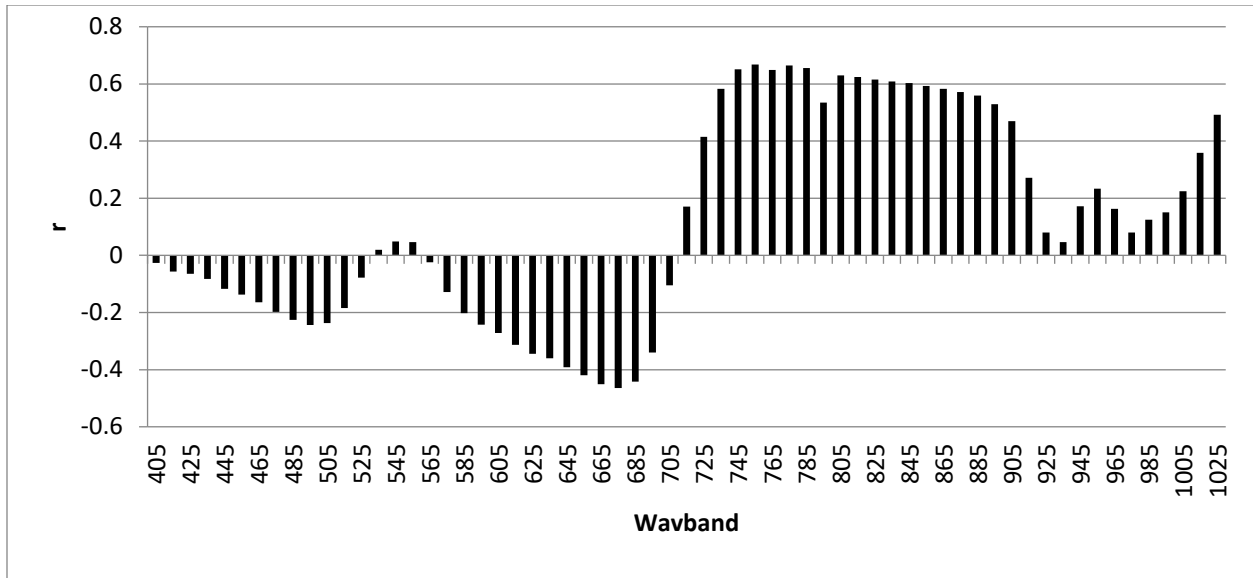


Figure 2.8 c. Pearson's correlation (r) between yield and season average waveband reflectance for the nested association mapping population grown at Rossville in 2016. Significant correlation at $\alpha = .05$ is equal to $r \leq -.15$ and $r \geq .15$. Significant correlation at $\alpha = .01$ is equal to $r \leq -.20$ and $r \geq .20$.

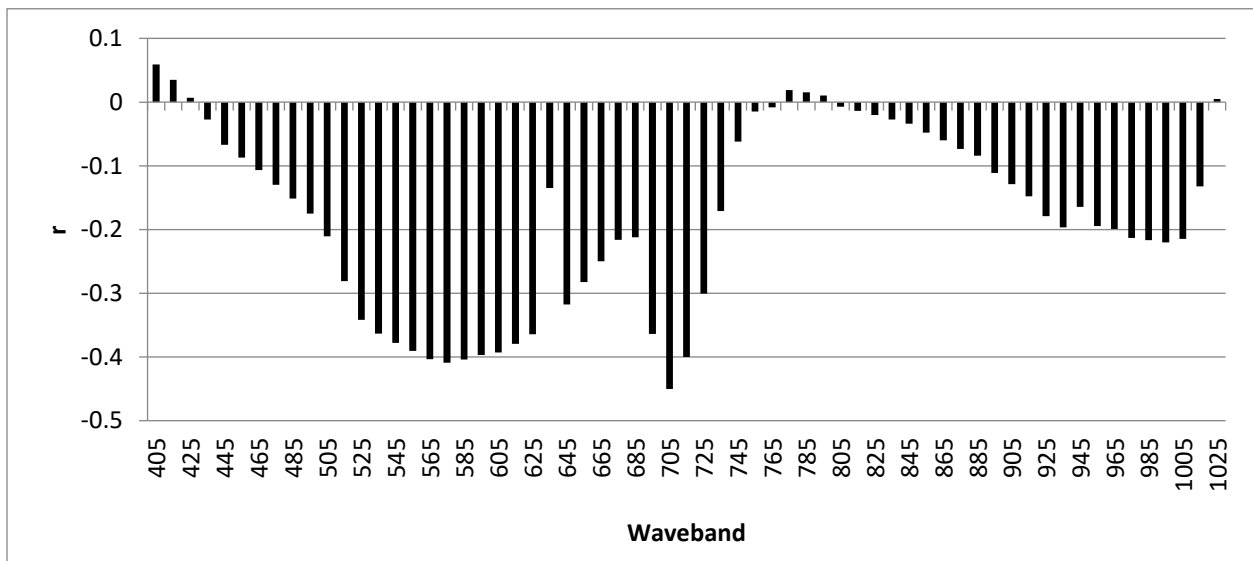


Figure 2.9 a. Pearson's correlation (r) between yield and August 8 waveband reflectance for a nested association mapping population grown at Rossville in 2016. Significant correlation at $\alpha = .05$ is equal to $r \leq -.15$ and $r \geq .15$. Significant correlation at $\alpha = .01$ is equal to $r \leq -.20$ and $r \geq .20$.

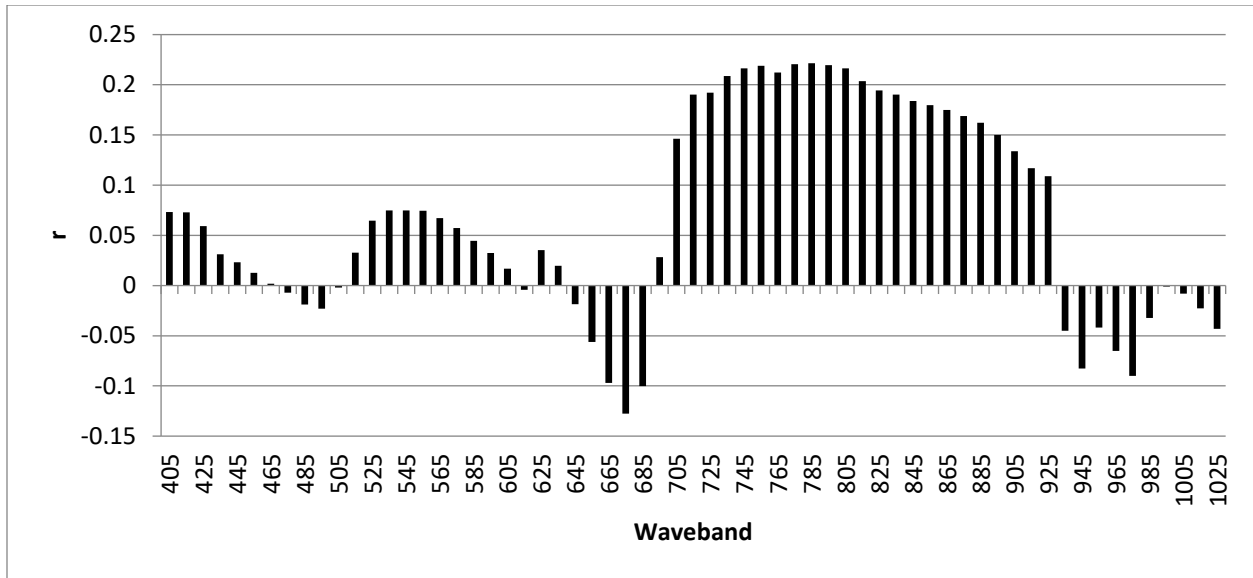


Figure 2.10 a. Pearson's correlation (r) between yield and season average waveband reflectance for the soybean variety performance test population grown at Manhattan in 2015. Significant correlation at $\alpha = .05$ is equal to $r \leq -0.15$ and $r \geq 0.15$. Significant correlation at $\alpha = .01$ is equal to $r \leq -0.20$ and $r \geq 0.20$.

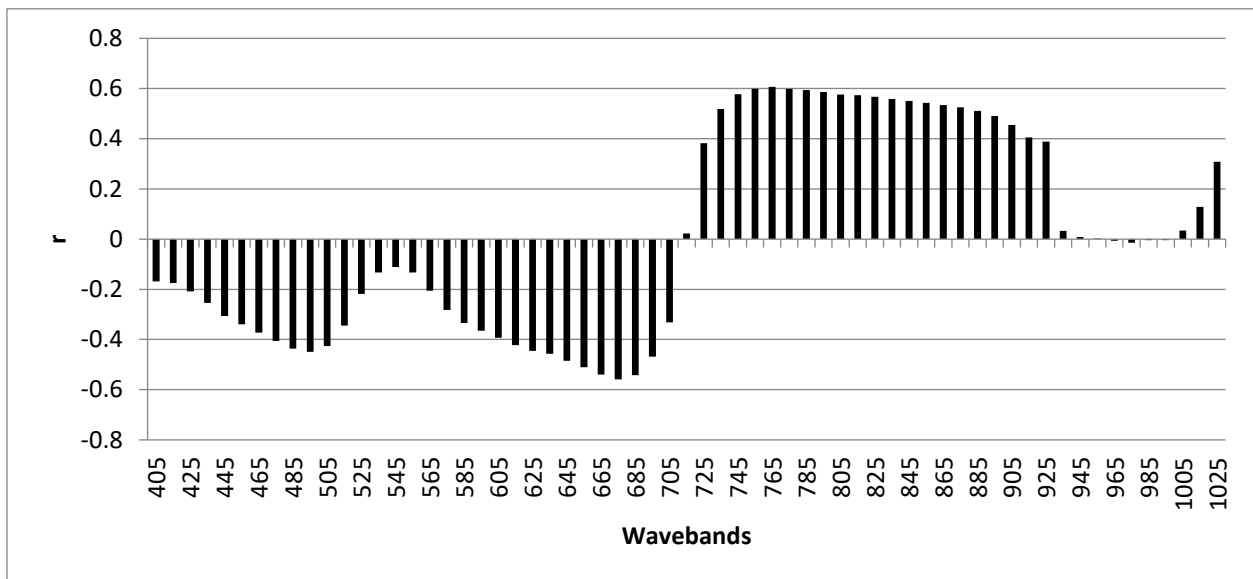


Figure 2.10 b. Pearson's correlation (r) between yield and season average waveband reflectance for the soybean variety performance test population grown at Manhattan in 2016. Significant correlation at $\alpha = .05$ is equal to $r \leq -0.15$ and $r \geq 0.15$. Significant correlation at $\alpha = .01$ is equal to $r \leq -0.20$ and $r \geq 0.20$.

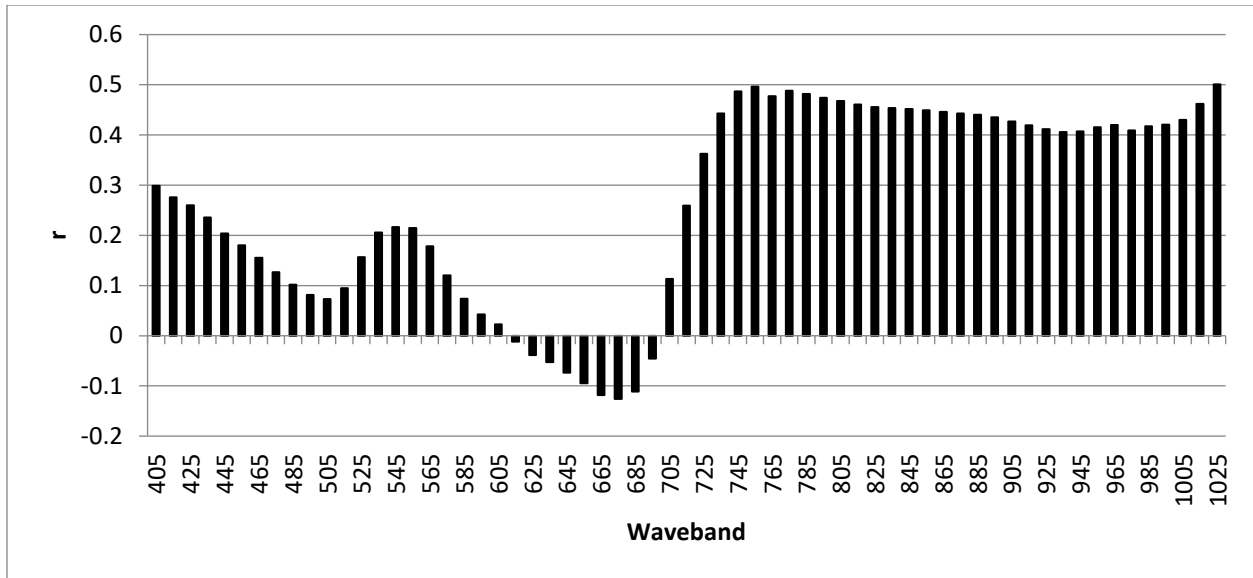


Figure 2.10 c. Pearson's correlation (r) between disease index and September 9 waveband reflectance for the soybean variety performance test population grown at Rossville in 2016. Significant correlation at $\alpha = .05$ is equal to $r \leq -.15$ and $r \geq .15$. Significant correlation at $\alpha = .01$ is equal to $r \leq -.20$ and $r \geq .20$.

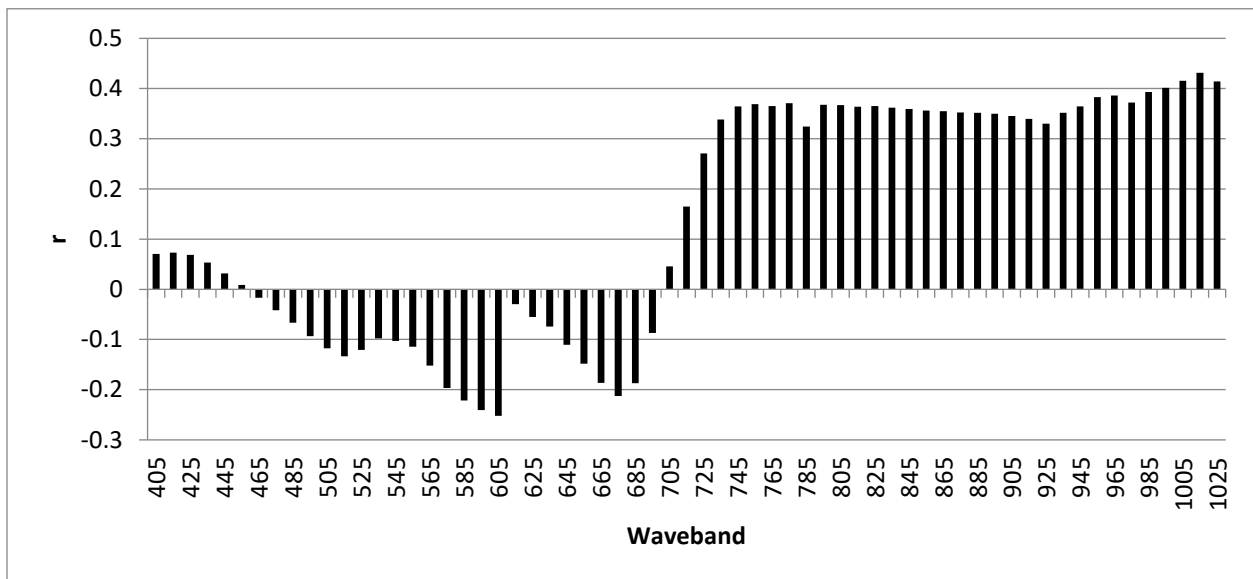


Figure 2.11 a. Pearson's correlation (r) between maturity and season average waveband reflectance for the nested association mapping population grown at Manhattan in 2015. Significant correlation at $\alpha = .05$ is equal to $r \leq -.15$ and $r \geq .15$. Significant correlation at $\alpha = .01$ is equal to $r \leq -.20$ and $r \geq .20$.

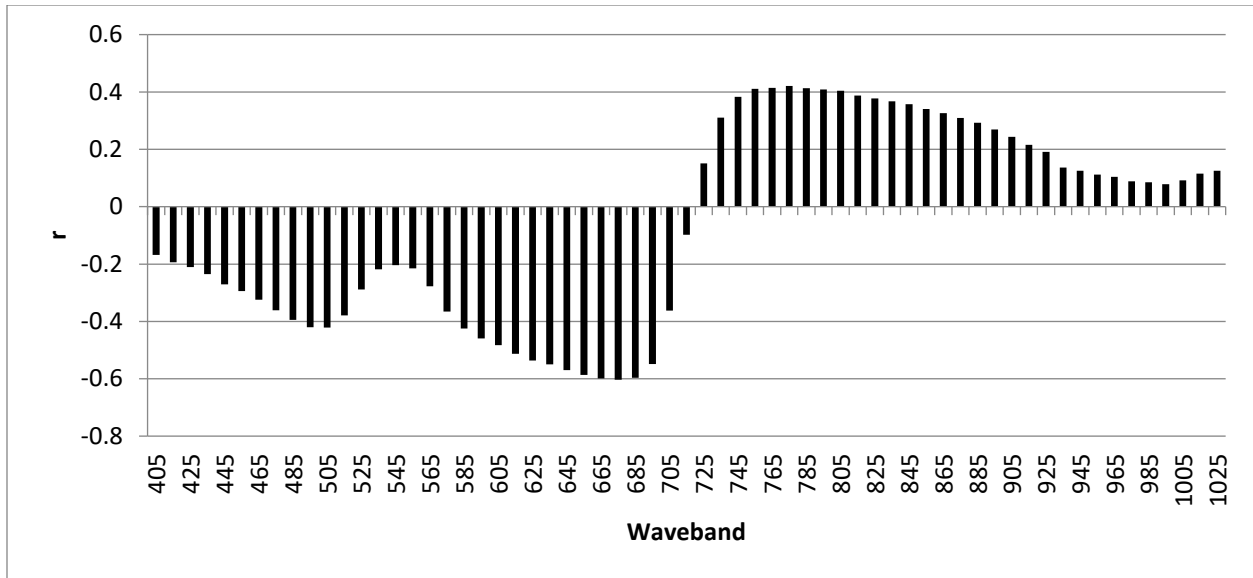


Figure 2.11 b. Pearson's correlation (r) between maturity and season average waveband reflectance of the Nested association mapping population grown at Manhattan in 2016. Significant correlation at $\alpha = .05$ is equal to $r \leq -.15$ and $r \geq .15$. Significant correlation at $\alpha = .01$ is equal to $r \leq -.20$ and $r \geq .20$.

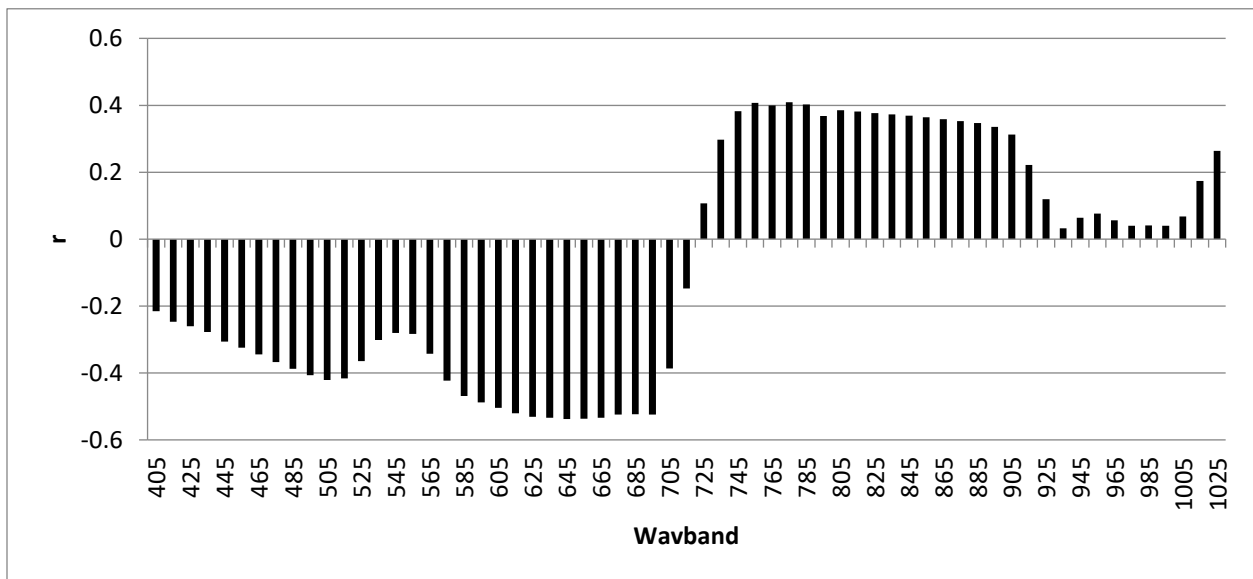


Figure 2.11 c. Pearson's correlation (r) between maturity and season average waveband reflectance for the nested association mapping population grown at Rossville in 2016. Significant correlation at $\alpha = .05$ is equal to $r \leq -.15$ and $r \geq .15$. Significant correlation at $\alpha = .01$ is equal to $r \leq -.20$ and $r \geq .20$.

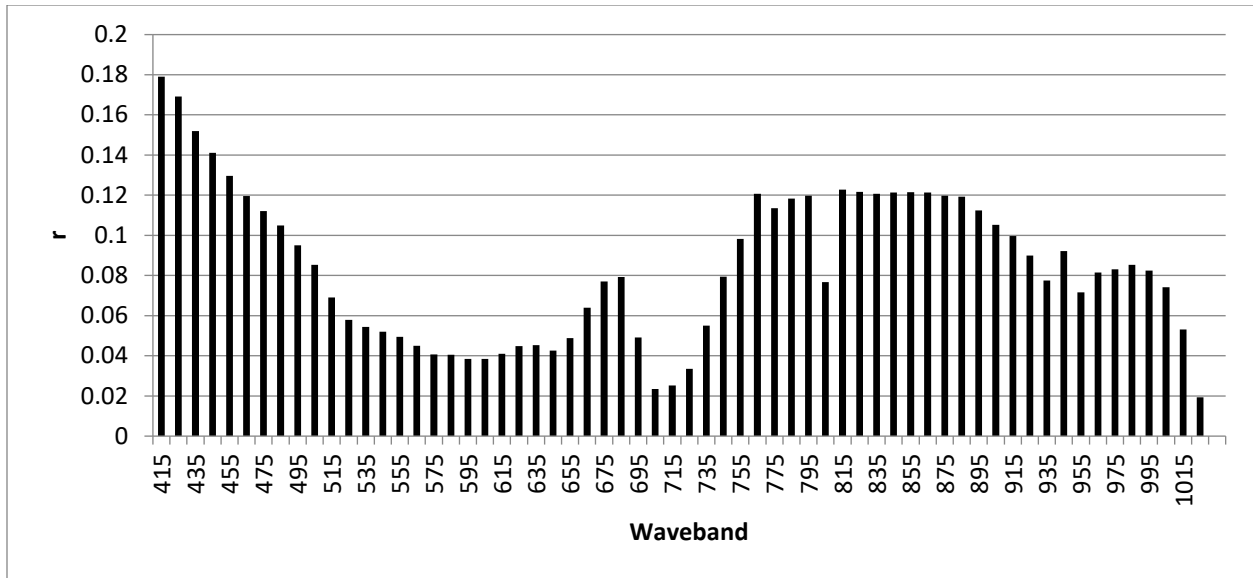


Figure 2.12 a. Pearson's correlation (r) between maturity and August 8 waveband reflectance for the nested association mapping population grown at Rossville in 2016. Significant correlation at $\alpha = .05$ is equal to $r \leq -.15$ and $r \geq .15$. Significant correlation at $\alpha = .01$ is equal to $r \leq -.20$ and $r \geq .20$.

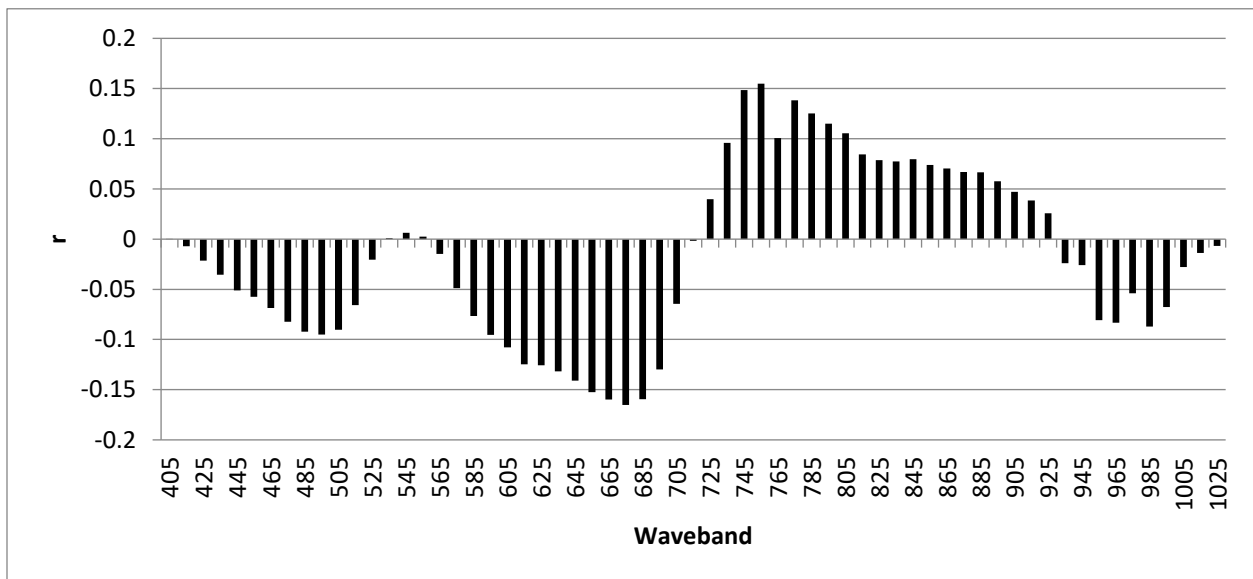


Figure 2.13 a. Pearson's correlation (r) between yield and season average waveband reflectance for the soybean variety performance test population grown at Manhattan in 2015. Significant correlation at $\alpha = .05$ is equal to $r \leq -.15$ and $r \geq .15$. Significant correlation at $\alpha = .01$ is equal to $r \leq -.20$ and $r \geq .20$.

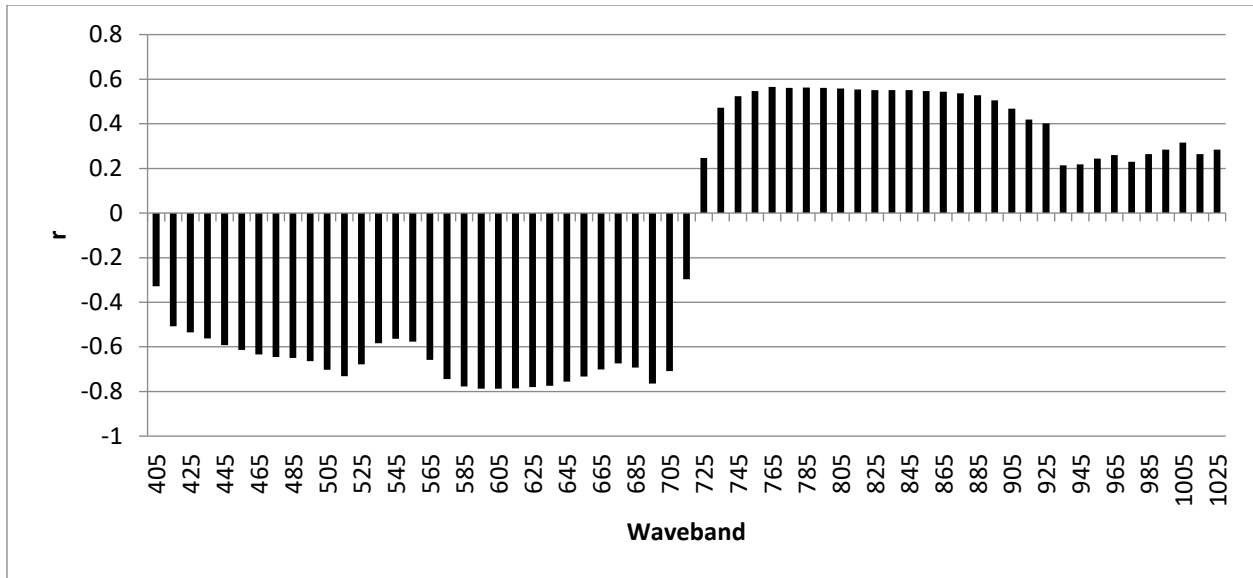


Figure 2.13 b. Pearson's correlation (r) between yield and season average waveband reflectance for the soybean variety performance test population grown at Manhattan in 2016. Significant correlation at $\alpha = .05$ is equal to $r \leq -.15$ and $r \geq .15$. Significant correlation at $\alpha = .01$ is equal to $r \leq -.20$ and $r \geq .20$.

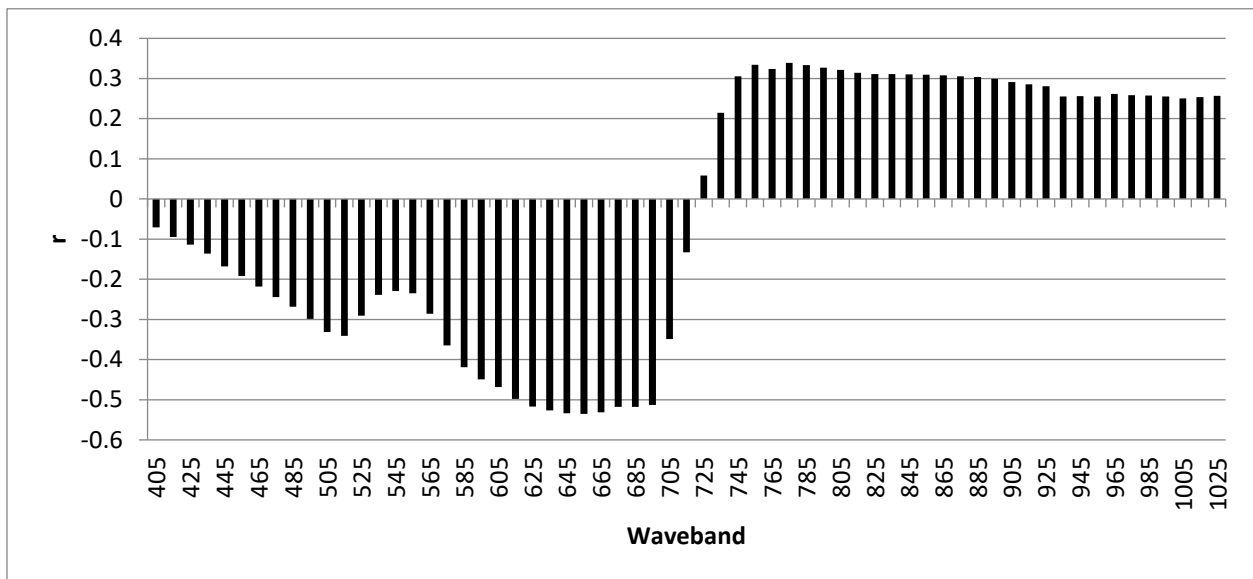


Figure 2.13 c. Pearson's correlation (r) between disease index and September 9 waveband reflectance for the soybean variety performance test population grown at Rossville in 2016. Significant correlation at $\alpha = .05$ is equal to $r \leq -.15$ and $r \geq .15$. Significant correlation at $\alpha = .01$ is equal to $r \leq -.20$ and $r \geq .20$.

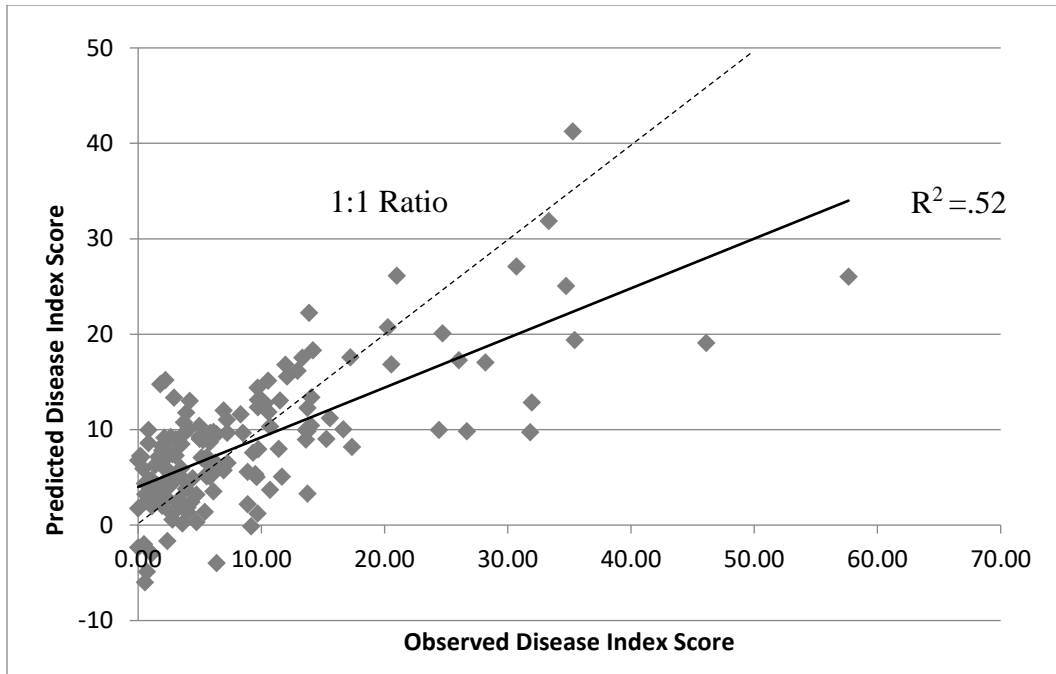


Figure 2.14 a. Relationship between observed disease index score and predicted disease index score based on stepwise regression model using season average reflectance values for the NAM population at Manhattan in 2015.

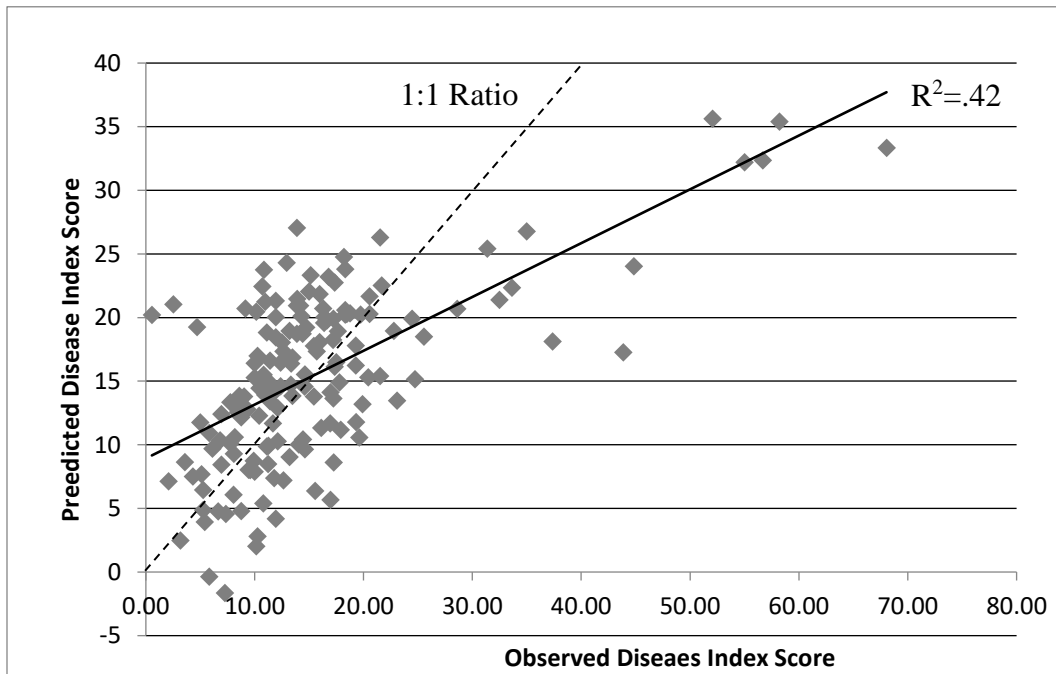


Figure 2.15 a. Relationship between observed disease index score and predicted disease index score based on stepwise regression model using season average reflectance values and maturity as a covariate for the NAM population at Rossville in 2016.

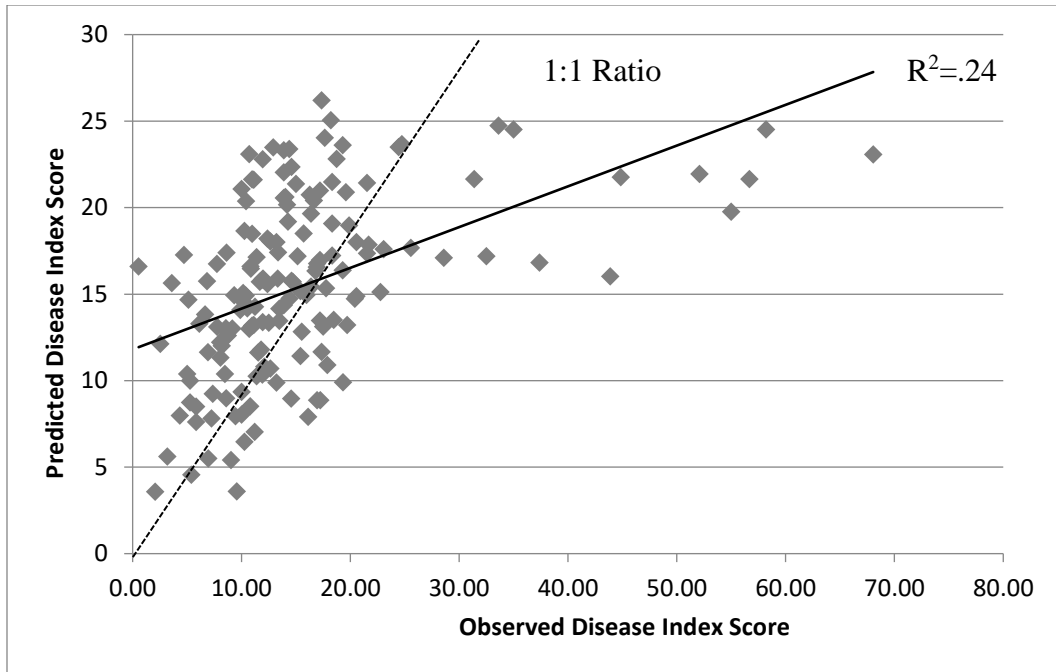


Figure 2.16 a. Relationship between observed disease index score and predicted disease index score based on stepwise regression model for September 2 reflectance values for the NAM population at Rossville 2016.

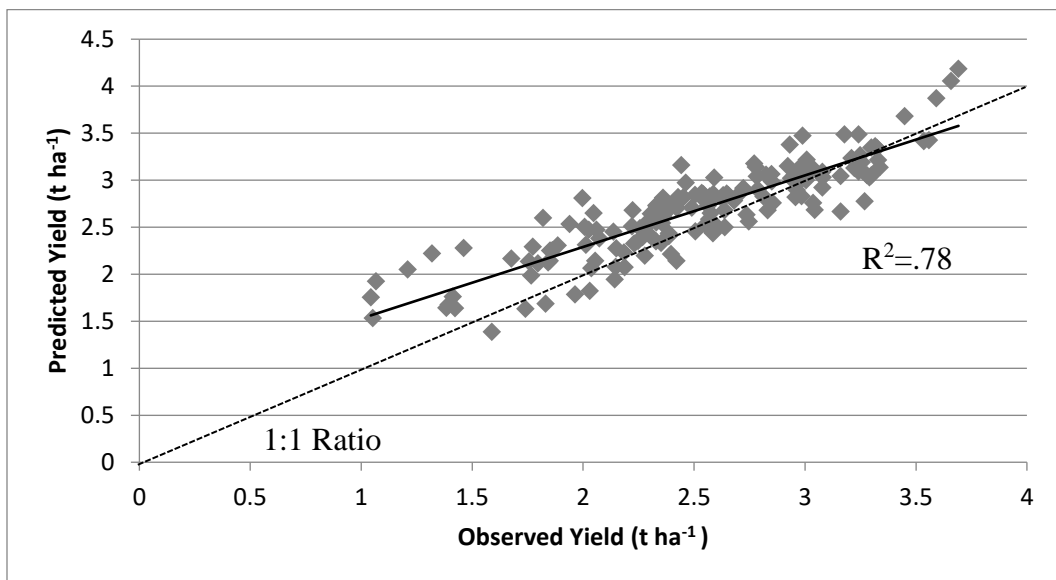


Figure 2.17 a. Relationship between observed yield and predicted yield based on a stepwise regression model using season average reflectance values for the NAM population at Rossville 2016.

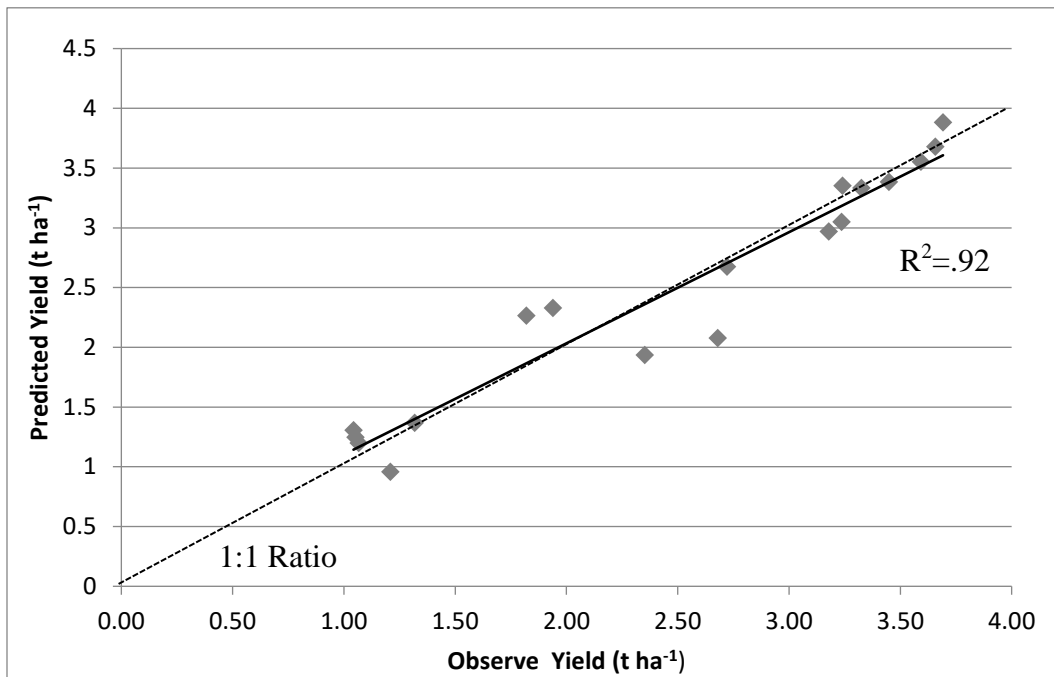


Figure 2.18 a. Relationship between observed yield and predicted yield based on a stepwise regression model for the check reflectance value for the NAM population at Rossville 2016.

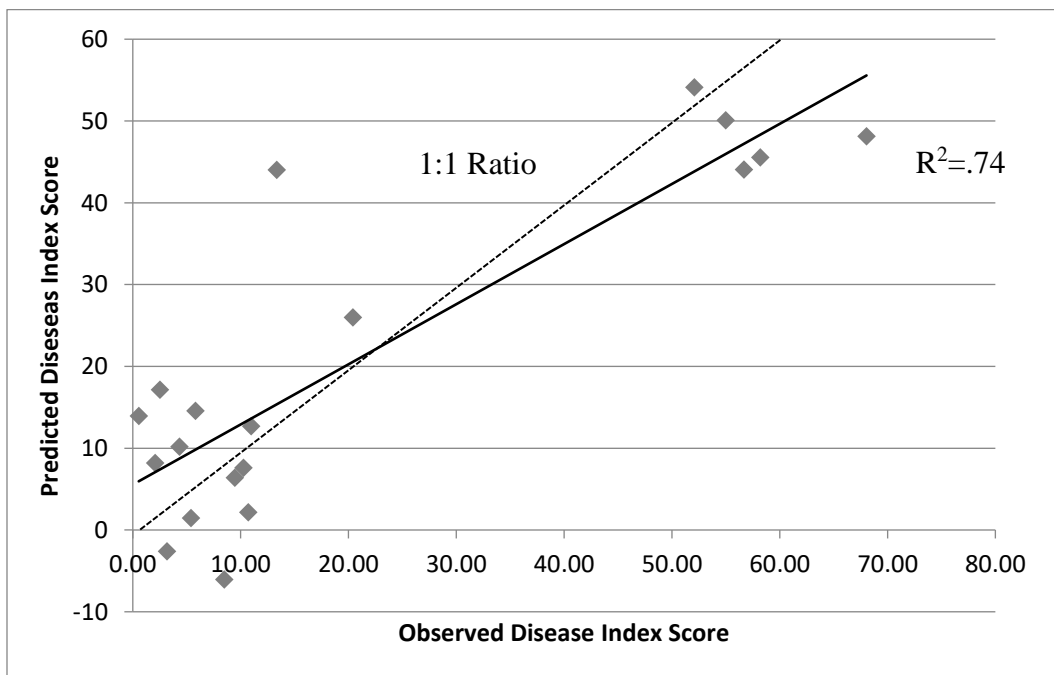


Figure 2.19 a. Relationship between observed disease index score and predicted disease index score for the check reflectance model for the NAM population at Rossville 2016.

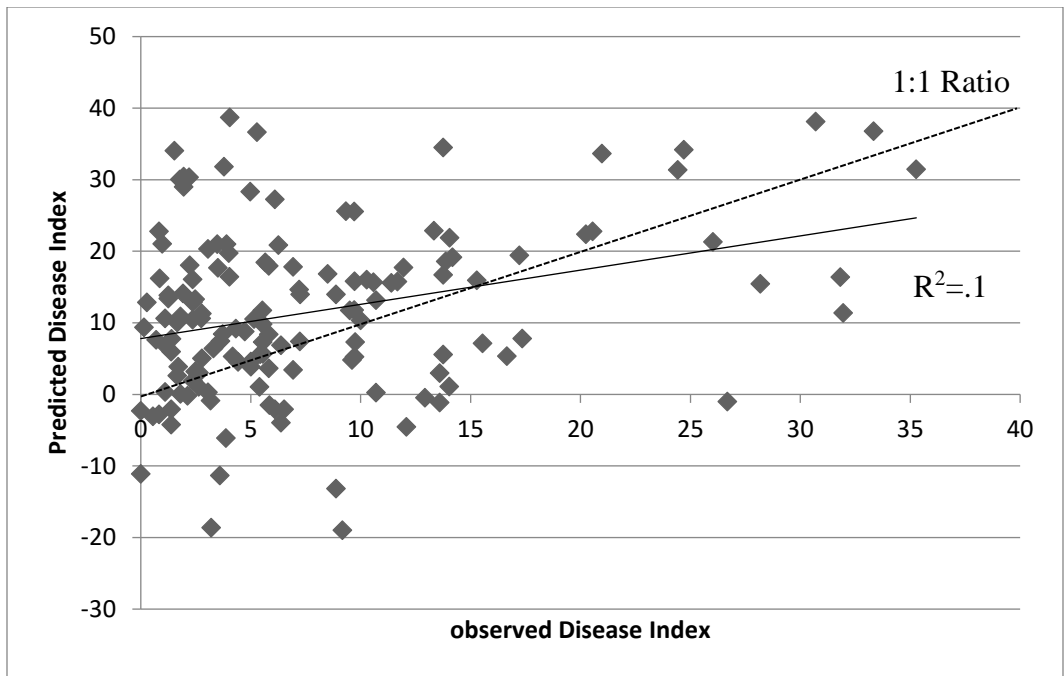


Figure 2.20 a. Relationship between observed disease index score and predicted disease index score for the NAM RILs based on the NAN Check model population at Manhattan 2015.

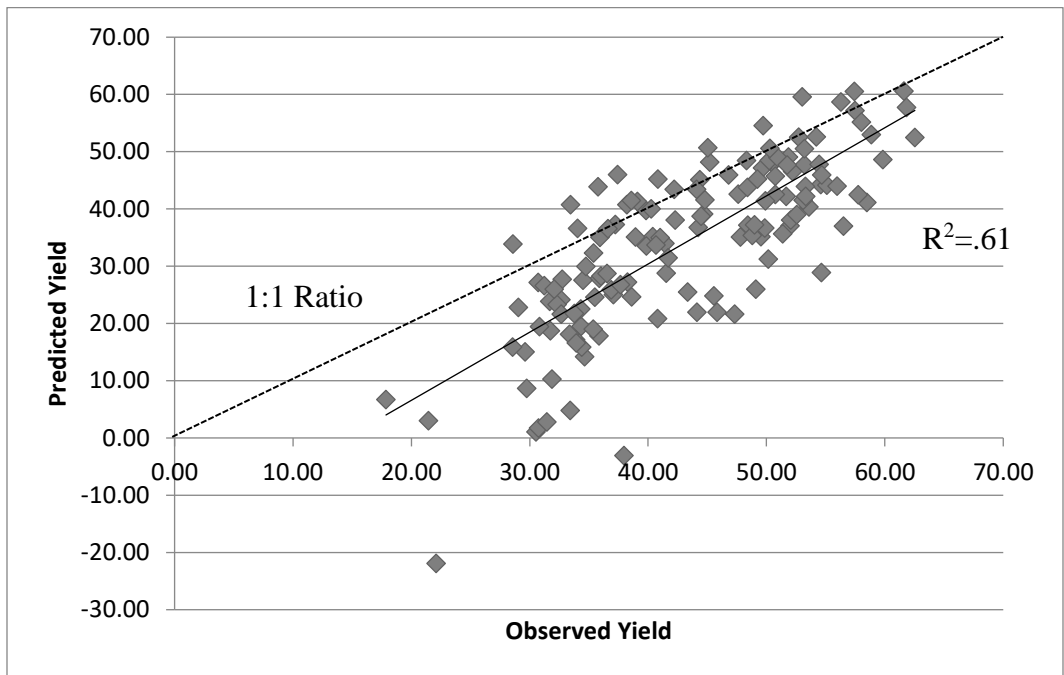


Figure 2.21 a. Relationship between observed yield and predicted yield for the NAM RILs based on the NAM Check model population at Rossville 2016.

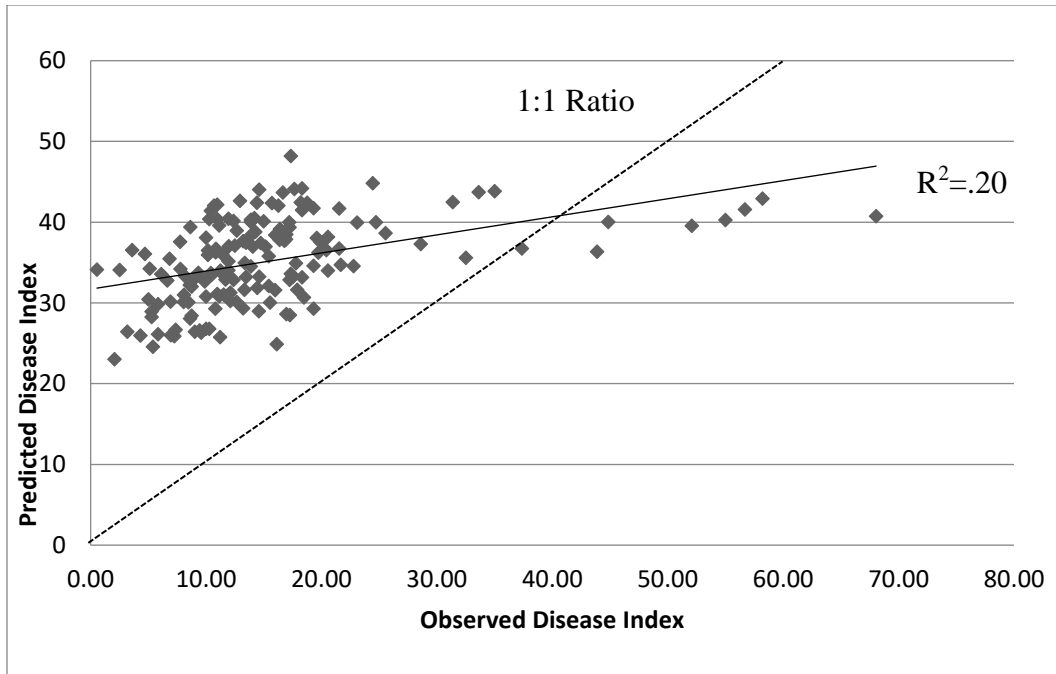


Figure 2.22 a. Relationship between observed disease index and predicted disease index for the NAM population at Rossville in 2016 based on the NAM Grand means model.

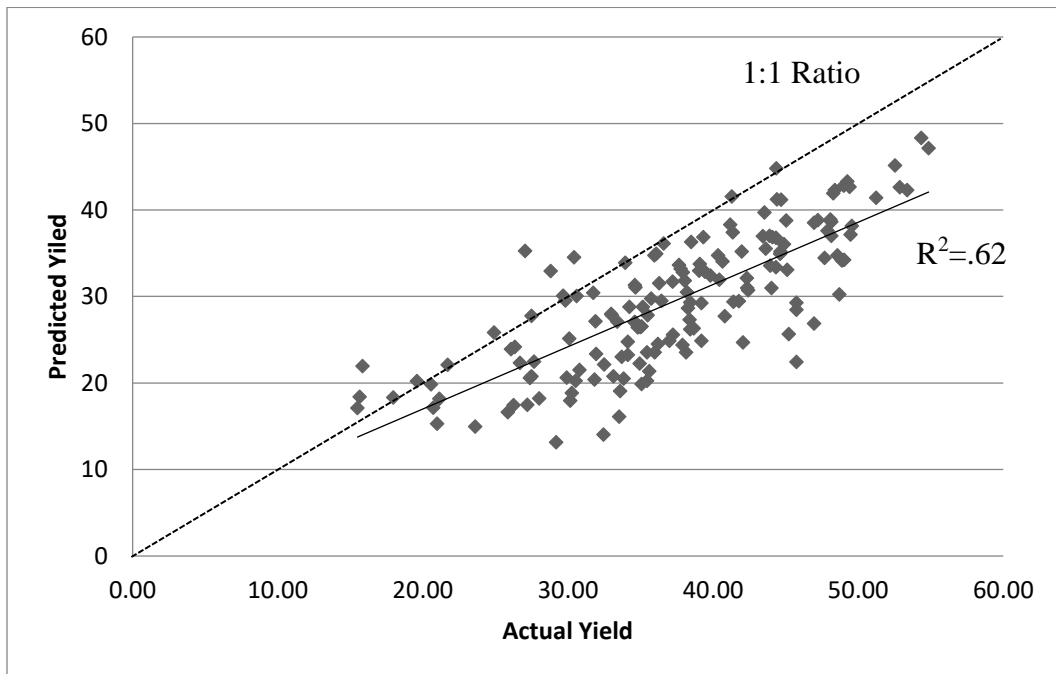


Figure 2.23 a. Relationship between observed yield and predicted yield for the NAM population at Rossville in 2016 based on the NAM Grand means model.

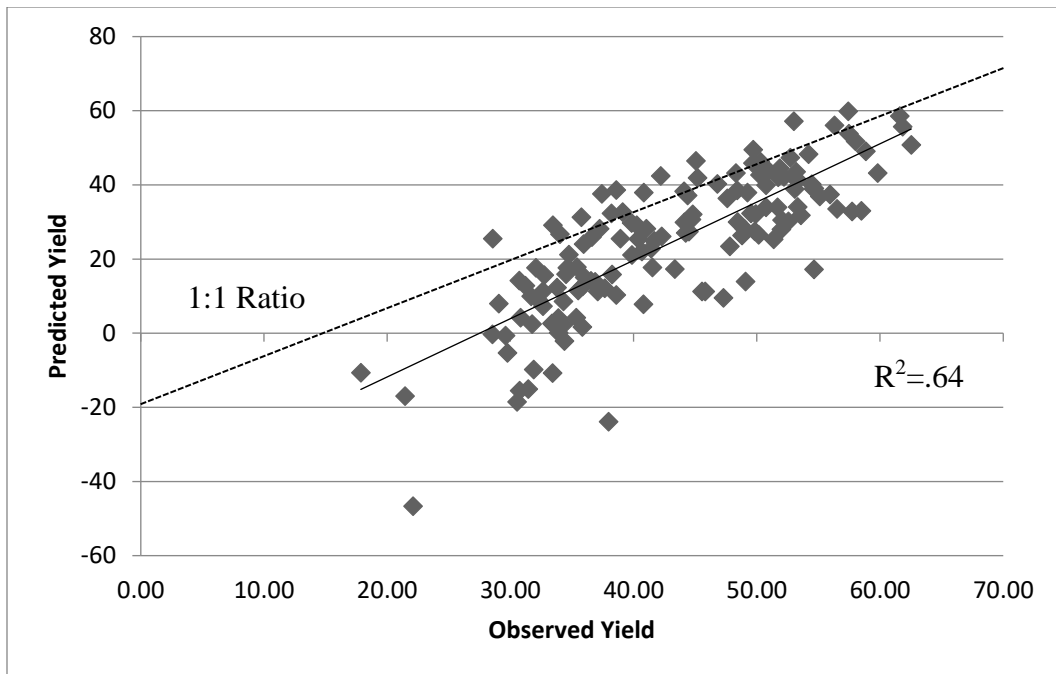


Figure 2.24 a. Relationship between observed yield and predicted yield for the NAM population at Manhattan in 2016 based on the NAM Grand means check model.

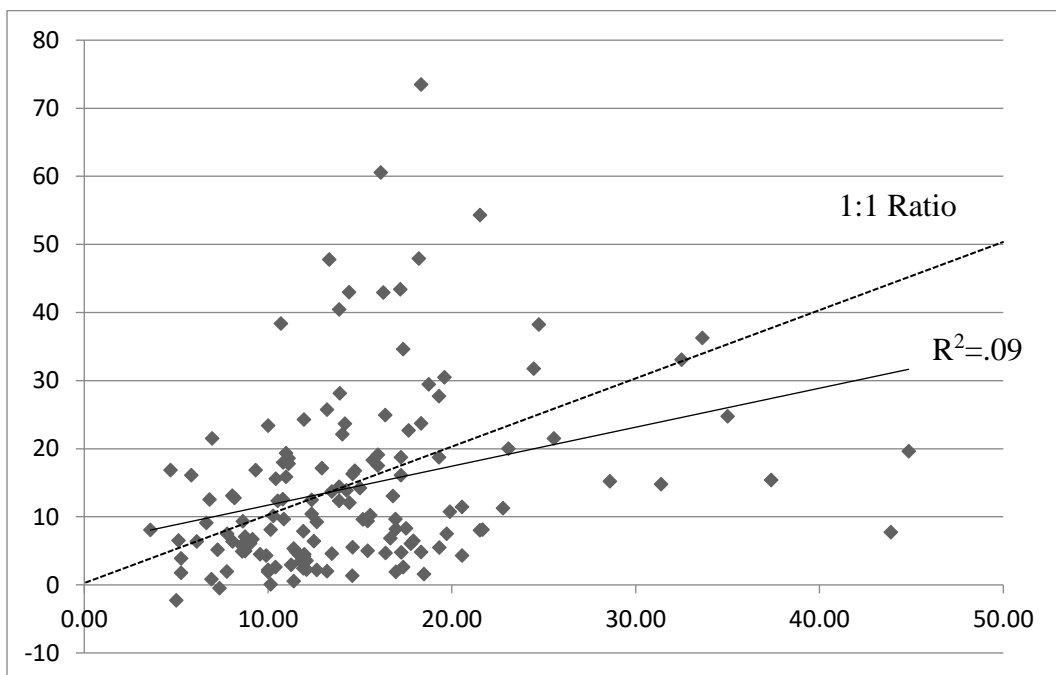


Figure 2.25 a. Relationship between observed disease index and predicted disease index for the NAM population at Rossville in 2016 based on the NAM Grand Means check model.